NOAA Project
Report

Development of two tsunami inundation maps in the GOM and inclusion of the Meteotsunami characterization for Panama City, FL

Final Report to the
National Tsunami Hazard Mitigation Program (NTHMP)
in Completion of Project Awards
NA18NWS4670078

Authors

Juan J Horrillo	Texas A&M University at Galveston
Wei Cheng	
Jens Figlus	
Williams Knight	

Collaborators:

Brad Baker	Santa Rosa County Emergency Management Director

Under the guidance of
NTHMP Mapping and Modeling Subcommittee

National Tsunami Hazard Mitigation Program

National Oceanic and Atmospheric Administration

Ocean Engineering
Texas A&M University at Galveston
Galveston, Texas, 77553

November 2019

Contents

List of Figures

List of Tables

1 Executive Summary

Potential tsunami sources for the GOM are local submarine landslides, which have been examined in the past by the Atlantic and Gulf of Mexico Tsunami Hazard Assessment Group [ten Brink et al., 2009b]. In their findings, they stated that submarine landslides in the GOM are considered a potential tsunami hazard. However, the probability of such an event (tsunamis generated by large landslides) is low. The probability of occurrence is related to ancient (historical) massive landslides which were probably active prior to 7,000 years ago when large quantities of sediments were emptied into the Gulf of Mexico. Nowadays, sediment continues to empty into the Gulf of Mexico mainly from the Mississippi River. This sediment supply contributes to the slope steepening and the increase of fluid pore pressure in sediments, which may lead to further landslide activities and hence, the reason for this study in determining the potential tsunami hazard and its effects in the Gulf of Mexico.

For the triggering mechanism (tsunami generation) we use five historical sources, i.e., the Eastbreaks, Mississippi Canyon, West Florida landslides, and two Yucatán landslides introduced in [Horrillo et al., 2018]. A probabilistic approach was implemented in our previous study, see [Horrillo et al., 2015], to fill gaps along the continental shelf between the historical landslide sources by adding synthetic landslide sources (four in total) to cover the entire northern part of the GOM. Our probabilistic approach confirmed a recurrence period of major landslide events of around 8000 years, consistent with findings by [Geist et al., 2013].

These historical and probabilistic tsunami sources (nine in total) are used as the maximum credible events that could happen in the region according to the local bathymetry, seafloor slope, and sediment information. These credible events are then used to determine the inundation impact on selected communities along the GOM. The extent and magnitude of the tsunami inundation in those selected locations are achieved by using a combination of 3D and 2D coupled-numerical models. For instance, the 3D model, TSUNAMI3D, is used for tsunami generation to determine the initial dynamic wave or initial source and results are passed as an input to the 2D non-hydrostatic model, NEOWAVE, to determine the tsunami wave propagation and the detailed runup and inundation extent in each of the communities. Tsunami flooding inland-extent, maximum inundation water depth, momentum flux and direction, current velocity and vorticity can then be determined within the inundation-prone areas of the selected communities. Also, tsunami inundation and hurricane category flooding can be compared to access tsunami hazard in unmapped locations.

This project focused on the implementation of recent developments in the tsunami science recommended by the National Tsunami Hazard Mitigation Program - Modeling Mapping Subcommittee - Strategic Plan (NTHMP-MMS-SP) into our current Gulf of Mexico (GOM) tsunami mitigation products. Three main developments for tsunami mitigation have been created under this project for communities in the GOM that will provide guidance to state emergency managers for tsunami hazard mitigation and warning purposes.

The first is the development of tsunami inundation maps in Grand Isle, LA and Freeport, TX. Maximum tsunami inundation extent, water height, and momentum flux magnitude and direction are determined from each landslide sources, as well as the maximum of maximum inundation maps from all nine landslide sources. The two new tsunami inundation map products add to the existing 12 mapped locations, which provide so far good coverage of the most populous coastal areas along the GOM.

The second is a continuing study of the comparison between existing SLOSH hurricane flooding data and our tsunami inundation result, in order to provide temporal-low-order estimate for tsunami hazard areas (community) where inundation studies have not yet been assigned/executed or where little bathymetric and elevation data exists. The adopted approach to define a quick estimate of tsunami vulnerability areas in the GOM has been taken from the existing hurricane storm surge flooding results along coastal areas, in which storm flooding map products are based on hurricane category. The existing storm surge flooding maps cover almost the entire GOM coastal regions and thus they are very well known among GOM regional emergency managers and other parties.

The third is to produce the velocity and vorticity magnitude maps for all the landslide scenarios, for Grand Isle, LA and Freeport, TX. Based on these maritime maps, location of strong currents and their damaging levels are identified. The tsunami hazard maritime products such as tsunami current magnitude, vorticity, safe/hazard zones would be central for future developments of maritime hazard maps, maritime emergency response and as well as infrastructure planning. We hope that the results herein may assist the maritime communities, port managers and other NTHMP's interested parties.

The fourth task is to identify meteotsunami physical parameters and to obtain an understanding of this phenomenon through the characterization of physical parameters both globally and locally in a specific region susceptible to meteotsunami in the GOM. We have chosen Panama City, Clearwater Beach, and Naples, FL as the prime locations for this pilot study to gain a better understanding of the meteotsunami phenomenon on the eastern Gulf of Mexico and west coast of Florida, and to determine which tools (methodology) are most appropriate for EMs and tsunami warning operators for mitigation and hindcasting/forecasting of these types of events.

Although the recurrence of destructive tsunami events have been verified to be quite low in the GOM, our work has confirmed that submarine landslide events with similar characteristics to those used here, have indeed the potential to cause severe damage to GOM coastal communities. Therefore, this work is intended to provide guidance to local emergency managers to help managing urban growth, evacuation planning, and public education with final objective to mitigate potential tsunami hazards in the GOM.

2 Introduction

2.1 Background

The U.S. Tsunami Warning System has included Gulf of Mexico (GOM) coasts since 2005 in order to enable local emergency management to act in response to tsunami warnings. To plan for the warning response, emergency managers must understand what specific areas within their jurisdictions are threatened by tsunamis. Coastal hazard areas susceptible to tsunami inundation can be determined by historical events, by modeling potential tsunami events (worst-case scenarios), or by using a probabilistic approach to determine the rate of recurrence or likelihood of exceeding a certain threshold. As the GOM coastal regions have no significant recent historical tsunami records, numerical modeling and probabilistic methodologies for source identification must be used to determine coastal hazard zones.

Potential tsunami sources for the GOM are local submarine landslides [ten Brink et al., 2009b]; sources outside the GOM are considered a very low threat and may not significantly impact GOM coastal communities or infrastructure [Knight, 2006]. Although a massive tsunamigenic underwater landslide in the GOM is considered a potential hazard, the frequency of such events (though not well-constrained) is probably quite low based on historical evidence [Dunbar and Weaver, 2008] and available data on ages of failures which suggest they were probably active prior to 7,000 years ago when large quantities of sediments were emptied into the GOM [ten Brink et al., 2009b]. However, sediments continue to empty into the GOM, mainly from the Mississippi River, contributing to slope steepening and the increase of fluid pore pressure in sediments which may lead to unstable slopes that can be subsequently triggered to failure by seismic loading [Masson et al., 2006, ten Brink et al., 2009a, Dugan and Stigall, 2010, Harbitz et al., 2014]. In addition, the unique geometry of the GOM basin makes even unlikely tsunami events potentially hazardous to the entire Gulf Coast. Waves tend to refract along continental slopes; thus, given the curved geomorphology of the GOM shelf and the concave shape of the coastline, any outgoing tsunami wave could potentially affect the opposite coast in addition to the coast close to the landslide source.

Five large-scale geological submarine landslides with tsunamigenic potential have been identified within the GOM [ten Brink et al., 2009b, Chaytor et al., 2016], representing possible worst-case tsunami scenarios affecting GOM coasts in the past. In order to generate a more complete picture of landslide tsunami potential in the GOM, a probabilistic approach has been implemented to develop four additional synthetic landslide sources which fill gaps along the continental shelf between the geological landslide sources [Pampell-Manis et al., 2016]. These probabilistic tsunami sources are considered to be the maximum credible events that could happen in a particular region of the GOM according to the local bathymetry, seafloor slope, sediment information, and seismic loading. The probabilistic maximum credible events together with the geological sources form a suite of tsunami sources that have been used within coupled 3D and 2D numerical models to model tsunami generation and propagation throughout the GOM and to develop high-resolution inundation maps for the inundation-prone areas of two new communities along the Gulf Coast: Grand Isle, LA and Freeport, TX. These inundation studies showed that tsunamis triggered by massive submarine landslides have the potential to cause widespread and significant inundation of coastal cities. All of the 14 communities from both previous and current work and nine landslide sources are shown in Fig. 1.

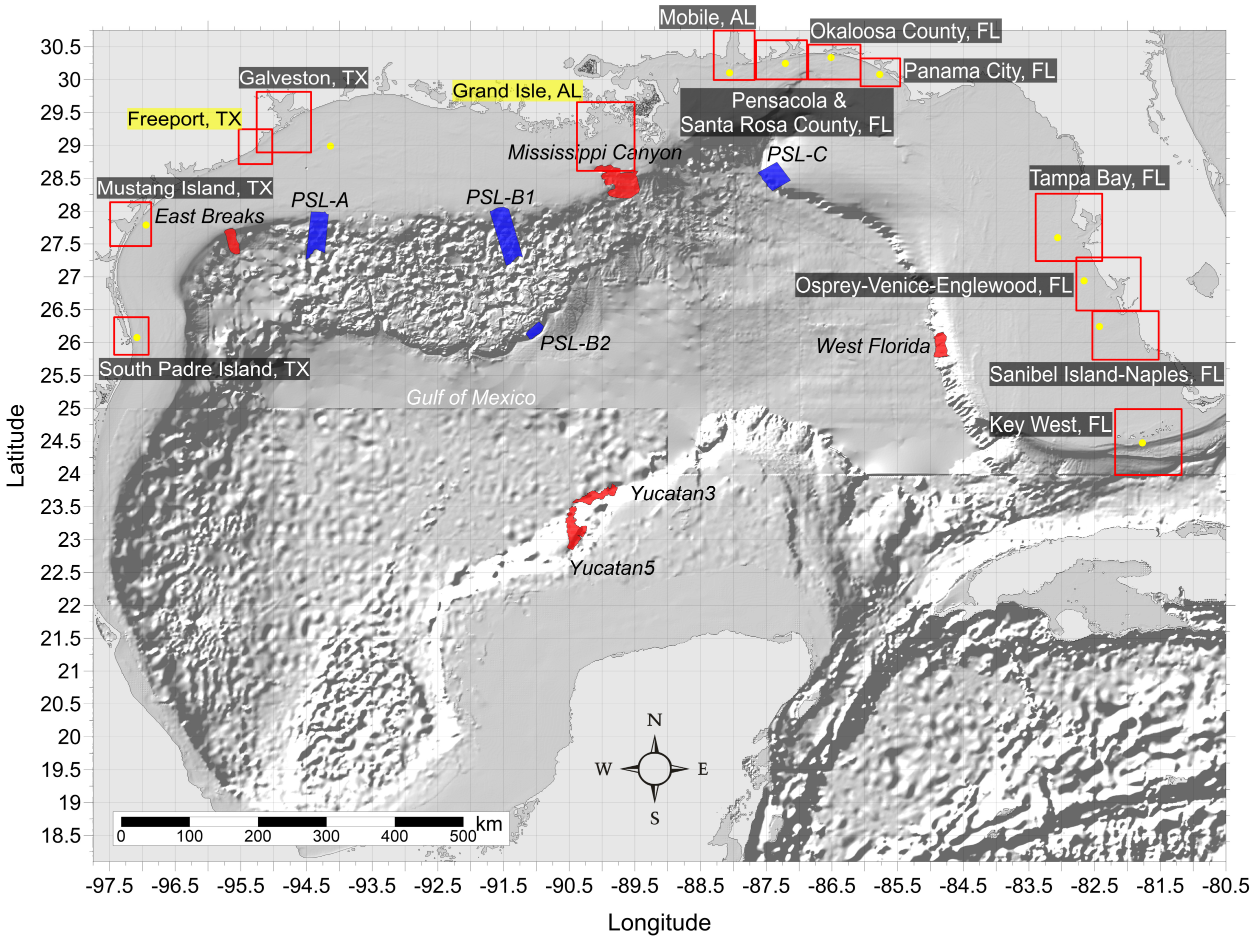

Figure 1: Selected communities or geography regions along the US GOM coastline where tsunami maps have been developed. Red rectangles denote 3 arcsecond (∼90m) domains of coastal communities where tsunami inundation has been modeled (highlighted Freeport, TX and Grand Isle, LA are developed in the current project); red hatched areas are geological landslide sources; blue hatched areas are Probabilistic Submarine Landslide (PSL) sources; yellow dots are locations of numerical wave gauges. The zero-meter elevation contour is drawn to show the GOM coastline.

While high-resolution tsunami inundation studies have been completed for these 14 communities and are planned for additional locations, vulnerability assessments are still essential for coastal locations where inundation studies have not yet been performed or planned, or where there is a lack of high-resolution bathymetric and/or elevation data. Therefore, we aim to extend the results of the completed mapping studies in order to provide estimates of tsunami inundation zones for hazard mitigation efforts in un-mapped locations. Inundation maps with even low resolution are useful to emergency managers to create first-order evacuation maps, and some methods currently exist to provide low-resolution estimates of hazard zones for regions which do not currently have or warrant high-resolution maps. For example, guidance given by the National Tsunami Hazard Mitigation Program (NTHMP) Mapping and Modeling Subcommittee in "Guidelines and Best Practices to Establish Areas of Tsunami Inundation for Non-modeled or Low-hazard Regions" (available from `https://nws.weather.gov/nthmp/documents/3nonmodeledregionguidelines.pdf`) recommends that coastal areas and areas along ocean-connected waterways that are below 10 m (33 ft) elevation are at risk for most tsunamis, and rare and large tsunamis may inundate above this elevation. However, in low-lying coastal regions such as along the Gulf Coast, the 10 m (33 ft) elevation contour is too far inland to be reasonably applicable for estimating potential tsunami inundation zones. The guidance additionally suggests that low-lying areas are prone to inundation within 3 km (1.9 mi) inland for locally-generated tsunamis and within 2 km (1.3 mi) inland for distant sources. While these distances may be reasonable for some regions of the Gulf Coast, prevalent bathymetric and topographic features such as barrier islands/peninsulas complicate the method of delineating inundation-prone areas based on distance from the shoreline. As a result, the purpose of the current work is to improve the methodology which compares modeled tsunami inundation to modeled/predicted hurricane storm surge. Specifically, we aim to identify the hurricane category which produces modeled maximum storm surge that best approximates the maximum tsunami inundation in the two new locations modeled in this project. Even though many physical aspects of storm surge inundation are completely different from those of tsunamis (time scale, triggering mechanism, inundation process, etc.), good agreement or clear trends between tsunami and storm surge flooding on a regional scale can be used to provide first-order estimates of potential tsunami inundation in communities where detailed inundation maps have not yet been developed or are not possible due to unavailability of high-resolution bathymetry/elevation data. Additionally, since tsunamis are not well-understood as a threat along the Gulf Coast, while hurricane hazards are well-known, this method of predicting tsunami inundation from storm surge provides a way for GOM emergency managers to better prepare for potential tsunami events based on more understandable and accessible information. This study was first carried out in Horrillo et al. [2016] (award number NA14NWS4670049) where five locations were studied, namely South Padre Island, TX, Galveston, TX, Mobile, AL, Panama City, FL, and Tampa, FL; then in Horrillo et al. [2017] (award number NA15NWS4670031 and NA16NWS4670039), where the comparison was performed in Pensacola, FL, Key West, FL, Okaloosa County, FL, Santa Rosa County, FL and Mustang Island, TX; lastly Osprey-Venice-Englewood, FL and Sanibel Island-Naples, FL were analyzed in Horrillo et al. [2018] (award number NA17NWS4670015).

Recent tsunamis have shown that the maritime community requires additional information and guidance about tsunami hazards and post-tsunami recovery [Wilson et al., 2012, 2013]. To accomplish mapping and modeling activities to meet NTHMP's planning/response purposes for the maritime community and port emergency management and other customer requirements, it is necessary to continue the process to include maritime products in our current inundation map development. These activities will include tsunami hazard maritime products generated by GOM's tsunami sources (submarine landslides) that may impact specifically ship channels, bay inlets, harbors, marinas, and oil infrastructures (e.g., designated lightering and oil tanker waiting zones), which has already been applied in other tsunami risk regions, e.g., California, Oregon and Washington. It is worth noting that Galveston was the first city where we implemented the maritime products [Horrillo et al., 2016]. South Padre Island, TX, Mobile, AL, Panama City, FL, and Tampa, FL, Pensacola, FL, Key West, FL, Okaloosa County, FL, Santa Rosa County, FL and Mustang Island, TX, were implemented in project NA15NWS4670031 and NA16NWS4670039 [Horrillo et al., 2017], and Osprey-Venice-Englewood, FL and Sanibel Island-Naples, FL implemented in Horrillo et al. [2018] (award number NA17NWS4670015). Grand Isle, LA and Freeport, TX, are added to the maritime portfolio in this project.

2.2 Regional and Historical Context

Grand Isle, LA

Grand Isle is a town on a barrier island of the same name located in Jefferson Parish, southeastern Louisiana, known for its fishing and birding habitat. Grand Isle is the state's only inhabited barrier island, which is connected to the mainland by the only land access – the Louisiana Highway 1 bridge. Grand Isle barrier island separates the Barataria Bay and Caminada Bay from the Gulf of Mexico. As of the 2010 census, Grand Isle's population was 1296. However, in summers tourists visiting the island sometimes increase the population to over 20000.

In this study, the finest grid (1/3 arcsec) covers most of the Grand Isle (except for west of Hebert Ln), Fifi Island, Grand Terre Islands, Beauregard Island, and the islands surrounding Raccoon Lake.

1909 Grand Isle hurricane was a large and deadly Category 3 hurricane that killed more than 400 people across Cuba and northern GOM. A Published article in 1909, reported that a "tidal wave" came in after the storm. It was debated whether that event was a hurricane storm surge or a tsunami wave caused by an offshore seismological event after the hurricane. The event was added to the Global Tsunami Database in 2002, with a low validity rating, which means that it was unlikely that this was a tsunami event, but needed further study. This particular event was flagged as suspect when NOAA began its intense review of the database in 2006.

On June 30, 2003, Tropical Storm Bill brought moderate storm surge to Louisiana coast and flooded many roads, including the only road to Grand Isle.

Tropical Storm Matthew made landfall on Louisiana on October 10, 2004 and resulted in severe beach erosion at Grand Isle.

The 2005 Hurricane Cindy first landed on Yucatán Peninsula on July 4 as a tropical depression, only to further develop into a Category 1 hurricane as it moved northward and finally landed near Grand Isle on July 5. Southeastern Louisiana was affected by a 1.2 to 1.8 m storm surge which caused beach erosion near Grand Isle.

Hurricane Katrina first made landfall in Florida on August 25, 2005, and weakened into a tropical storm and traveled to GOM the next day where it intensified into a Category 5 hurricane. When it made landfall again in southeast Louisiana and Mississippi, it becomes Category 3. However, Hurricane Katrina made extensive damage, making it the deadliest hurricane in the US and the most costliest Atlantic tropical cyclone. In Grand Isle, LA, more than half of the homes on the island were destroyed. Storm surge of 3.7 m was recorded by a tidal gauge in Plaquemines Parish.

In late August, 2012, Hurricane Isaac crossed Florida Keys as a tropical storm and later became Category 1 when making landfall in Louisiana. Isaac produced storm surge as high as 3.4 m across Louisiana coasts and wind gusts reached 137 km/h on Grand Isle. Hundreds of thousands of people suffered from power loss and close to 60000 homes were damage in southeastern Louisiana.

Freeport, TX

Freeport is a city in southern Brazoria County where the Brazos River joins the gulf. Freeport is located approximately 60 miles south of Houston, TX, and is accessible via State Highway 36 (to Brazoria) and State Highway 288 (to Angleton). Port Freeport is ranked 19th nationwide and 26th internationally in total tonnage, and is top 10 fastest growing US ports for exports. According to 2018 census, Freeport's population was 12,195.

In this study, the finest grid (1/3 arcsec) covers the whole Freeport City limits, as well as Quintana Beach, Surfside Beach, and the western portion of Galveston barrier island.

Hurricane Ike was a Category 4 hurricane before it made landfall first over eastern Cuba on September 8, 2008. The hurricane weakened but then picked up intensity to become Category 2 before making its second landfall on Galveston, TX. Though at Category 2 near Texas, Hurricane Ike created in storm surge (about 5 m) in Galveston comparable to Category 5 hurricanes. As a result, Ike caused upwards of $37 billion damage and 160 deaths (directly and indirectly) across Texas, Cuba and Bahamas, etc. The Brazoria County sustained hours of 75 to 110 mph winds while the hurricane traveled over Galveston Bay. Manufacturers suffered the most loss in Brazoria Country (more than $500 million). The Blue Water Highway connecting San Luis Pass was also severely damaged making it impassible.

Summary

Although the probability of a large-scale tsunami event in the GOM is low, this and previous studies have indicated that tsunami events with characteristics similar to those detailed in Horrillo et al. [2015] have the potential to cause severe flooding and damage to GOM coastal communities that is similar to or even greater than that seen from major hurricanes, particularly in open beach and barrier island regions. Tsunami hazard maritime products such as tsunami current magnitude, vorticity, safe/hazard zones would be central for future developments of maritime hazard maps, maritime emergency response as well as infrastructure planning. The results of this work are intended to provide guidance to local emergency managers to help with managing urban growth, evacuation planning, and public education with the vision to mitigate potential GOM tsunami hazards.

This report is organized as follows. Section 3 briefly describes all 9 landslide sources used for tsunami modeling (3.1) and the numerical models used for simulations (3.2). Section 4 covers the inundation and momentum flux maps for Grand Isle, LA and Freeport, TX. The comparison between tsunami inundation and hurricane storm surge inundation is given in Section 5 for the two new Gulf Coast communities. Current velocity and vorticity maps are described in Section 6 for the two new communities. Section 7 presents numerical results for a Florida gulf coast meteotsunami event and several possible scenarios for characterization of physical parameters both, globally and locally in specific regions susceptible to meteotsunami in the GOM. Concluding remarks on general trends seen among the communities and practical applications for other regions are given in Section 8.

3 Tsunami Inundation Modeling

3.1 Landslide Tsunami Sources

Nine large-scale landslide configurations were created assuming an unstable (gravity-driven) sediment deposit condition. Five of these landslide configurations are historical events identified by ten Brink et al. [2009b]: the Eastbreaks, Mississippi Canyon, and West Florida submarine landslides; and Chaytor et al. [2016]: the Yucatán #3 and Yucatán #5 landslides, which are shown as red hatched regions in Fig. 1. The Yucatán Shelf/Campeche Escarpment was the last remaining area of the GOM that had not been evaluated for landslide tsunami hazards, until high-resolution mapping data collected in 2013 [Paull et al., 2014] shows that the Yucatan Shelf/Campeche Escarpment margin has been subjected to intense modifications by Cenozoic mass wasting processes. Although no known tsunami events have been linked to these Yucatan sources, numerical modeling result shows that they are capable of generating tsunamis that could propagate throughout the GOM Basin [Chaytor et al., 2016]. The other four were obtained using a probabilistic methodology based on work by Maretzki et al. [2007] and Grilli et al. [2009] and extended for the GOM by Pampell-Manis et al. [2016]. The probabilistic landslide configurations were determined based on distributions of previous GOM submarine landslide dimensions through a Monte Carlo Simulation (MCS) approach. The MCS methodology incorporates a statistical correlation method for capturing trends seen in observational data for landslide size parameters while still allowing for randomness in the generated landslide dimensions. Slope stability analyses are performed for the MCS-generated trial landslide configurations using landslide and sediment properties and regional seismic loading (Peak Horizontal ground Acceleration, PHA) to determine landslide configurations which fail and produce a tsunami. The probability of each tsunamigenic failure is calculated based on the joint probability of the earthquake PHA and the probability that the trial landslide fails and produces a tsunami wave above a certain threshold. Those failures which produce the largest tsunami amplitude and have the highest probability of occurrence are deemed the most extreme probabilistic events, and the dimensions of these events are averaged to determine maximum credible probabilistic sources. The four maximum credible Probabilistic Submarine Landslides (PSLs) used as tsunami sources for this study are termed PSL-A, PSL-B1, PSL-B2, and PSL-C and are shown as blue hatched regions in Fig. 1. For a more complete discussion of GOM submarine landslide sources, the reader can consult Horrillo et al. [2015, 2018], Pampell-Manis et al. [2016].

Table 1: Submarine Landslide general information.

Submarine Landslide	Location (Lon, Lat)	Age/Recurrence (Years)	Area (km^2)	Volume (km^3)	Excavation Depth (m)	Modeled Volume (km^3)
East Breaks	-95.68, 27.70	$\sim 10000 - 25000$	~ 519.52	~ 21.95	~ 160	26.7
Mississippi	-90.00, 28.60	$\sim 7500 - 11000$	~ 3687.26	~ 425.54	~ 300	425
West Florida	-84.75, 25.95	> 10000	~ 647.57	~ 16.2	~ 150	18.4
Yucatan #3	-90.07, 23.00	–	~ 578	~ 38	~ 278	39.3
Yucatan #5	-89.80, 23.54	–	~ 1094	~ 70.2	~ 385	69.5
PSL-A	-94.30, 27.98	$\sim 7700 - 7800$	~ 1686	~ 57	~ 67	58
PSL-B1	-91.56, 28.05	$\sim 5400 - 5500$	~ 3118	~ 69	~ 44	57.3
PSL-B2	-91.01, 26.17	$\sim 4700 - 4800$	~ 282	~ 45	~ 323	68
PSL-C	-87.20, 28.62	$\sim 550 - 650$	~ 1529	~ 315	~ 404	357

3.2 Numerical Models

For the nine landslide tsunami sources considered here, tsunami wave development and subsequent propagation and inundation of coastal communities was modeled using coupled 3D and 2D numerical models [Horrillo et al., 2015]. The tsunami generation phase was modeled using the 3D model TSUNAMI3D [Horrillo, 2006, Horrillo et al., 2013], which solves the finite difference approximation of the full Navier-Stokes equations and the incompressibility (continuity) equation. Water and landslide material are represented as Newtonian fluids with different densities, and the landslide-water and water-air interfaces are tracked using the Volume of Fluid (VOF) method of Hirt and Nichols [1981], which is simplified to account for the large horizontal/vertical aspect ratio of the tsunami wave and the selected computational cell size required to construct an efficient 3D grid. The pressure term is split into hydrostatic and non-hydrostatic components. Although TSUNAMI3D has the capability of variable grids, the nesting capability necessary for modeling detailed inundation of coastal regions is too computationally intensive within the fully 3D model; thus, detailed inundation modeling is achieved by coupling the 3D model to a 2D model. Once the tsunami wave generated by the 3D model is fully developed, the wave is passed as an initial condition to the 2D model for modeling wave propagation and coastal inundation. The generated wave is considered fully developed when the total wave energy (potential plus kinetic) reaches a maximum and before the wave leaves the computational domain, as discussed in López-Venegas et al. [2015]. The 2D model used here is NEOWAVE [Yamazaki et al., 2008], a depth-integrated and non-hydrostatic model built on the nonlinear shallow water equations which includes a momentum-conserved advection scheme to model wave breaking and two-way nested grids for modeling higher-resolution wave runup and inundation. Propagation and inundation are calculated via a series of nested grids of increasing resolution, from 15 arcsecond (450 m) resolution for a domain encompassing the entire northern GOM (Fig. 1), to finer resolutions of 3 arcseconds (90 m, from NOAA NCEI Coastal Relief Models), 1 arcsecond (30 m), and 1/3 arcsecond (10 m, from NOAA NCEI Tsunami Inundation Digital Elevation Models [DEMs]) to model detailed inundation of the most populated/ inundation-prone areas of each coastal community. The 3 arcsecond (90 m) subdomains encompassing each coastal community studied here are shown by red rectangles in Fig. 1.

4 Tsunami Maps

Tsunami inundation depth and extent has been modeled for two selected coastal communities: Grand Isle, LA and Freeport, TX. Inundation (flooding) is determined by subtracting land elevation from water elevation, and elevations used are in reference to the Mean High Water (MHW) tidal datum. For this study, the tsunami inundation depth/extent modeled for each community is the maximum-of-maximums (MOM) inundation, which is calculated as the maximum inundation depth from an ensemble of inundation depths produced by each of the nine tsunami sources considered. That is, once inundation in a community has been modeled for each of the nine sources, the overall maximum inundation depth in each computational grid cell is taken as the MOM tsunami inundation in that cell. This approach gives a worst-case scenario perspective of estimated tsunami inundation for each coastal community.

In this section, the numerical results (inundation and momentum flux maps) for each landslide source are presented for Grand Isle, LA and Freeport, TX. The maximum of maximum inundation map from all sources and the maximum inundation map by source are also shown. A summary table of each location's numerical gauge (at an approximate water depth of 20 m) is presented, showing maximum wave amplitude and arrival time after landslide failure.

It is worth noting, however, that for both communities, the MOM tsunami inundation is produced solely by the Mississippi Canyon submarine landslide failure. That historical failure is the largest in both area and volume of material removed, and therefore produces the highest amplitude wave of all sources simulated. The two sources, Yucatán #3 and Yucatán #5, made little impact to the selected communities.

4.1 Grand Isle, LA

Table 2: Maximum tsunami wave amplitude and corresponding arrival time after landslide failure at Grand Isle, LA numerical wave gauge: 26°56'19.22"N, 82°39'34.28"W (Fig. 1), approximate water depth 20 m.

Tsunami Source	Maximum Wave Amplitude (m)	Arrival Time After Landslide Failure (hr)
East Breaks	0.85	2.2
PSL-A	0.73	1.8
PSL-B1	0.61	0.9
PSL-B2	0.48	1.3
Mississippi Canyon	6.44	0.1
PSL-C	10.87	1.0
West Florida	0.83	1.7
Yucatán #3	1.10	1.6
Yucatán #5	0.62	1.6

Grand Isle, LA
East Breaks submarine landslide
Maximum Momentum Flux

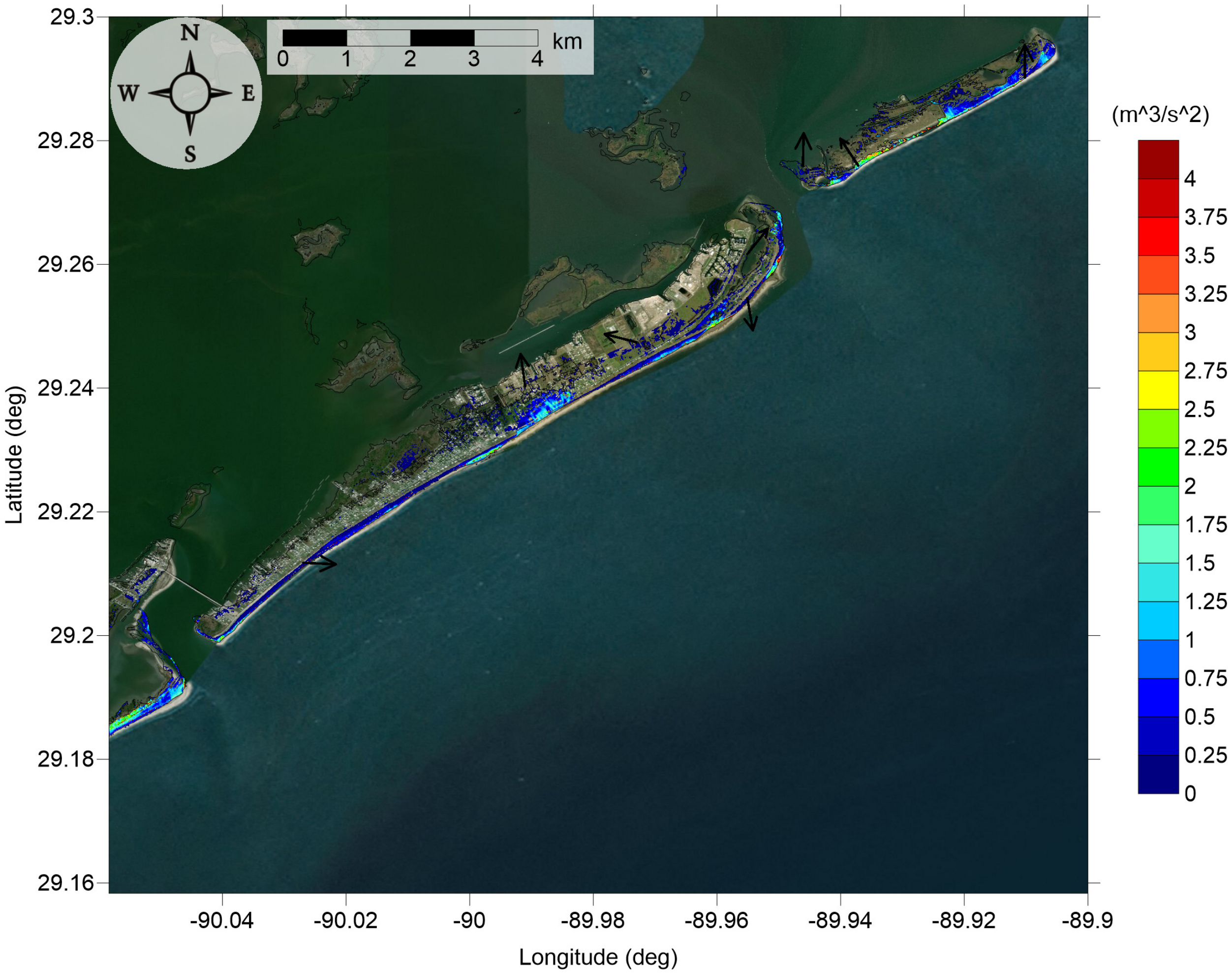

Figure 2: Maximum momentum flux (m^3/s^2) caused by the East Breaks submarine landslide in Grand Isle, LA. Arrows represent direction of maximum momentum flux. Contour drawn is the zero-meter contour for land elevation.

Grand Isle, LA
East Breaks submarine landslide
Maximum Inundation Depth

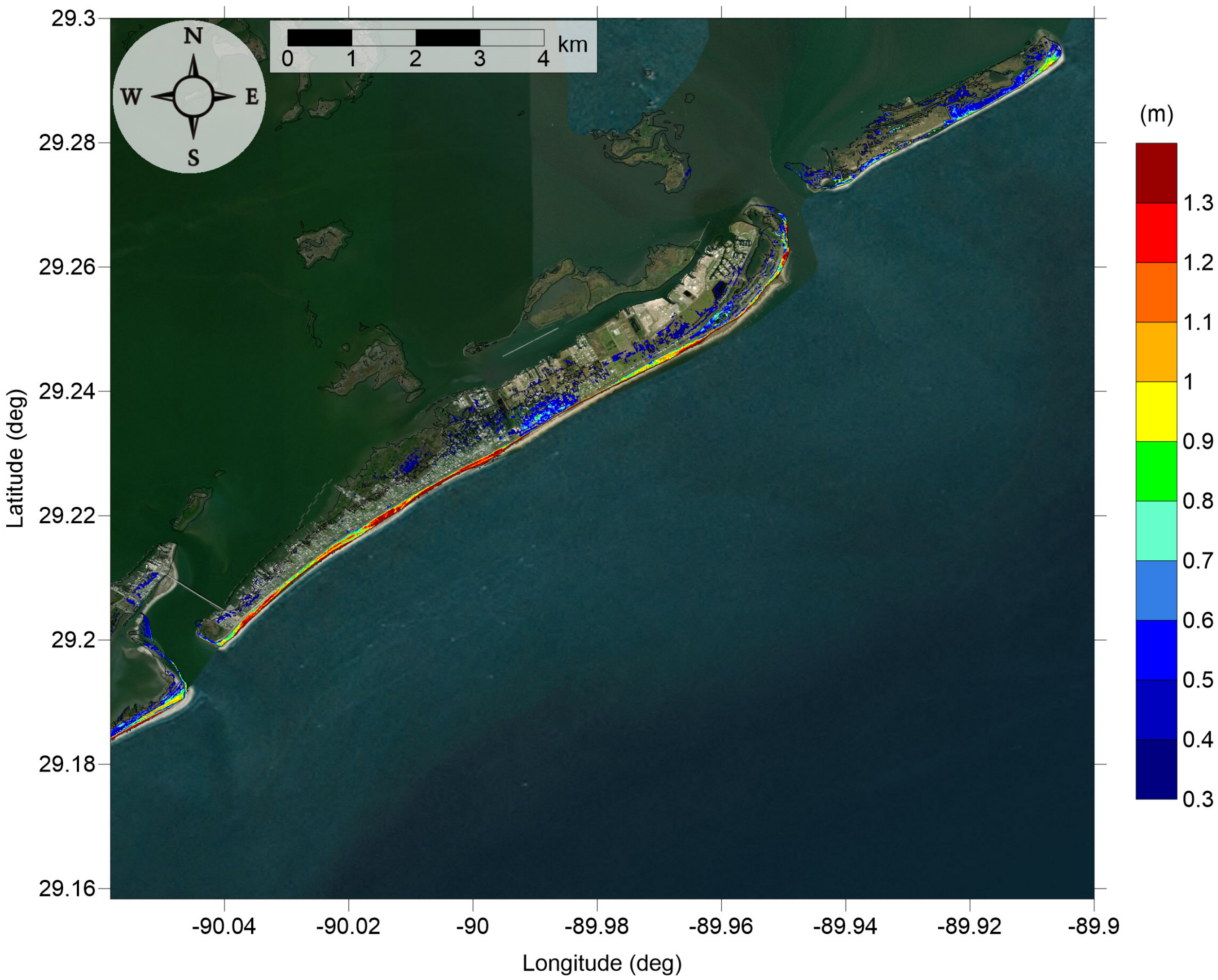

Figure 3: Maximum inundation depth (m) caused by the East Breaks submarine landslide in Grand Isle, LA. Contour drawn is the zero-meter contour for land elevation.

Grand Isle, LA
Probabilistic Submarine Landslide A
Maximum Momentum Flux

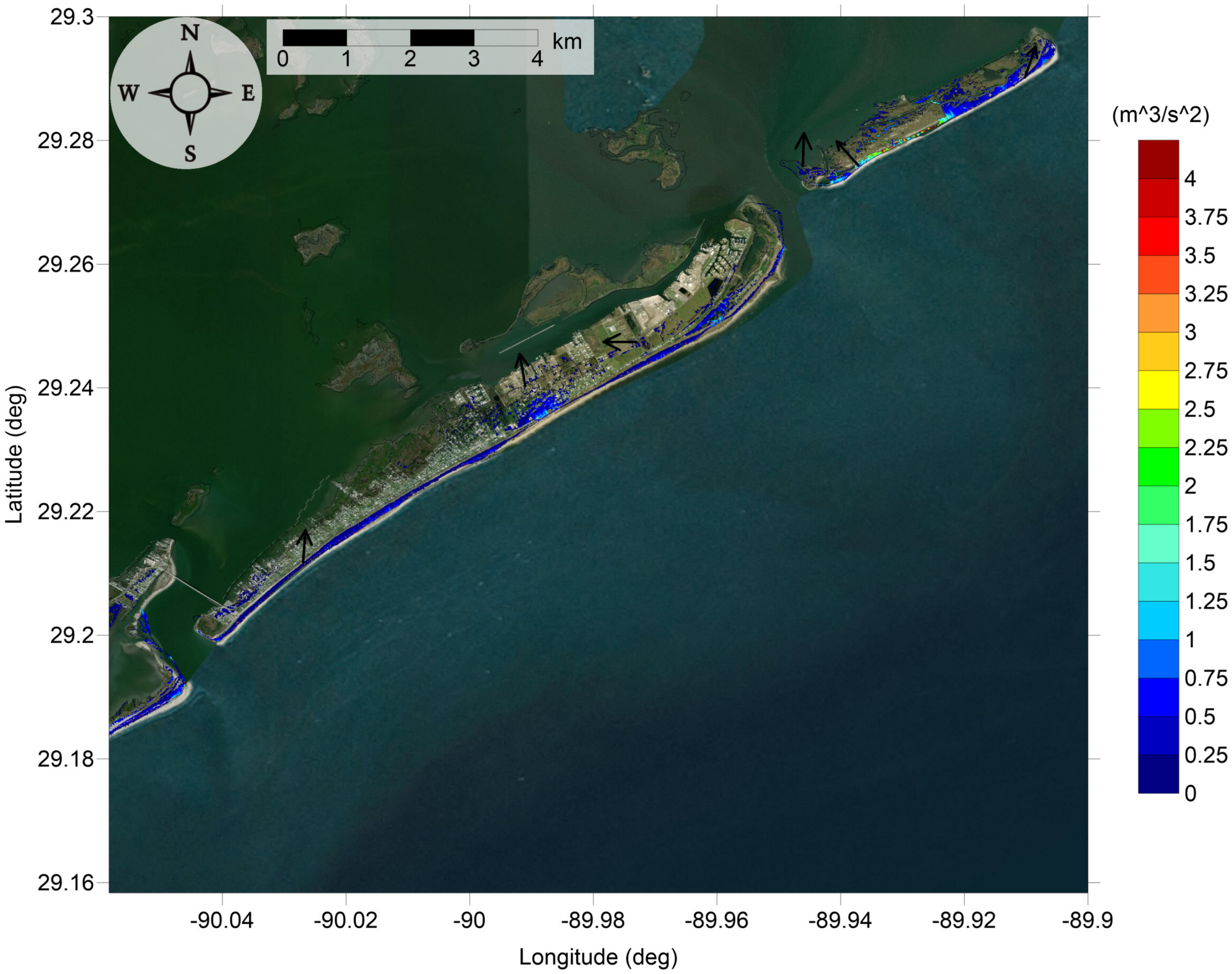

Figure 4: Maximum momentum flux (m^3/s^2) caused by the Probabilistic Submarine Landslide A in Grand Isle, LA. Arrows represent direction of maximum momentum flux. Contour drawn is the zero-meter contour for land elevation.

Grand Isle, LA
Probabilistic Submarine Landslide A
Maximum Inundation Depth

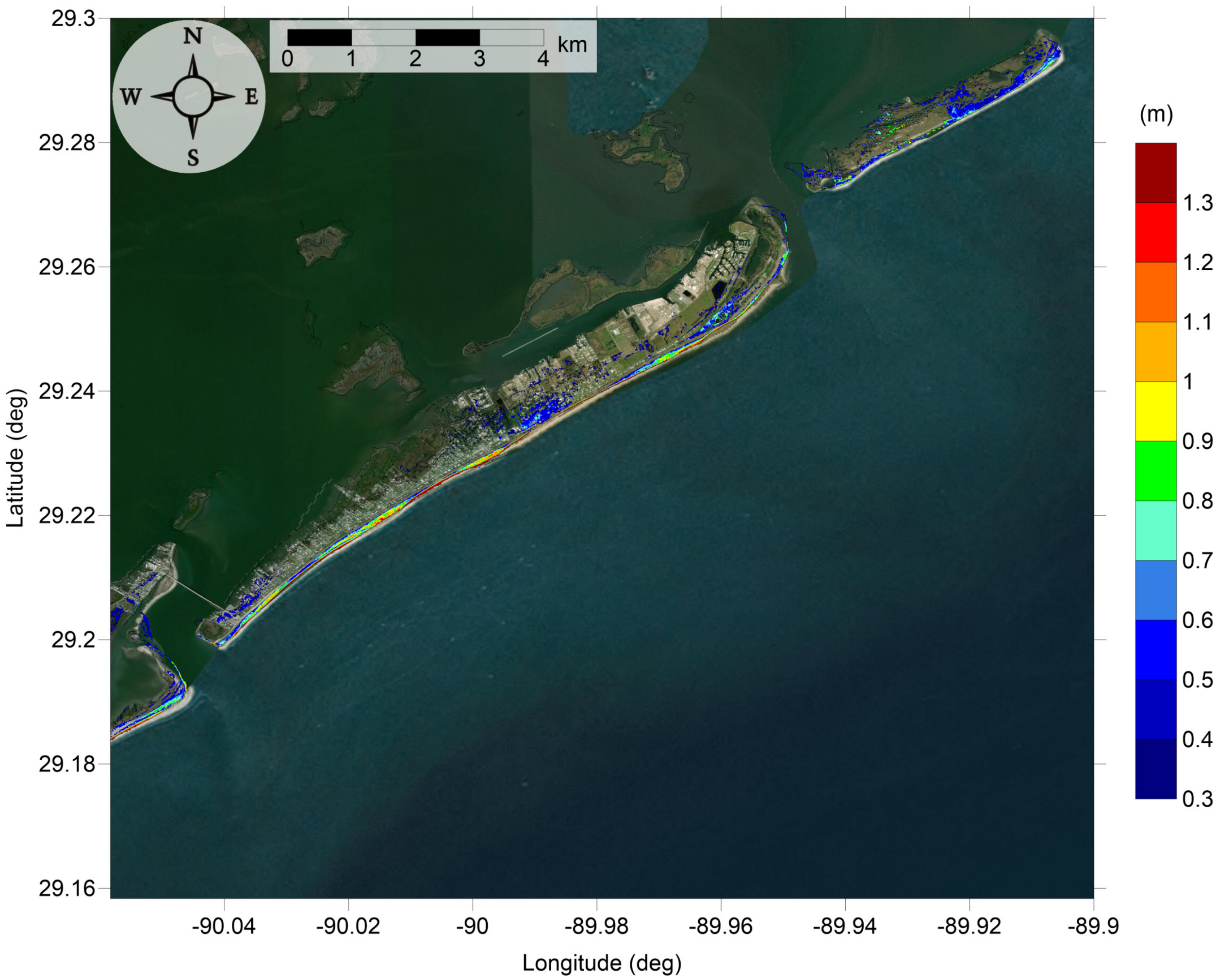

Figure 5: Maximum inundation depth (m) caused by the Probabilistic Submarine Landslide A in Grand Isle, LA. Contour drawn is the zero-meter contour for land elevation.

Grand Isle, LA
Probabilistic Submarine Landslide B1
Maximum Momentum Flux

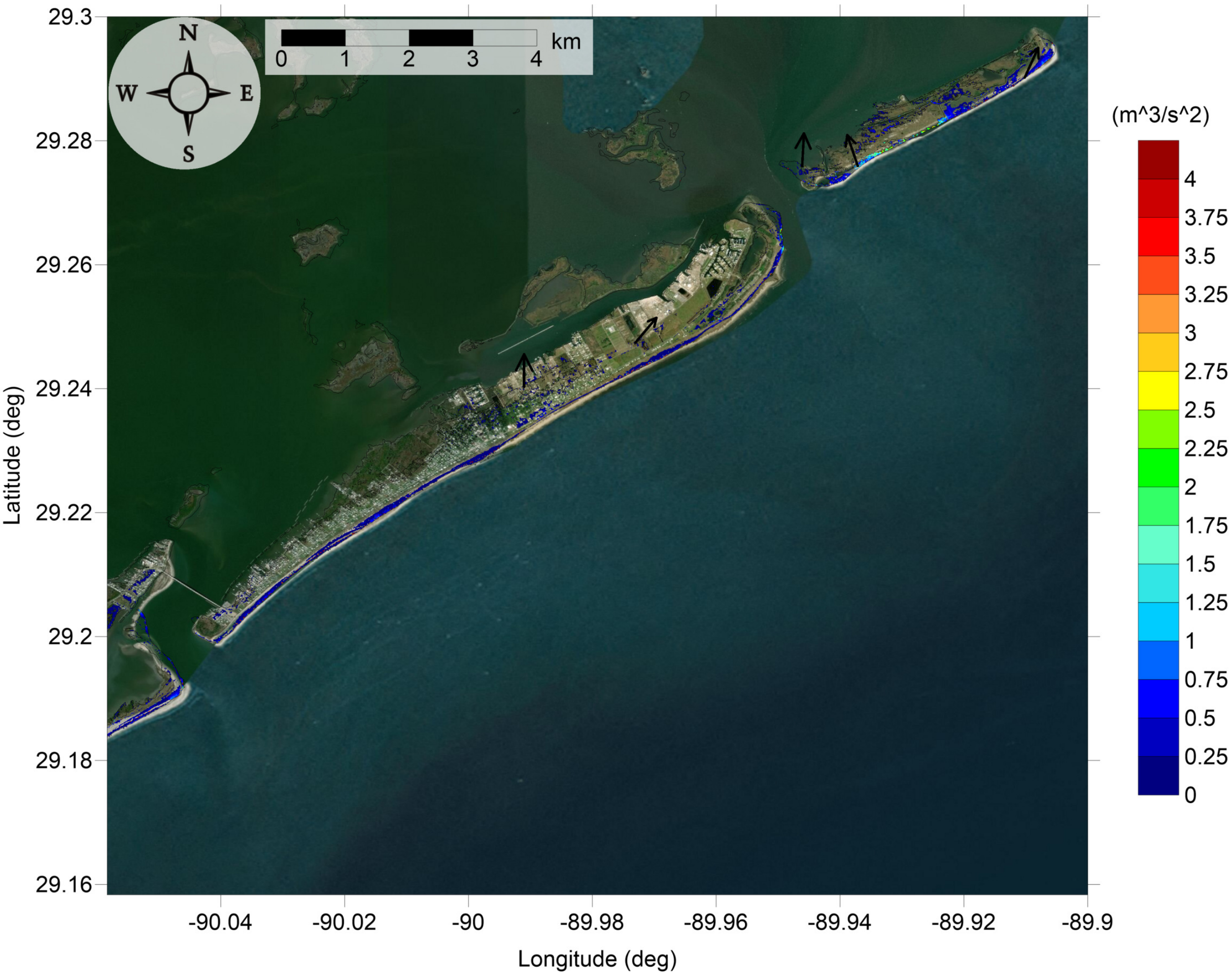

Figure 6: Maximum momentum flux (m^3/s^2) caused by the Probabilistic Submarine Landslide B1 in Grand Isle, LA. Arrows represent direction of maximum momentum flux. Contour drawn is the zero-meter contour for land elevation.

Grand Isle, LA
Probabilistic Submarine Landslide B1
Maximum Inundation Depth

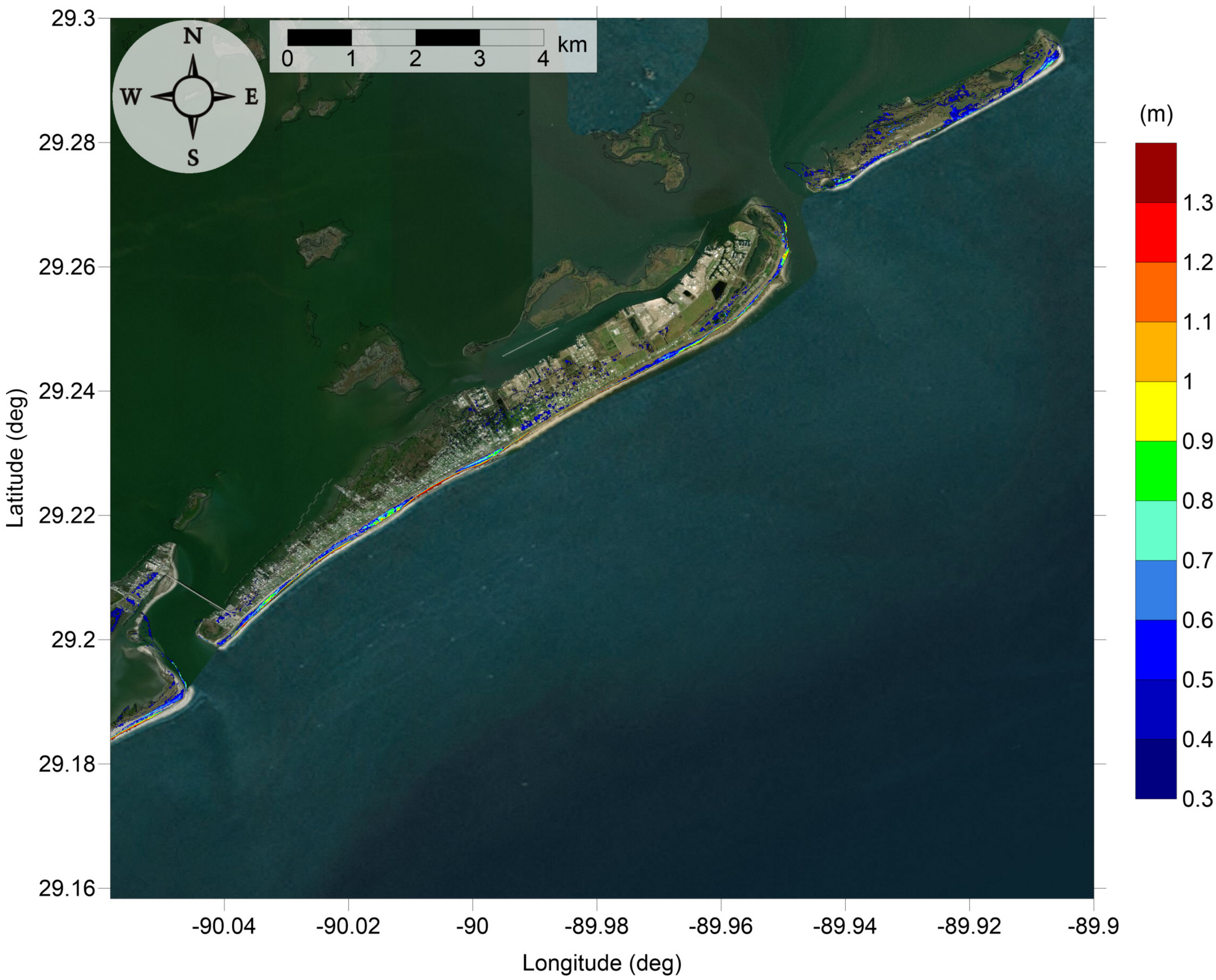

Figure 7: Maximum inundation depth (m) caused by the Probabilistic Submarine Landslide B1 in Grand Isle, LA. Contour drawn is the zero-meter contour for land elevation.

Grand Isle, LA
Probabilistic Submarine Landslide B2
Maximum Momentum Flux

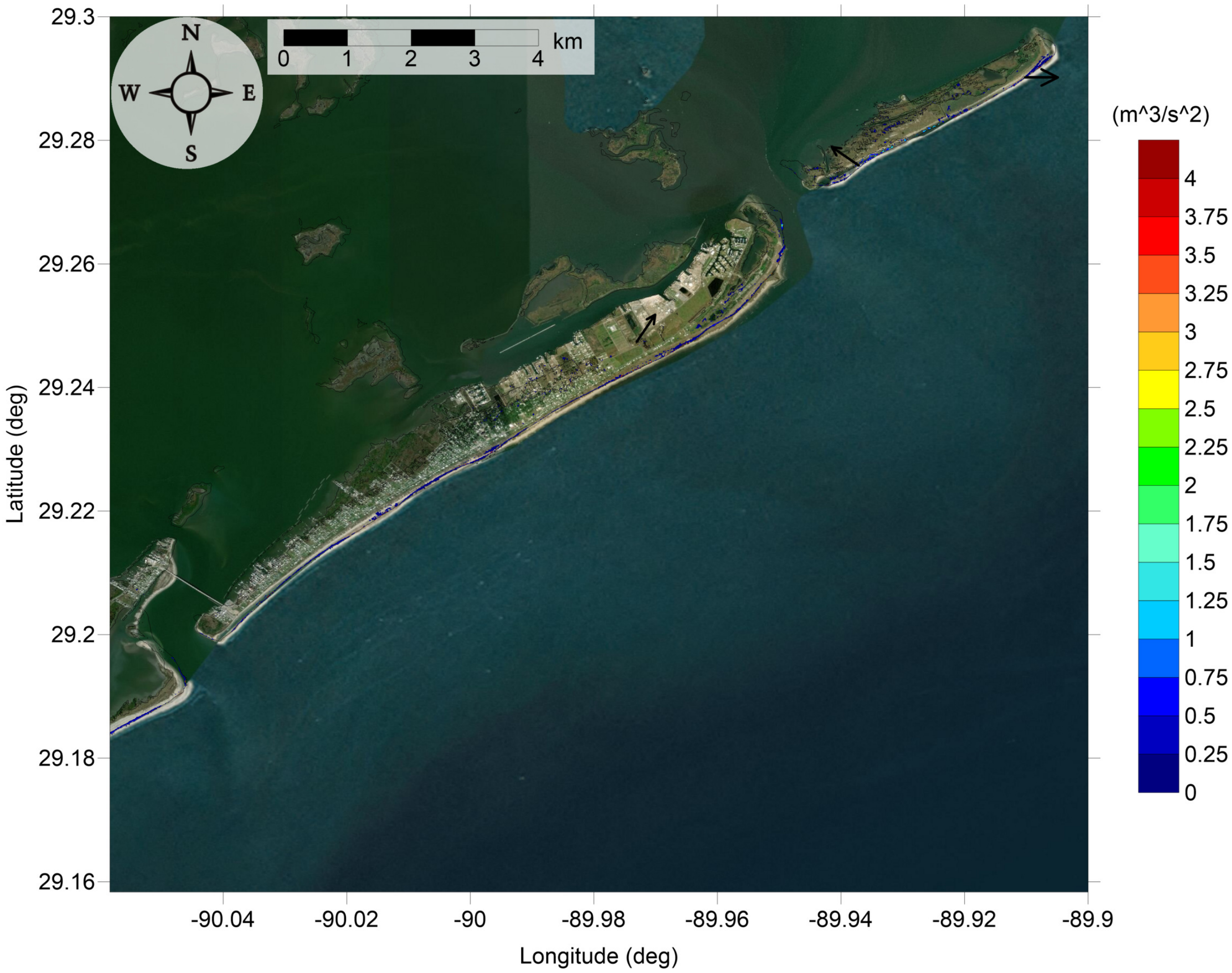

Figure 8: Maximum momentum flux (m^3/s^2) caused by the Probabilistic Submarine Landslide B2 in Grand Isle, LA. Arrows represent direction of maximum momentum flux. Contour drawn is the zero-meter contour for land elevation.

Grand Isle, LA
Probabilistic Submarine Landslide B2
Maximum Inundation Depth

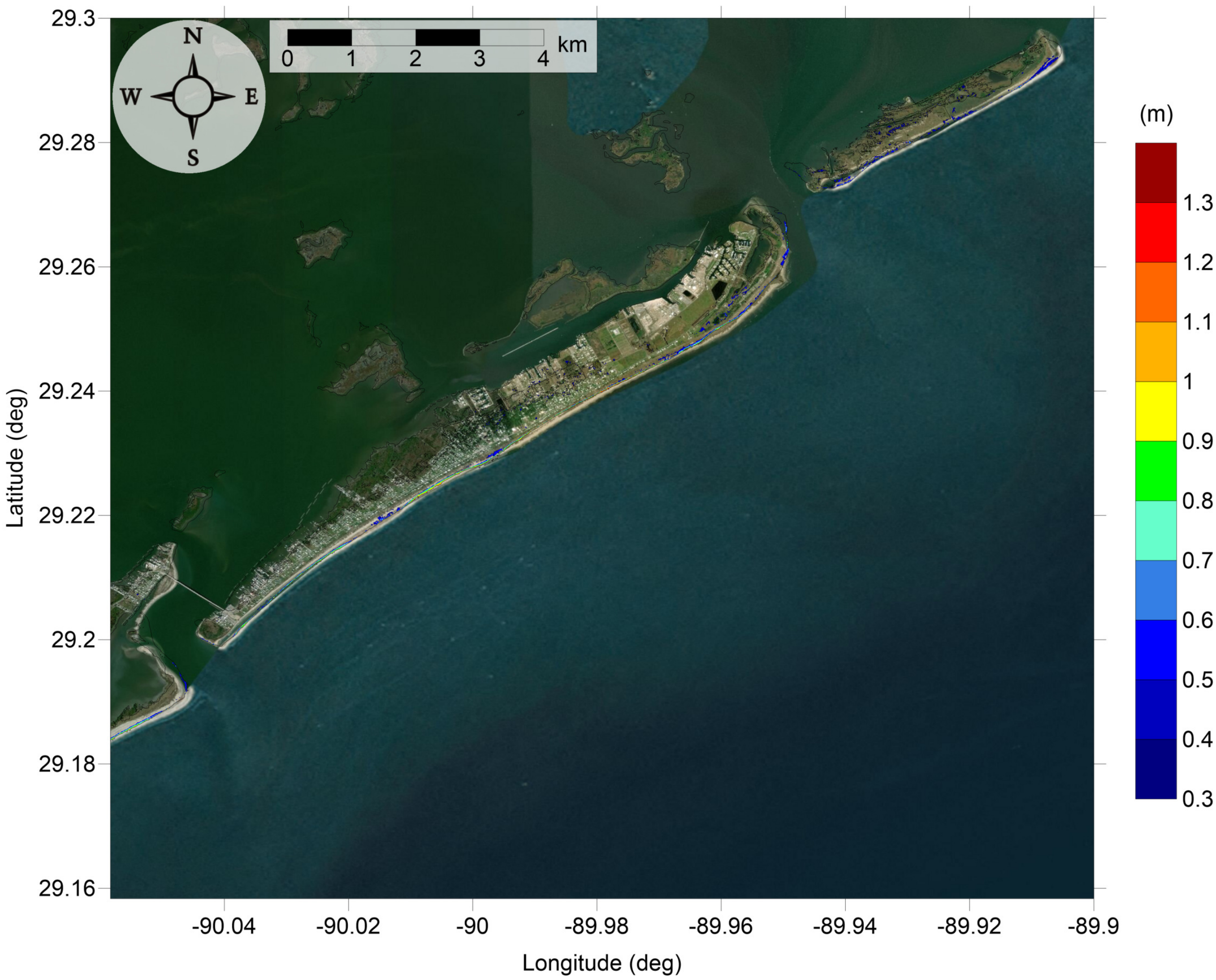

Figure 9: Maximum inundation depth (m) caused by the Probabilistic Submarine Landslide B2 in Grand Isle, LA. Contour drawn is the zero-meter contour for land elevation.

Grand Isle, LA
Mississippi Canyon submarine landslide
Maximum Momentum Flux

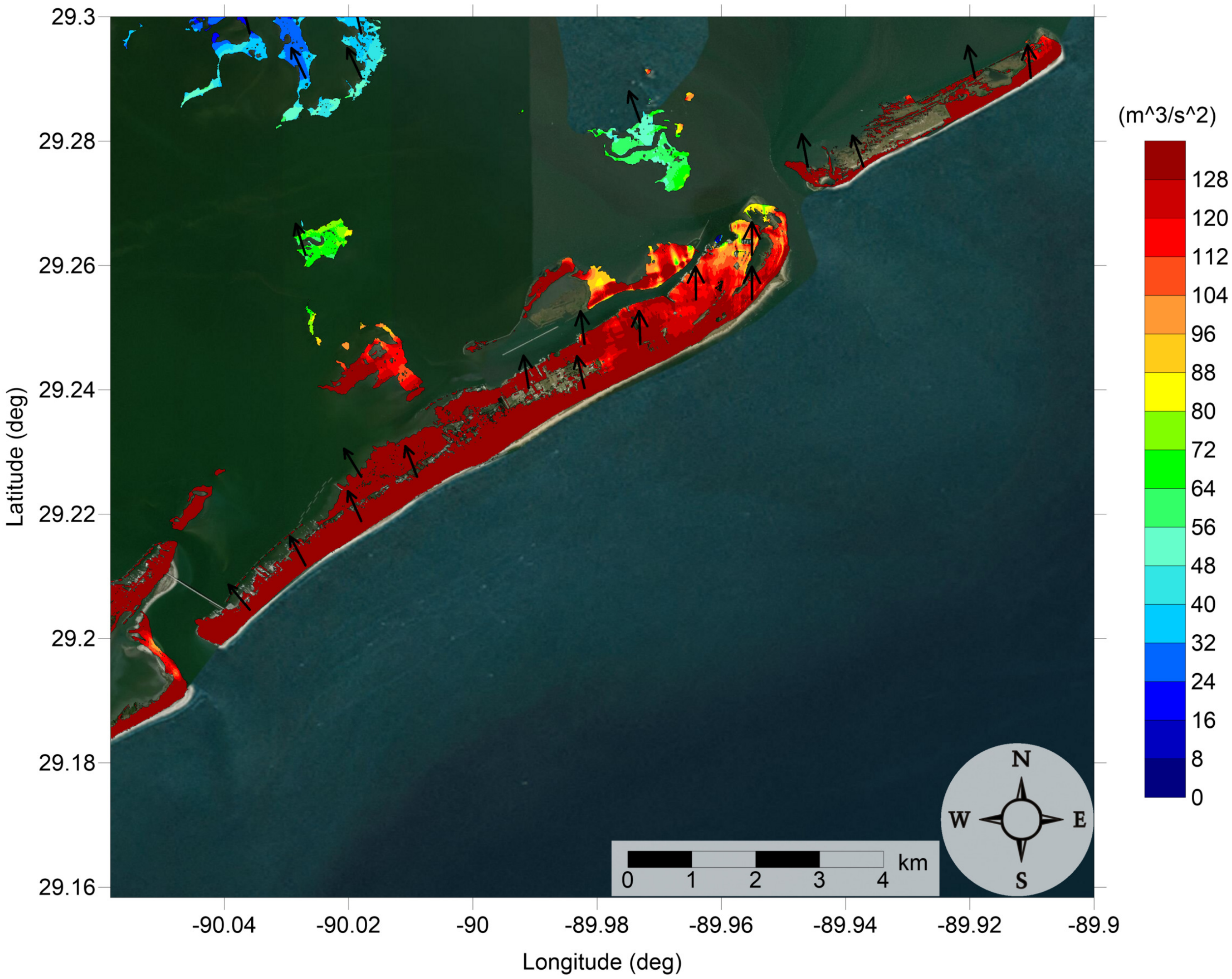

Figure 10: Maximum momentum flux (m^3/s^2) caused by the Mississippi Canyon submarine landslide in Grand Isle, LA. Arrows represent direction of maximum momentum flux. Contour drawn is the zero-meter contour for land elevation.

Grand Isle, LA
Mississippi Canyon submarine landslide
Maximum Inundation Depth

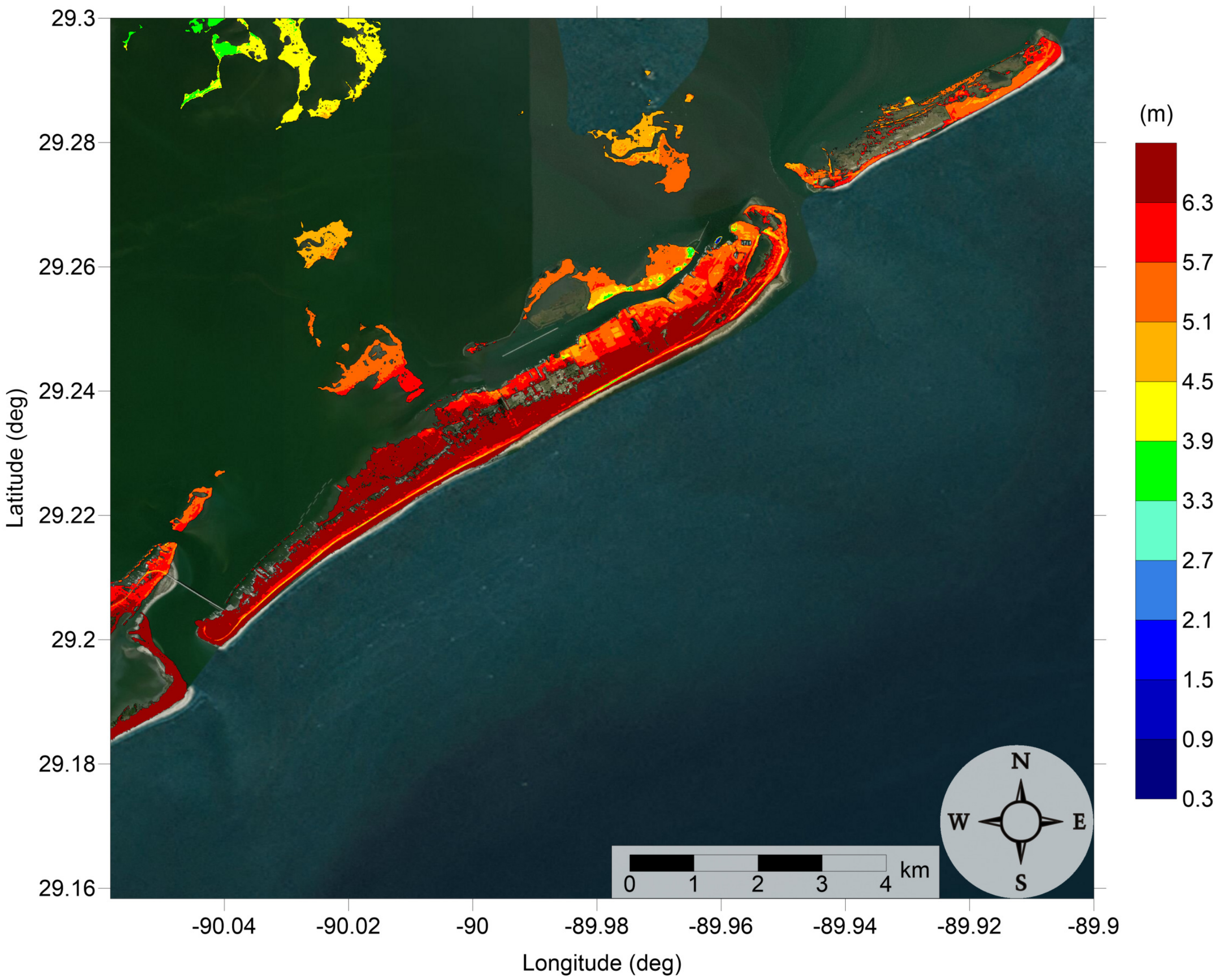

Figure 11: Maximum inundation depth (m) caused by the Mississippi Canyon submarine landslide in Grand Isle, LA. Contour drawn is the zero-meter contour for land elevation.

Grand Isle, LA
Probabilistic Submarine Landslide C
Maximum Momentum Flux

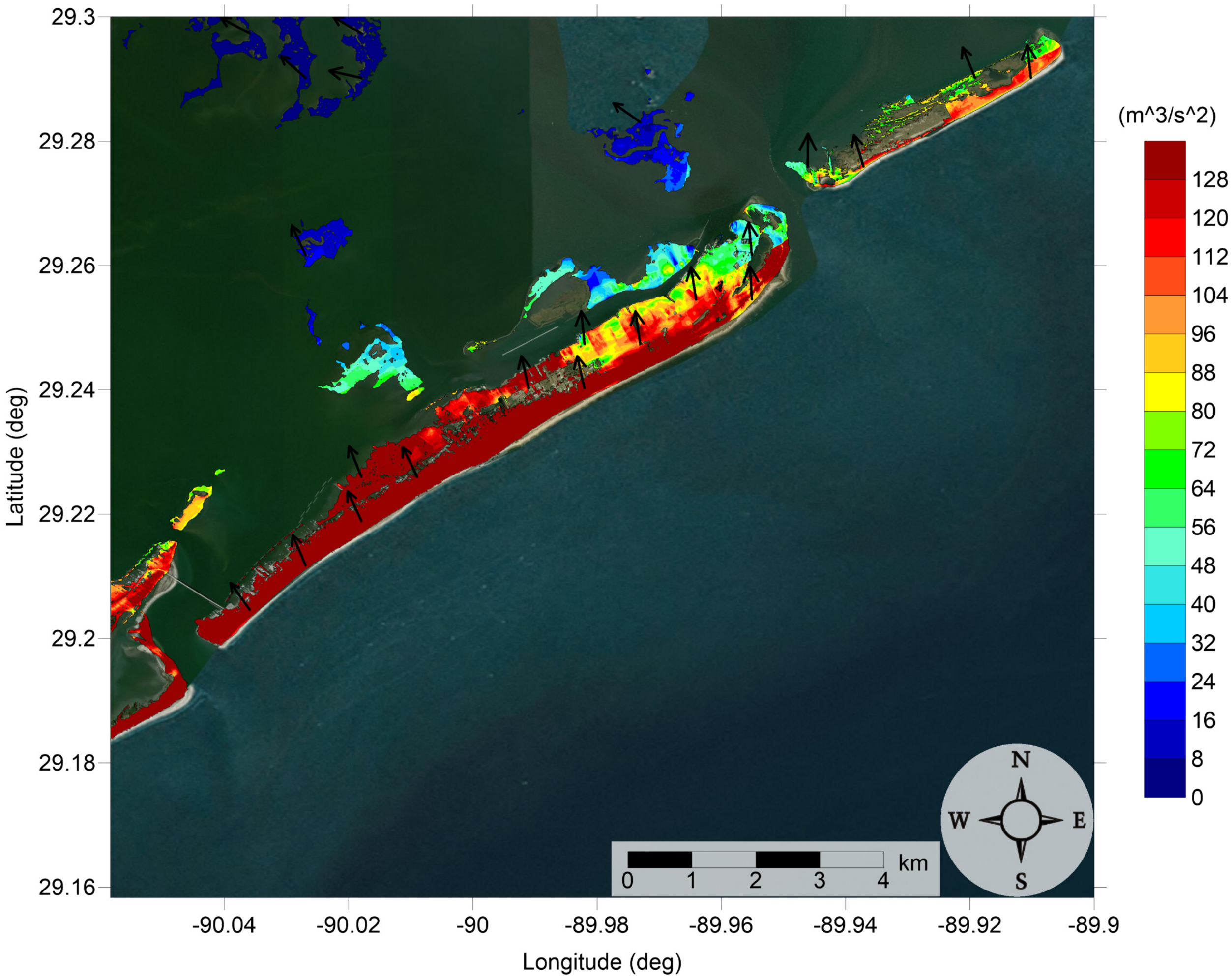

Figure 12: Maximum momentum flux (m^3/s^2) caused by the Probabilistic Submarine Landslide C in Grand Isle, LA. Arrows represent direction of maximum momentum flux. Contour drawn is the zero-meter contour for land elevation.

Grand Isle, LA
Probabilistic Submarine Landslide C
Maximum Inundation Depth

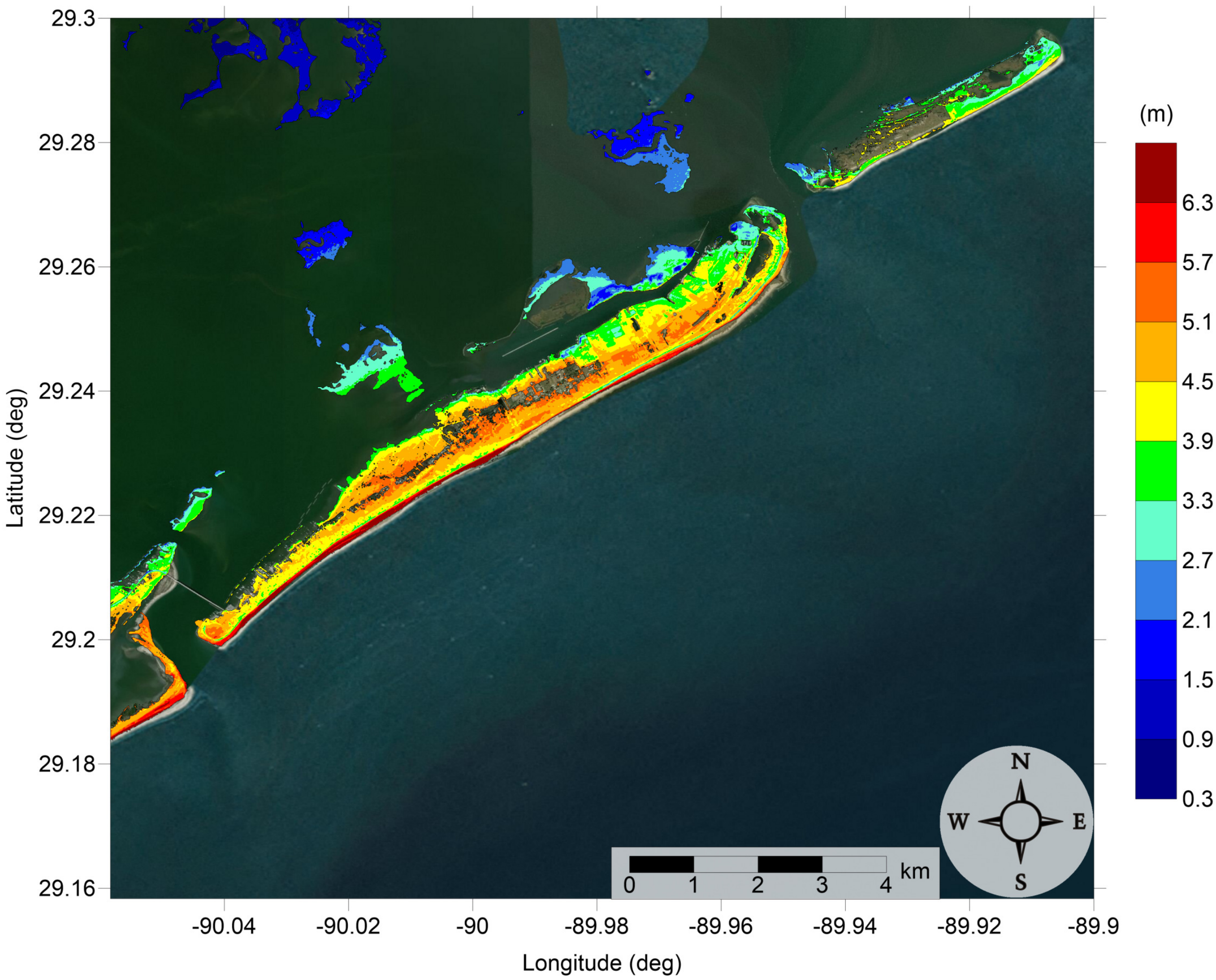

Figure 13: Maximum inundation depth (m) caused by the Probabilistic Submarine Landslide C in Grand Isle, LA. Contour drawn is the zero-meter contour for land elevation.

Grand Isle, LA
West Florida submarine landslide
Maximum Momentum Flux

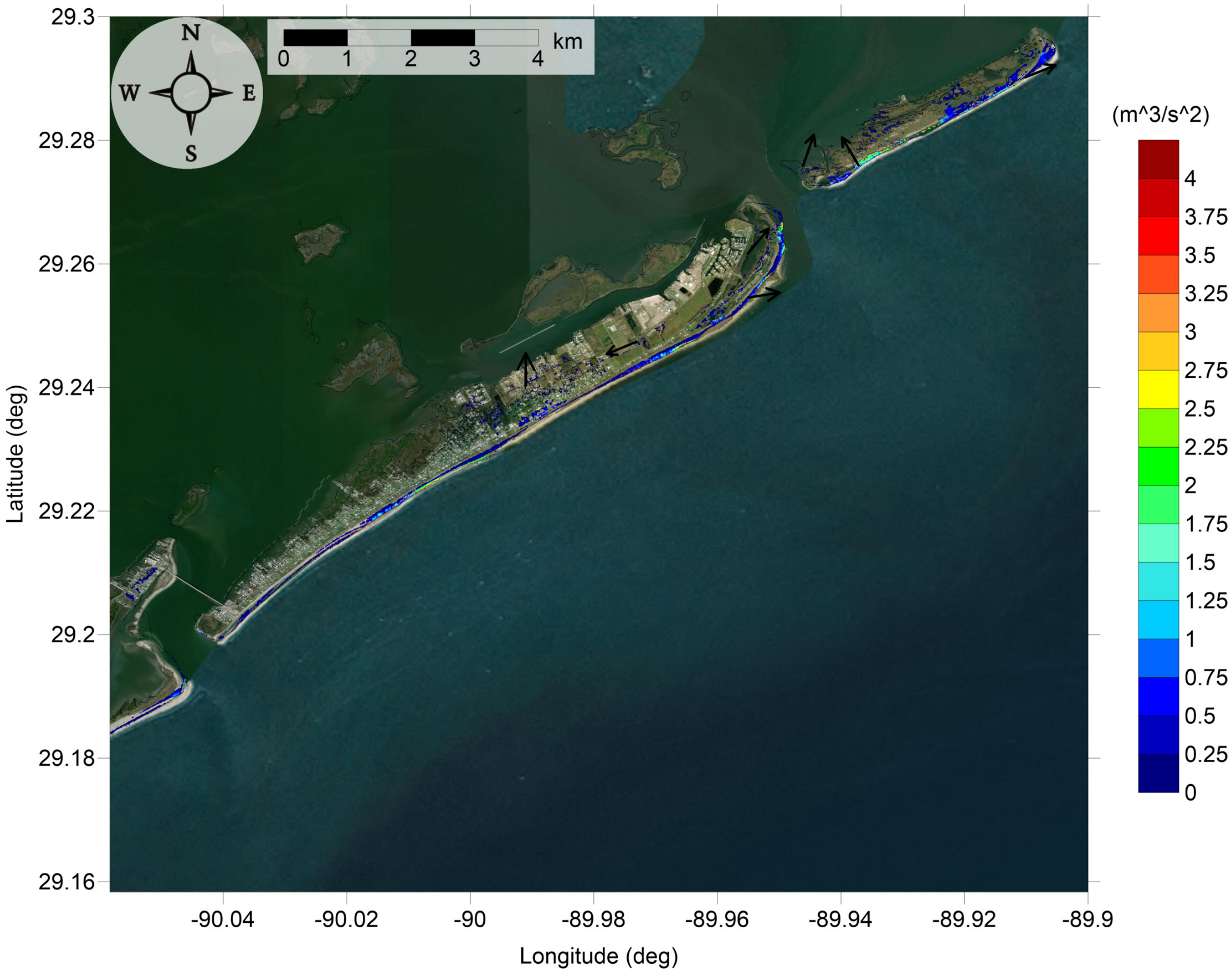

Figure 14: Maximum momentum flux (m^3/s^2) caused by the West Florida submarine landslide in Grand Isle, LA. Arrows represent direction of maximum momentum flux. Contour drawn is the zero-meter contour for land elevation.

Grand Isle, LA
West Florida submarine landslide
Maximum Inundation Depth

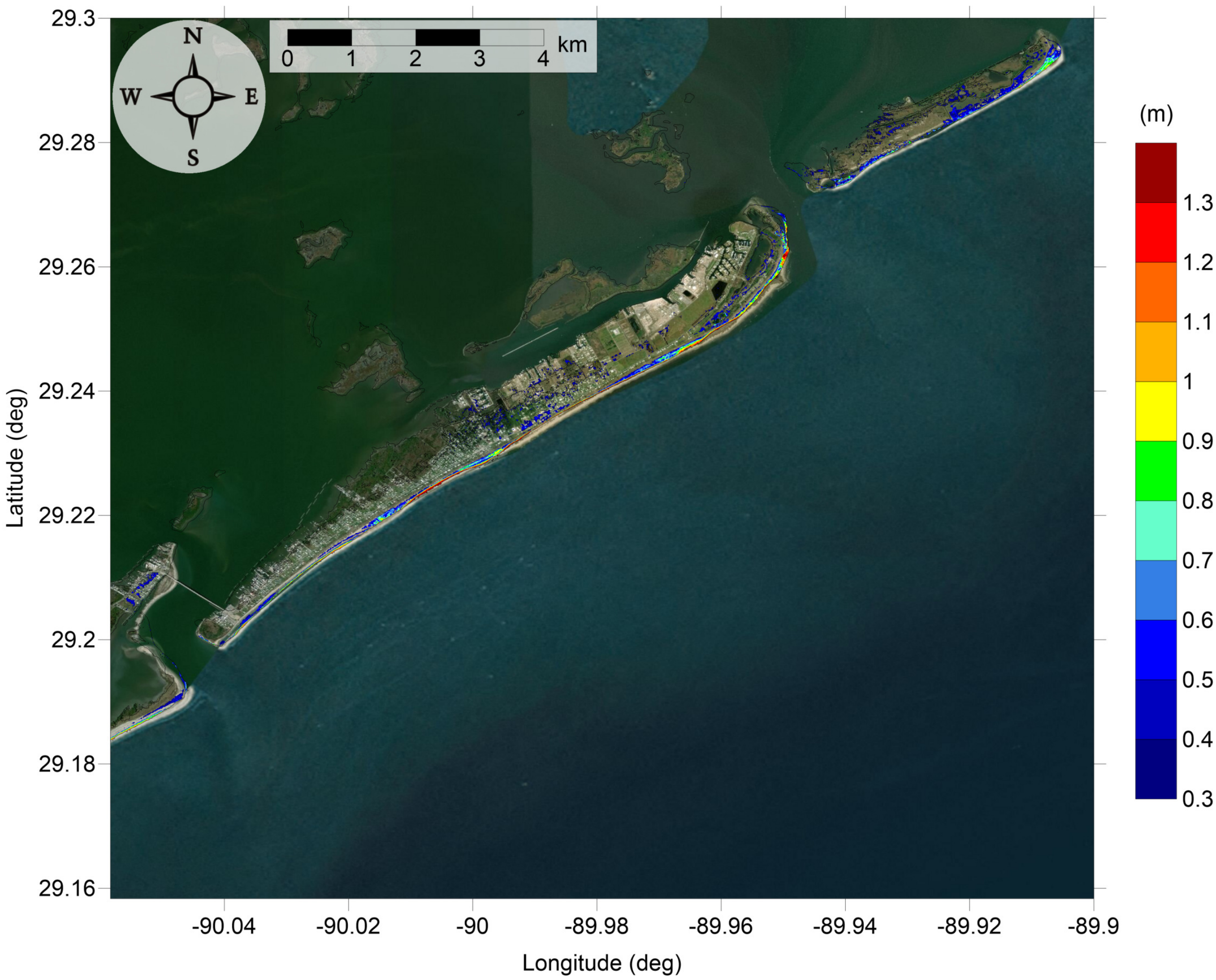

Figure 15: Maximum inundation depth (m) caused by the West Florida submarine landslide in Grand Isle, LA. Contour drawn is the zero-meter contour for land elevation.

Grand Isle, LA
Yucatán 3 submarine landslide
Maximum Momentum Flux

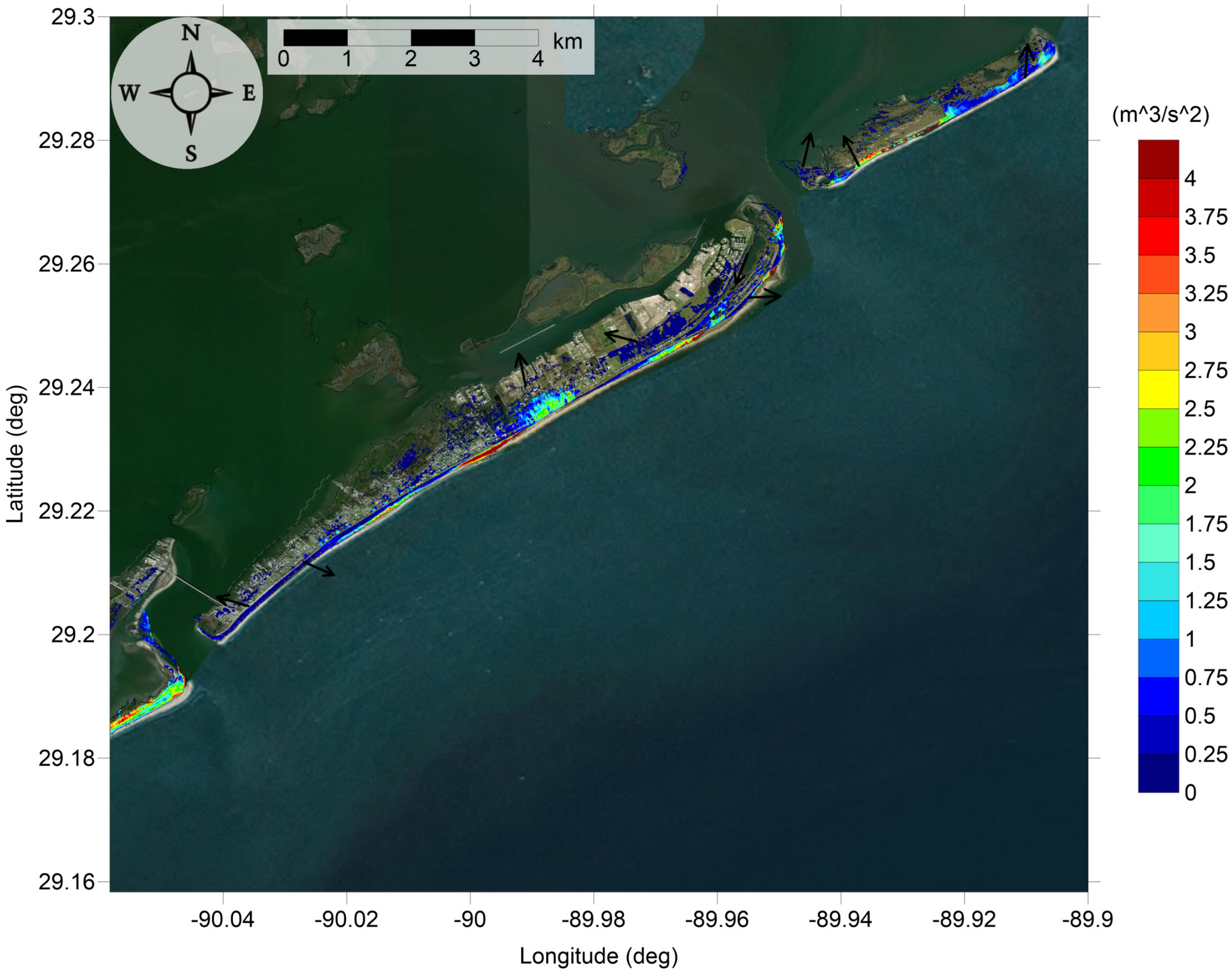

Figure 16: Maximum momentum flux (m^3/s^2) caused by the Yucatán 3 submarine landslide in Grand Isle, LA. Arrows represent direction of maximum momentum flux. Contour drawn is the zero-meter contour for land elevation.

Grand Isle, LA
Yucatán 3 submarine landslide
Maximum Inundation Depth

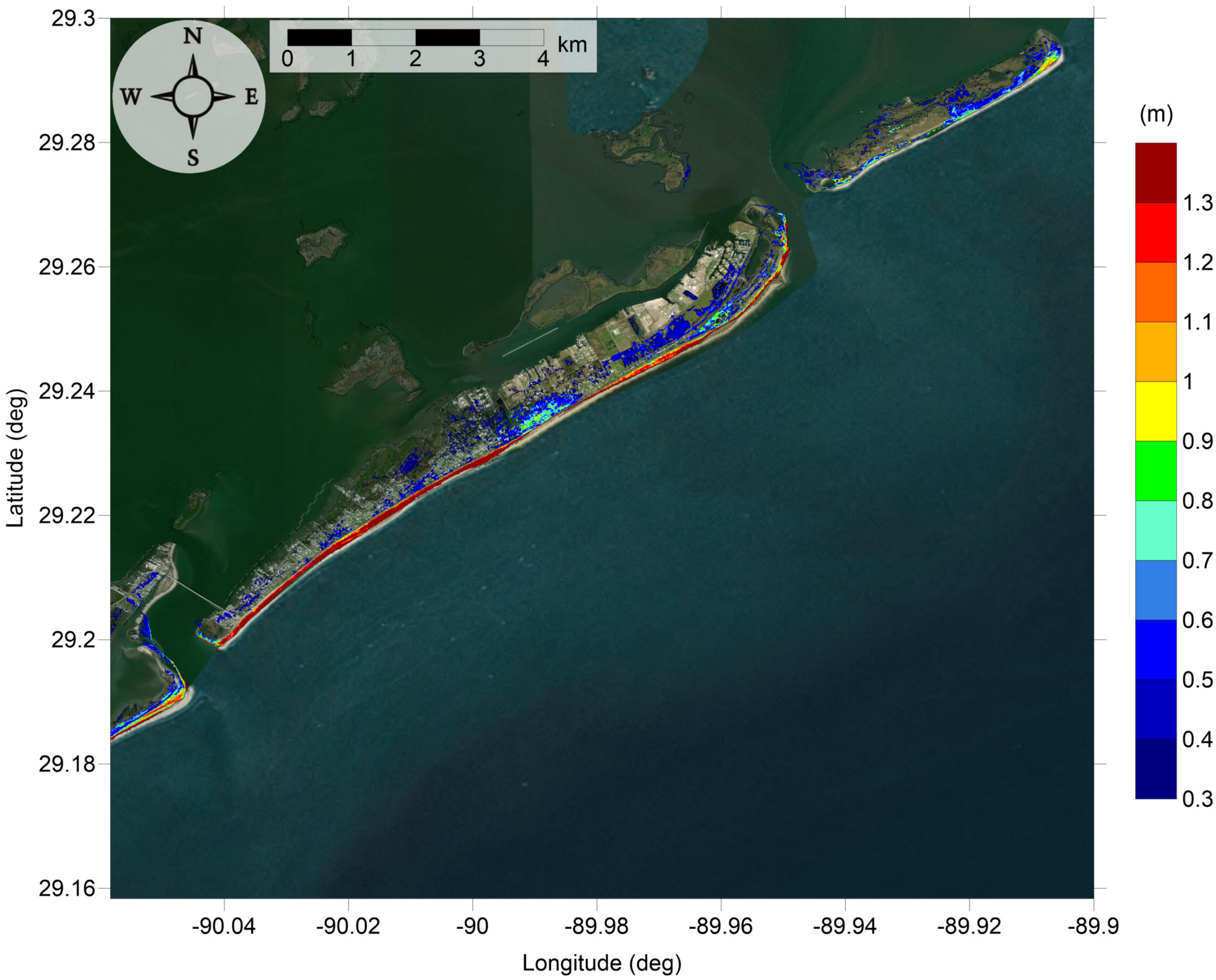

Figure 17: Maximum inundation depth (m) caused by the Yucatán 3 submarine landslide in Grand Isle, LA. Contour drawn is the zero-meter contour for land elevation.

Grand Isle, LA
Yucatán 5 submarine landslide
Maximum Momentum Flux

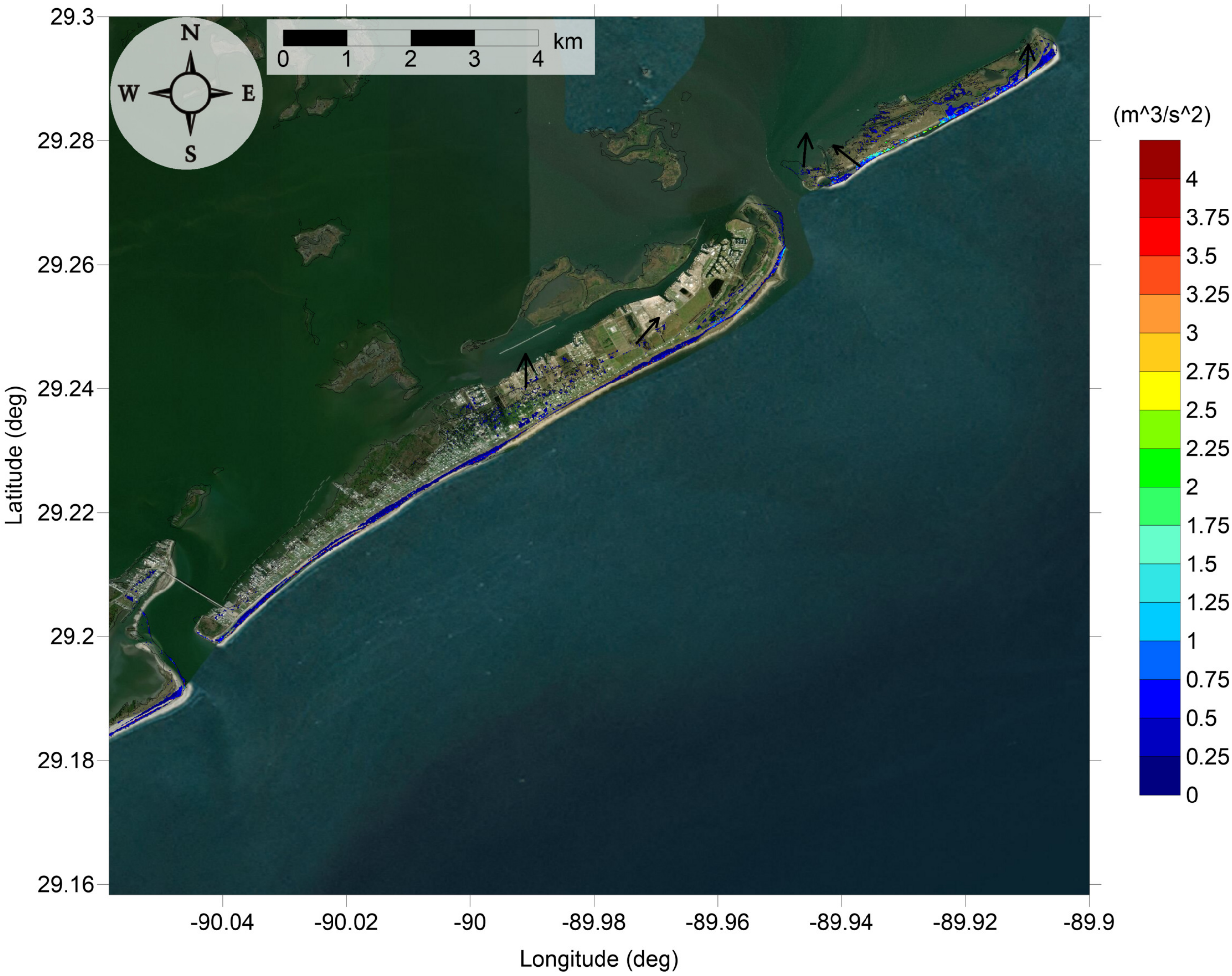

Figure 18: Maximum momentum flux (m^3/s^2) caused by the Yucatán 5 submarine landslide in Grand Isle, LA. Arrows represent direction of maximum momentum flux. Contour drawn is the zero-meter contour for land elevation.

Grand Isle, LA
Yucatán 5 submarine landslide
Maximum Inundation Depth

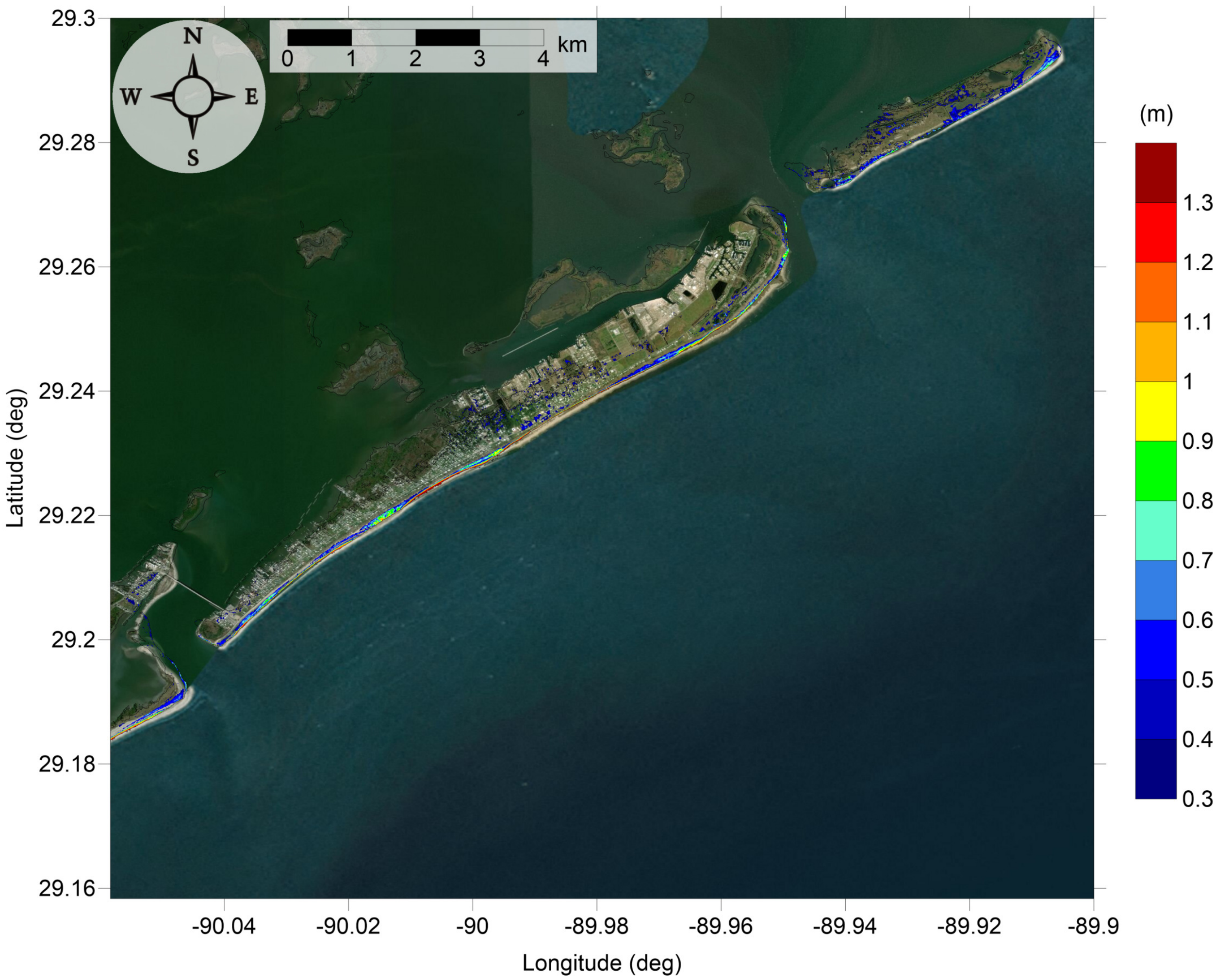

Figure 19: Maximum inundation depth (m) caused by the Yucatán 5 submarine landslide in Grand Isle, LA. Contour drawn is the zero-meter contour for land elevation.

Grand Isle, LA
All Sources
Maximum of Maximum Inundation Depth

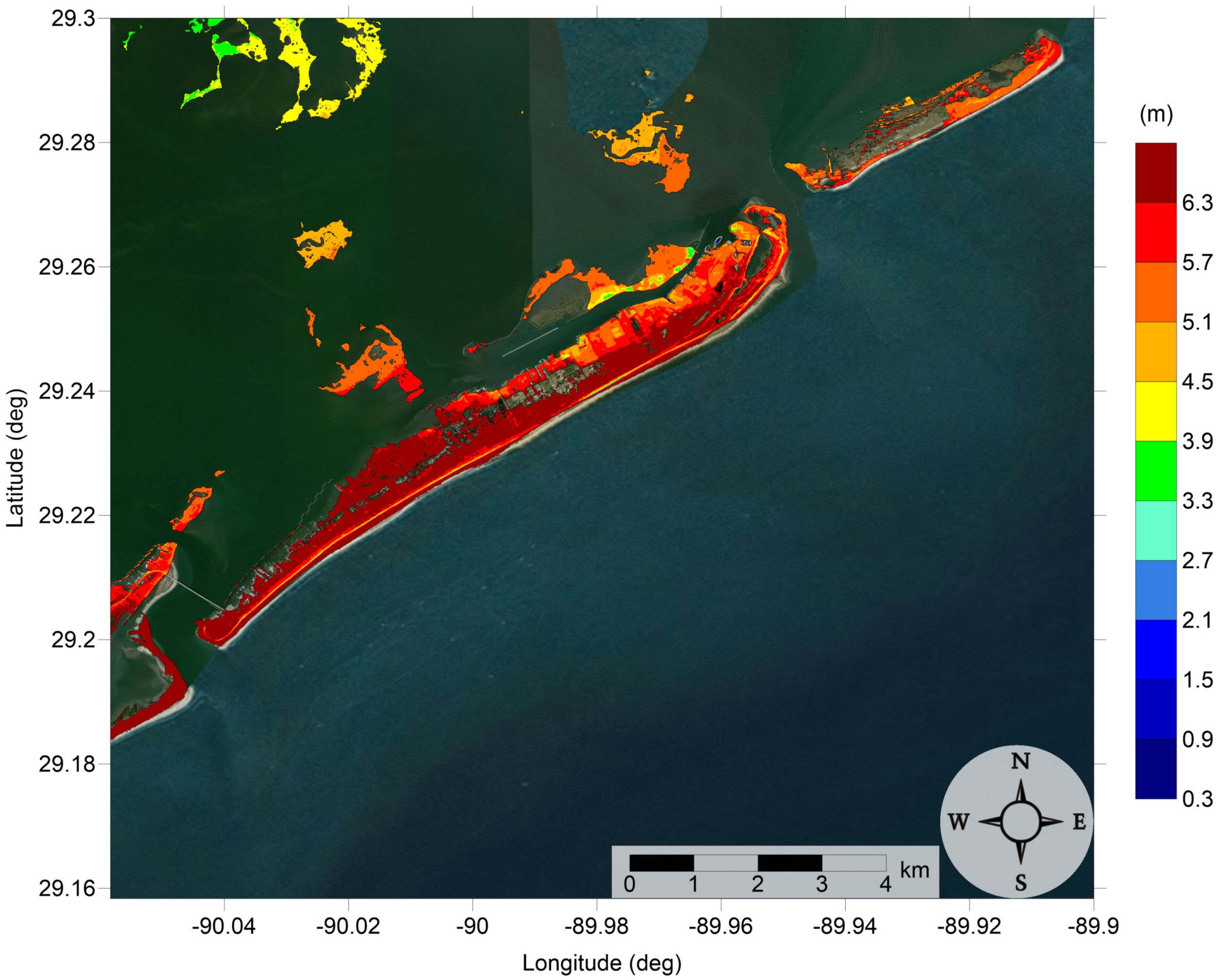

Figure 20: Maximum of maximums inundation depth (m) in Grand Isle, LA, calculated as the maximum inundation depth in each grid cell from an ensemble of all tsunami sources considered. Contour drawn is the zero-meter contour for land elevation.

Grand Isle, LA
All Sources
Maximum Inundation Depth by Source

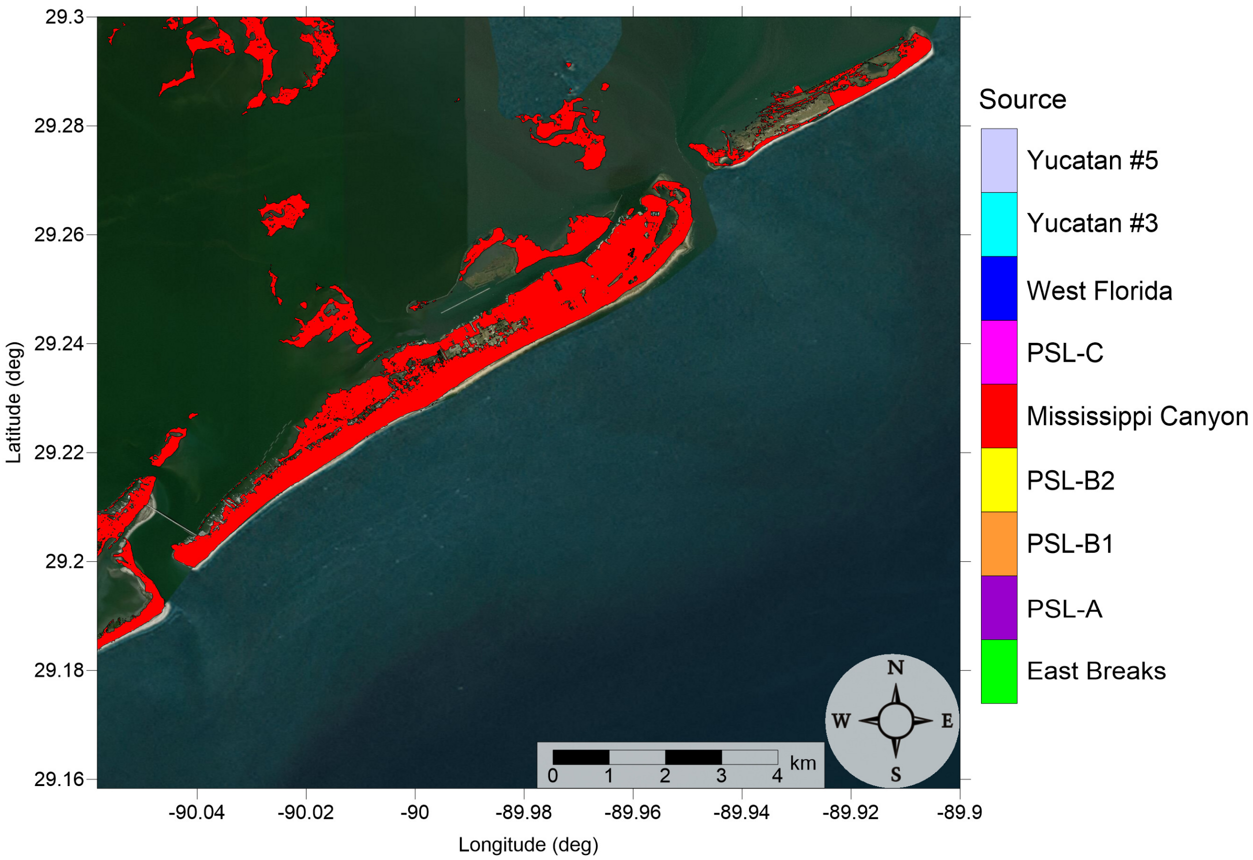

Figure 21: Indication of the tsunami source which causes the maximum of maximums inundation depth (m) in each grid cell from an ensemble of all tsunami sources in Grand Isle, LA. Contour drawn is the zero-meter contour for land elevation.

4.2 Freeport, TX

Table 3: Maximum tsunami wave amplitude and corresponding arrival time after landslide failure at Freeport, TX numerical wave gauge: 26°14'34.61"N, 82°25'32.45"W, approximate water depth 20 m.

Tsunami Source	Maximum Wave Amplitude (m)	Arrival Time After Landslide Failure (hr)
East Breaks	1.15	1.5
PSL-A	1.00	1.4
PSL-B1	1.07	2.1
PSL-B2	0.63	2.4
Mississippi Canyon	3.69	2.6
PSL-C	2.98	3.1
West Florida	0.40	3.4
Yucatán #3	1.00	2.7
Yucatán #5	1.09	2.6

Freeport, TX
East Breaks submarine landslide
Maximum Momentum Flux

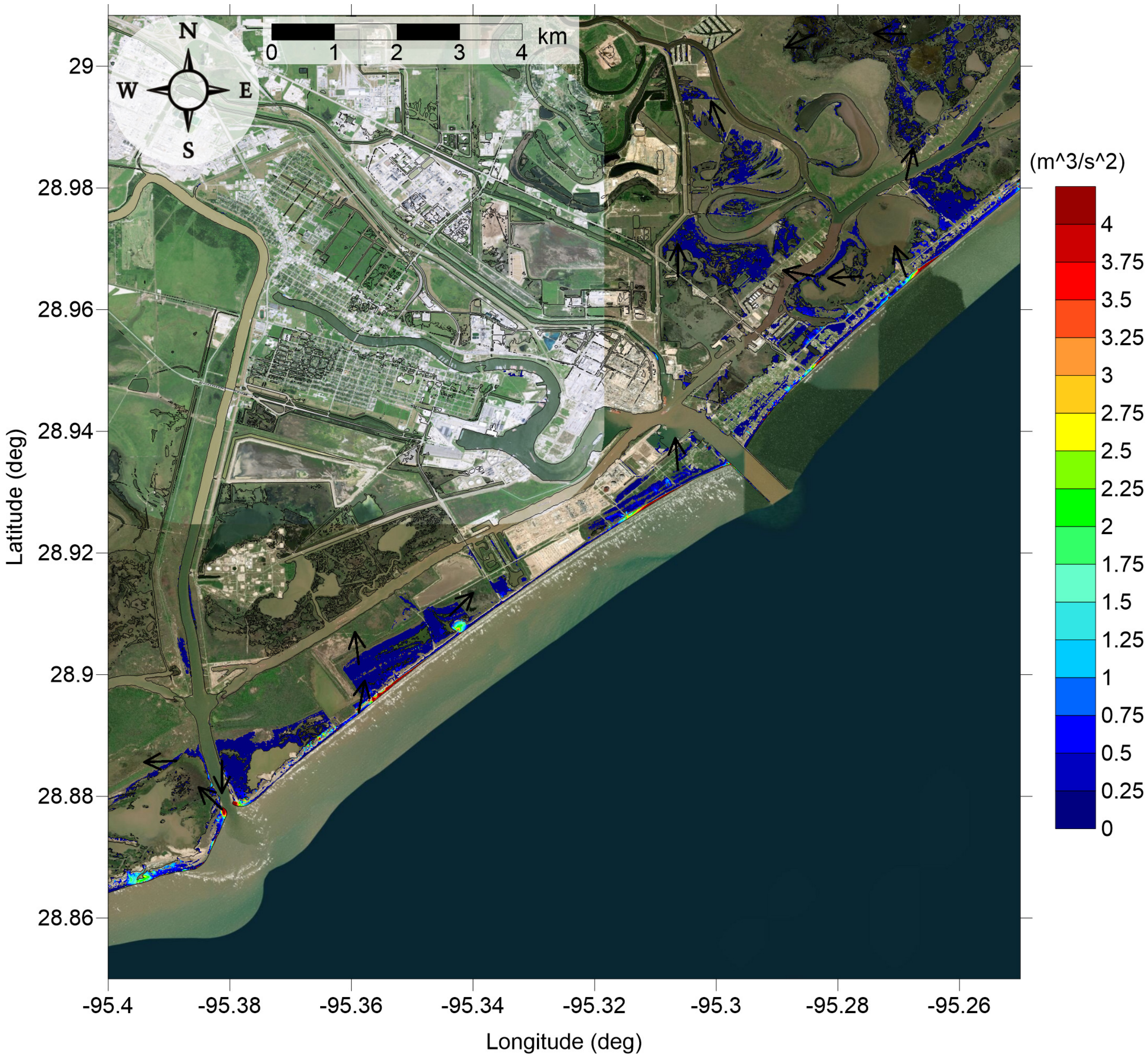

Figure 22: Maximum momentum flux (m^3/s^2) caused by the East Breaks submarine landslide in Freeport, TX. Arrows represent direction of maximum momentum flux. Contour drawn is the zero-meter contour for land elevation.

San Luis Pass, TX
East Breaks submarine landslide
Maximum Momentum Flux

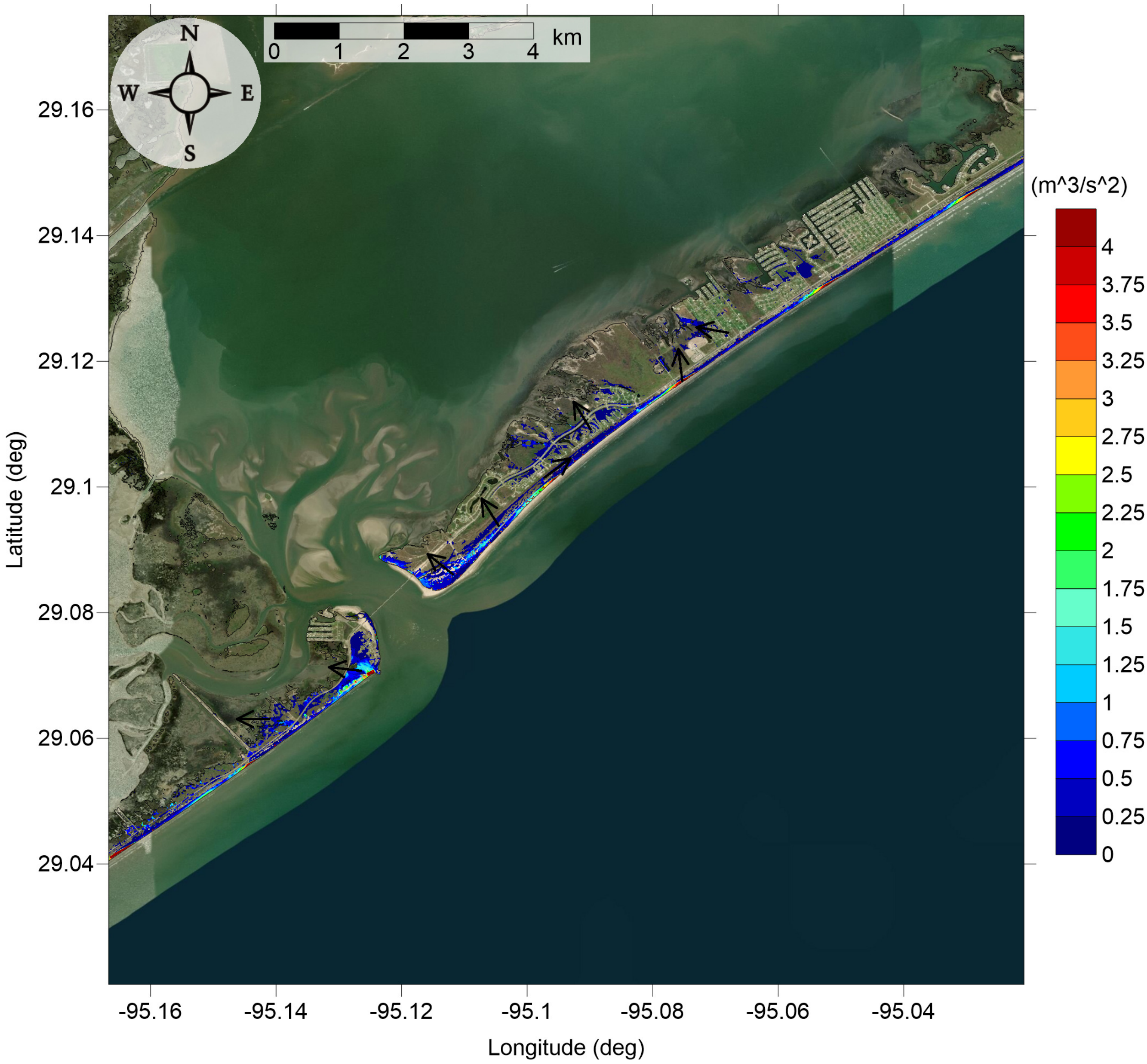

Figure 23: Maximum momentum flux (m^3/s^2) caused by the East Breaks submarine landslide in San Luis Pass, TX. Arrows represent direction of maximum momentum flux. Contour drawn is the zero-meter contour for land elevation.

Freeport, TX
East Breaks submarine landslide
Maximum Inundation Depth

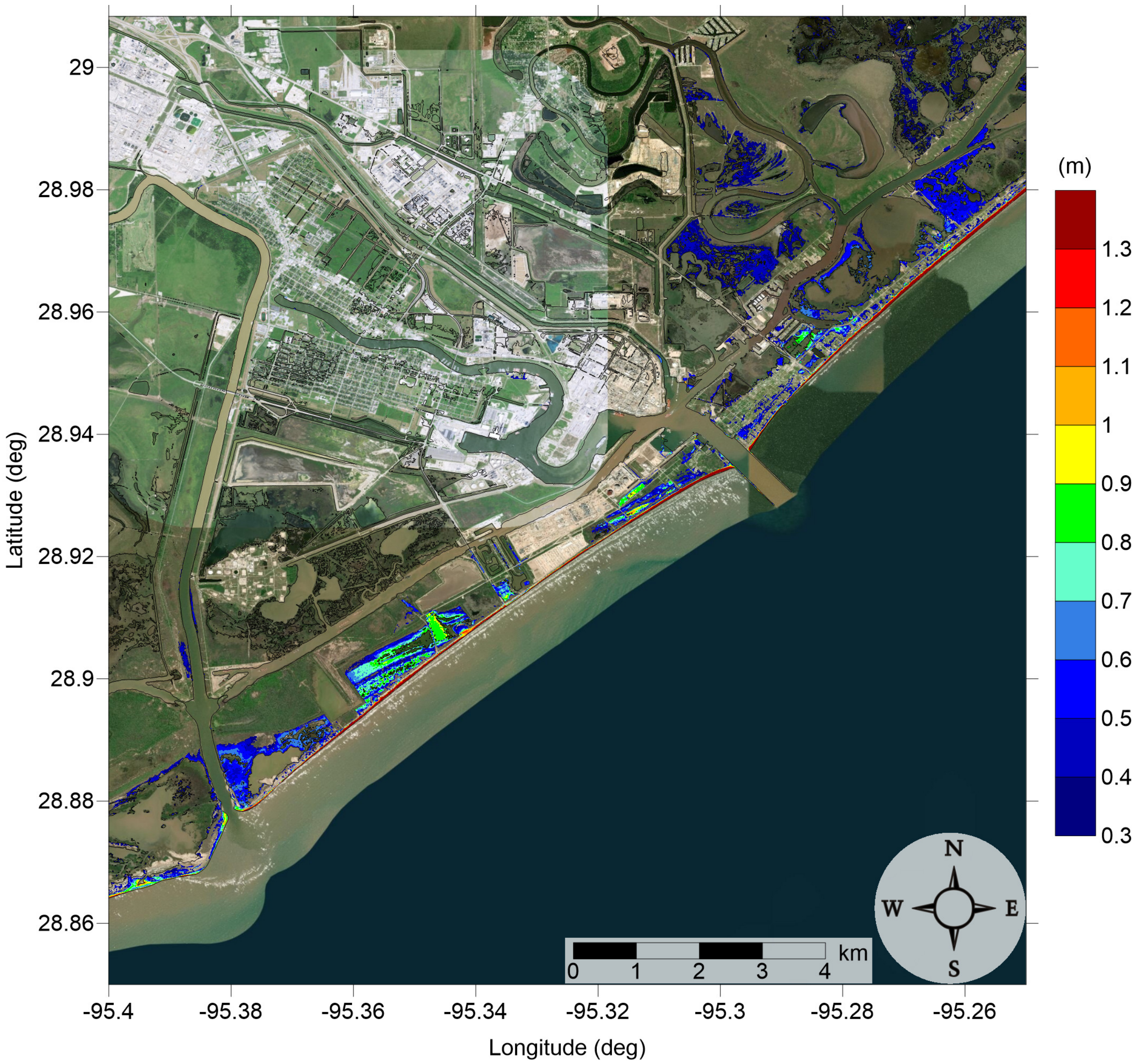

Figure 24: Maximum inundation depth (m) caused by the East Breaks submarine landslide in Freeport, TX. Contour drawn is the zero-meter contour for land elevation.

San Luis Pass, TX
East Breaks submarine landslide
Maximum Inundation Depth

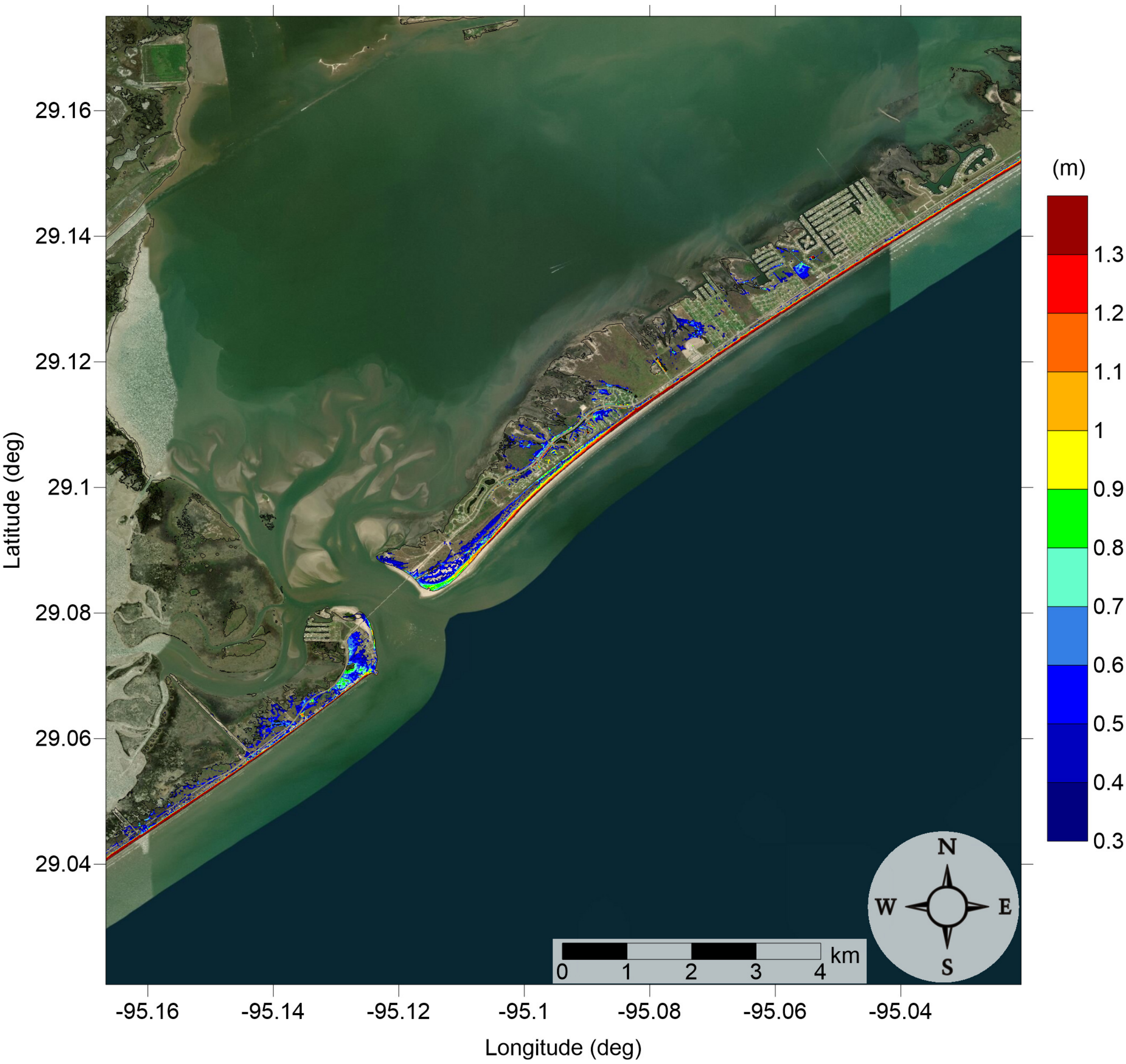

Figure 25: Maximum inundation depth (m) caused by the East Breaks submarine landslide in San Luis Pass, TX. Contour drawn is the zero-meter contour for land elevation.

Freeport, TX
Probabilistic Submarine Landslide A
Maximum Momentum Flux

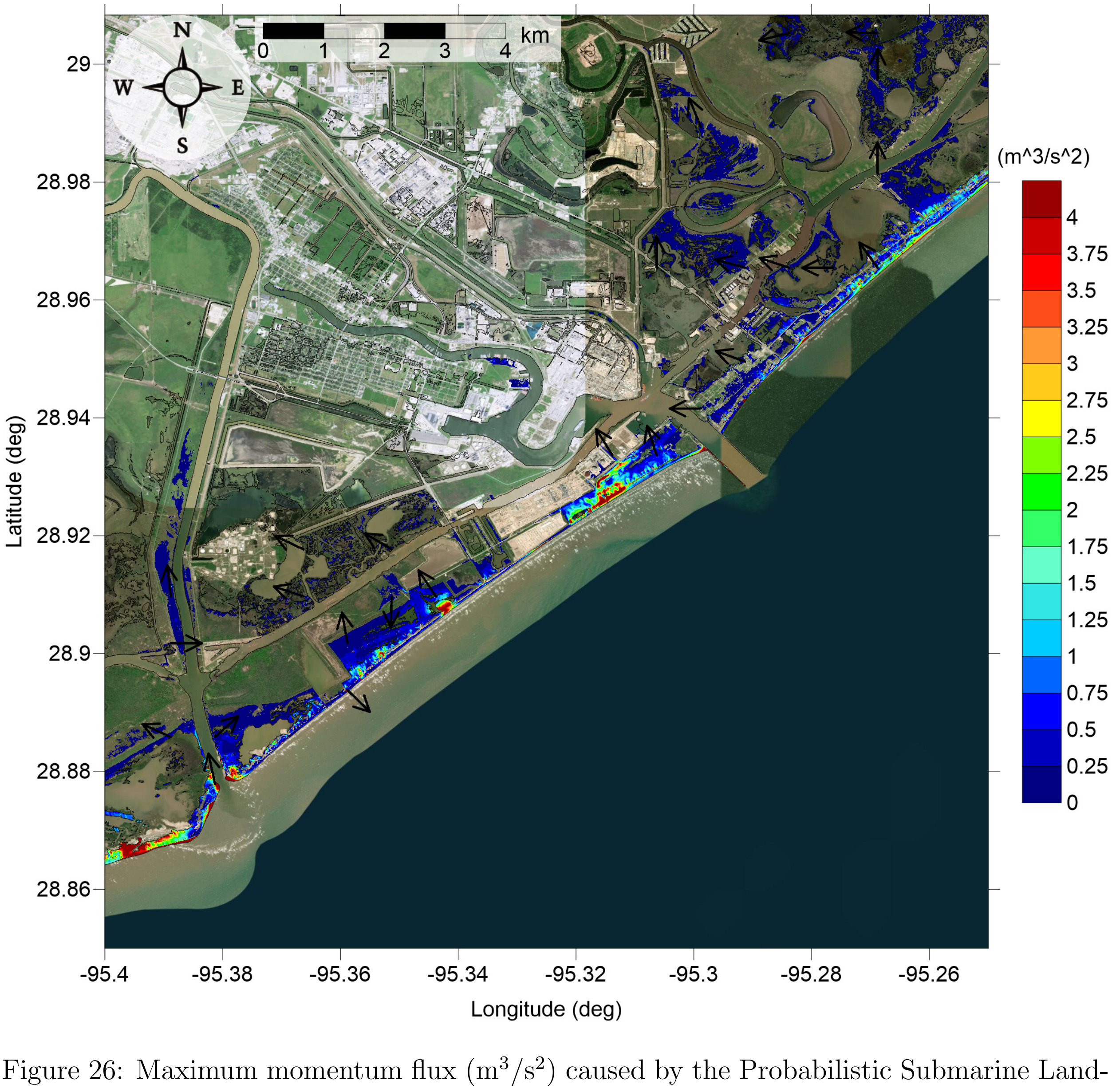

Figure 26: Maximum momentum flux (m^3/s^2) caused by the Probabilistic Submarine Landslide A in Freeport, TX. Arrows represent direction of maximum momentum flux. Contour drawn is the zero-meter contour for land elevation.

San Luis Pass, TX
Probabilistic Submarine Landslide A
Maximum Momentum Flux

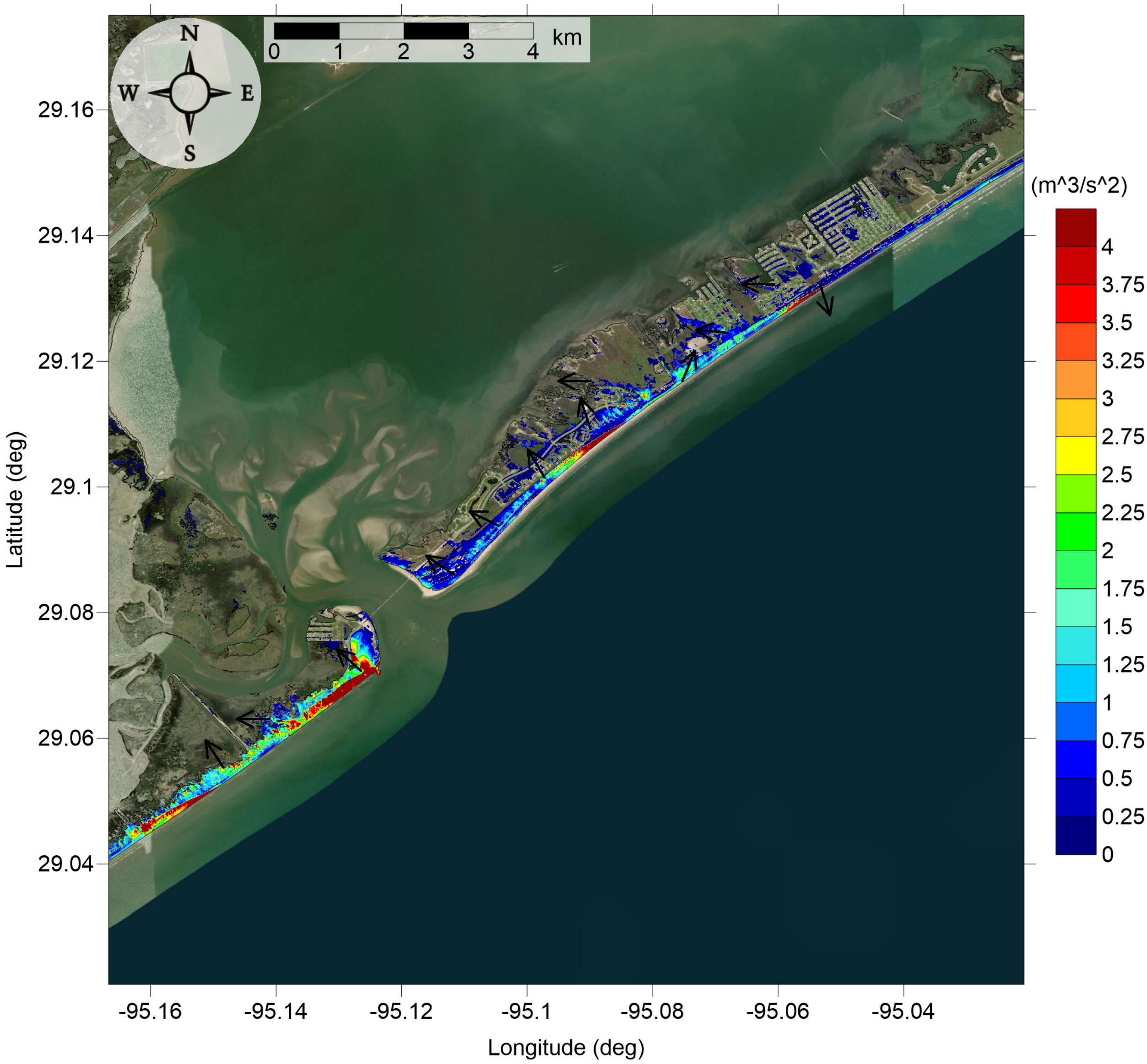

Figure 27: Maximum momentum flux (m^3/s^2) caused by the Probabilistic Submarine Landslide A in San Luis Pass, TX. Arrows represent direction of maximum momentum flux. Contour drawn is the zero-meter contour for land elevation.

Freeport, TX
Probabilistic Submarine Landslide A
Maximum Inundation Depth

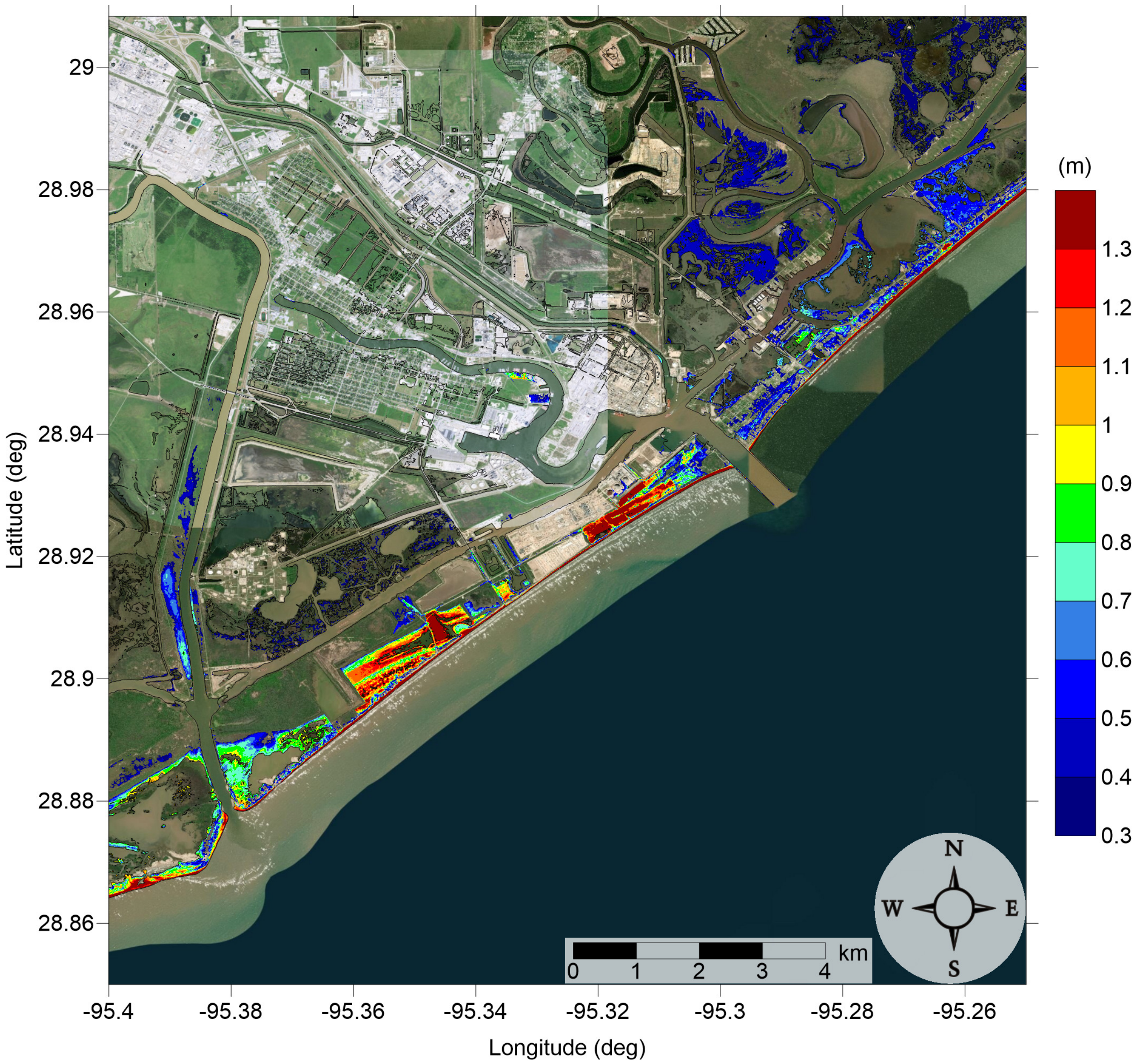

Figure 28: Maximum inundation depth (m) caused by the Probabilistic Submarine Landslide A in Freeport, TX. Contour drawn is the zero-meter contour for land elevation.

San Luis Pass, TX
Probabilistic Submarine Landslide A
Maximum Inundation Depth

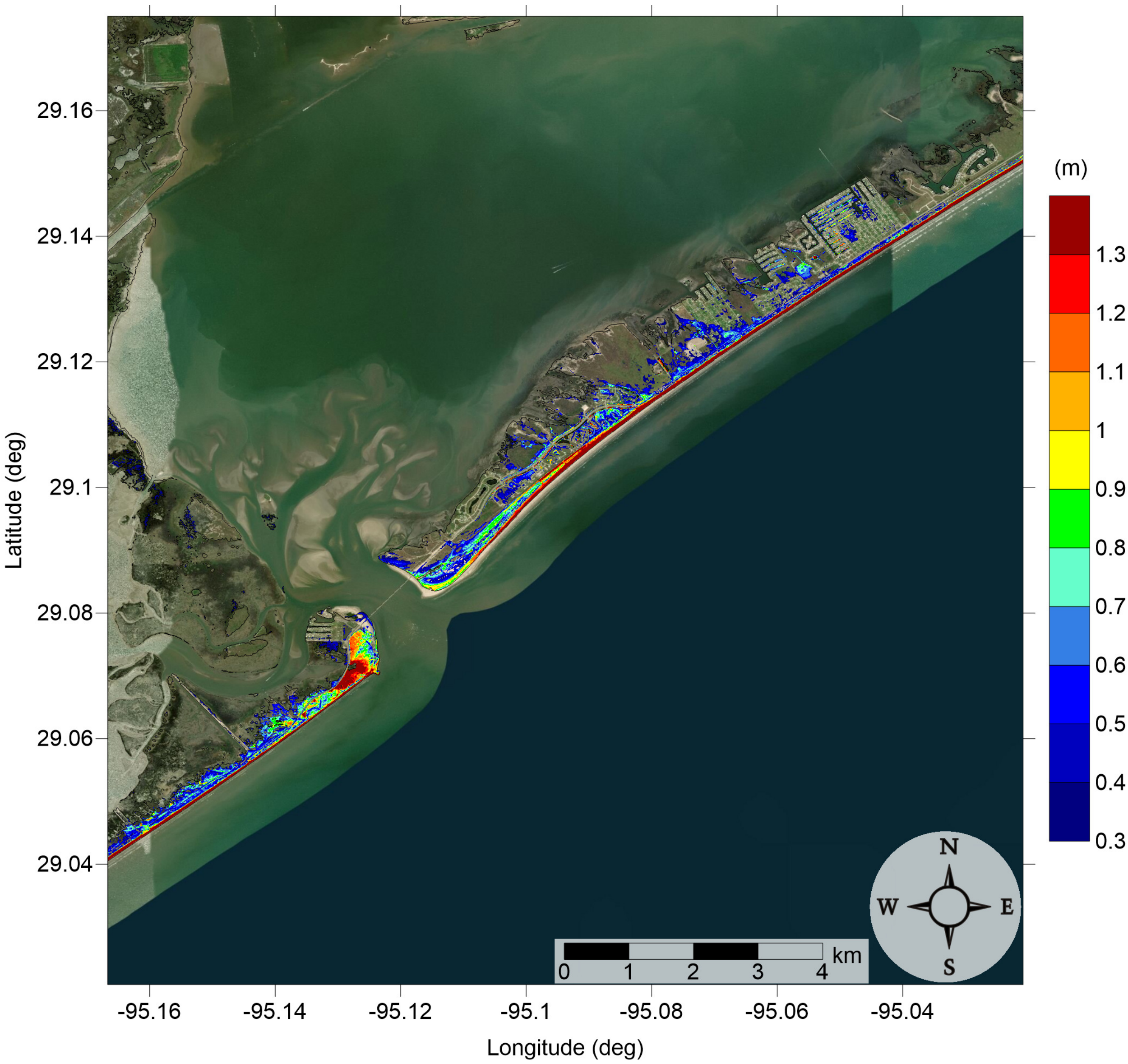

Figure 29: Maximum inundation depth (m) caused by the Probabilistic Submarine Landslide A in San Luis Pass, TX. Contour drawn is the zero-meter contour for land elevation.

Freeport, TX
Probabilistic Submarine Landslide B1
Maximum Momentum Flux

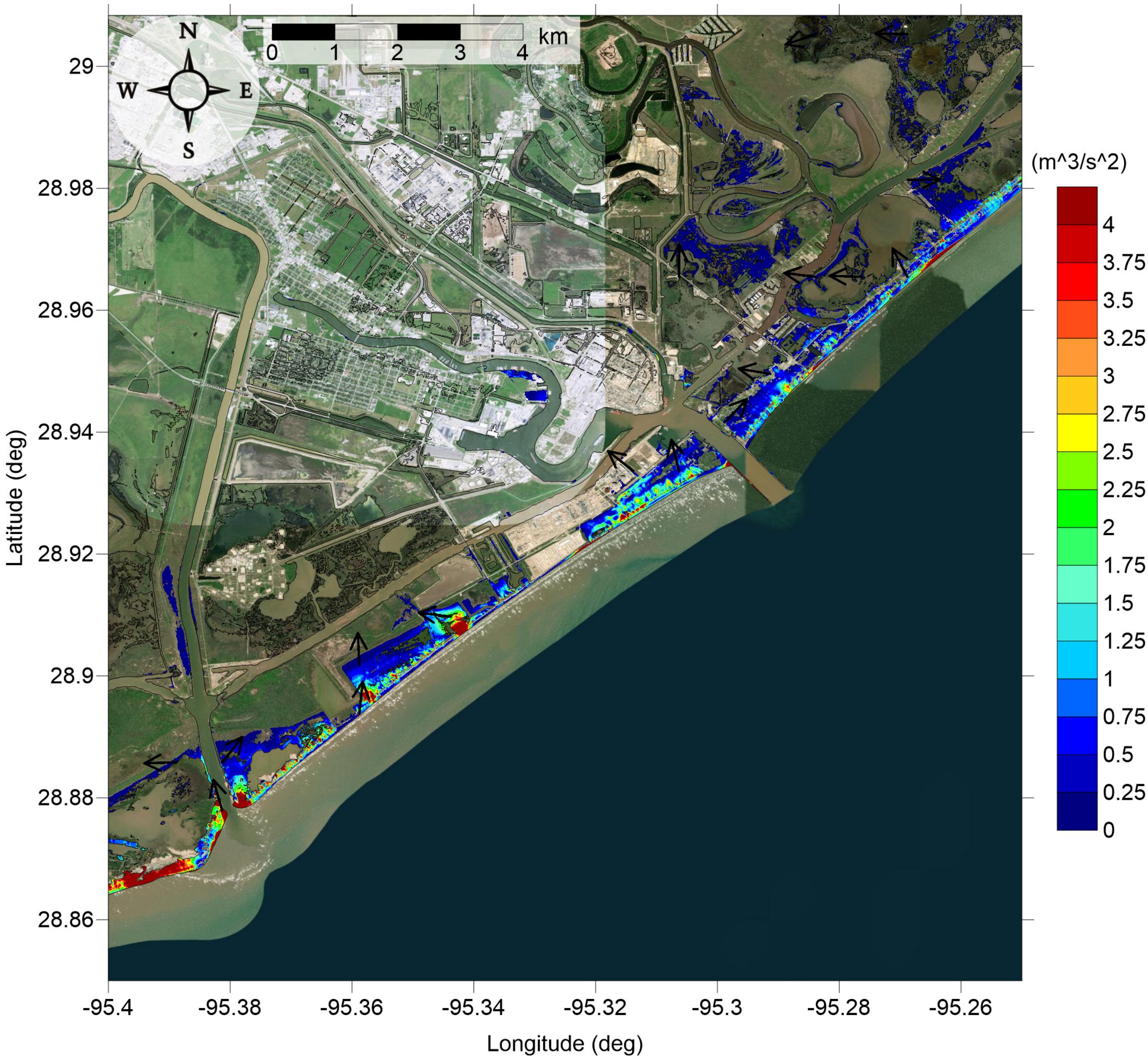

Figure 30: Maximum momentum flux (m^3/s^2) caused by the Probabilistic Submarine Landslide B1 in Freeport, TX. Arrows represent direction of maximum momentum flux. Contour drawn is the zero-meter contour for land elevation.

San Luis Pass, TX
Probabilistic Submarine Landslide B1
Maximum Momentum Flux

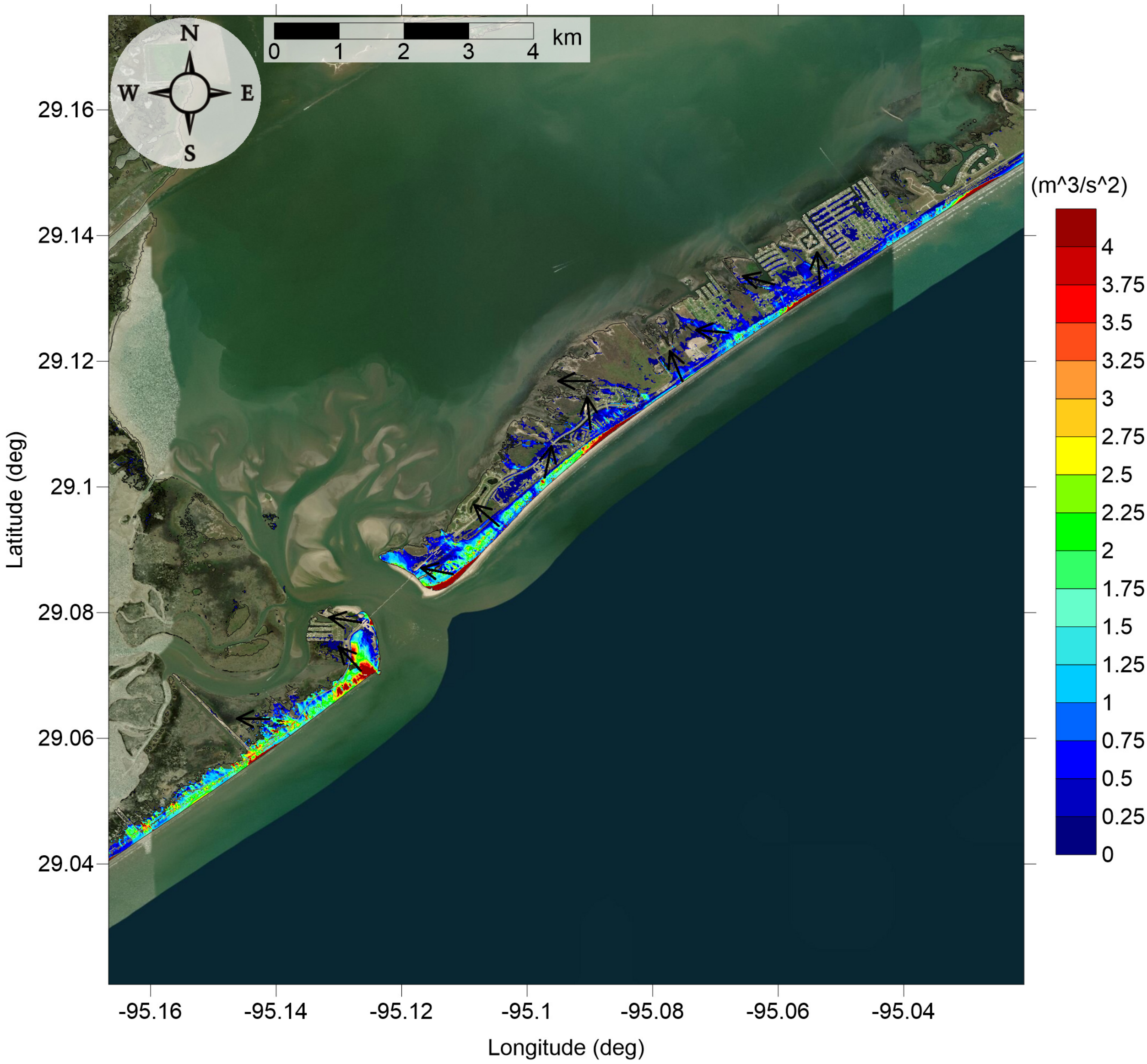

Figure 31: Maximum momentum flux (m^3/s^2) caused by the Probabilistic Submarine Landslide B1 in San Luis Pass, TX. Arrows represent direction of maximum momentum flux. Contour drawn is the zero-meter contour for land elevation.

Freeport, TX
Probabilistic Submarine Landslide B1
Maximum Inundation Depth

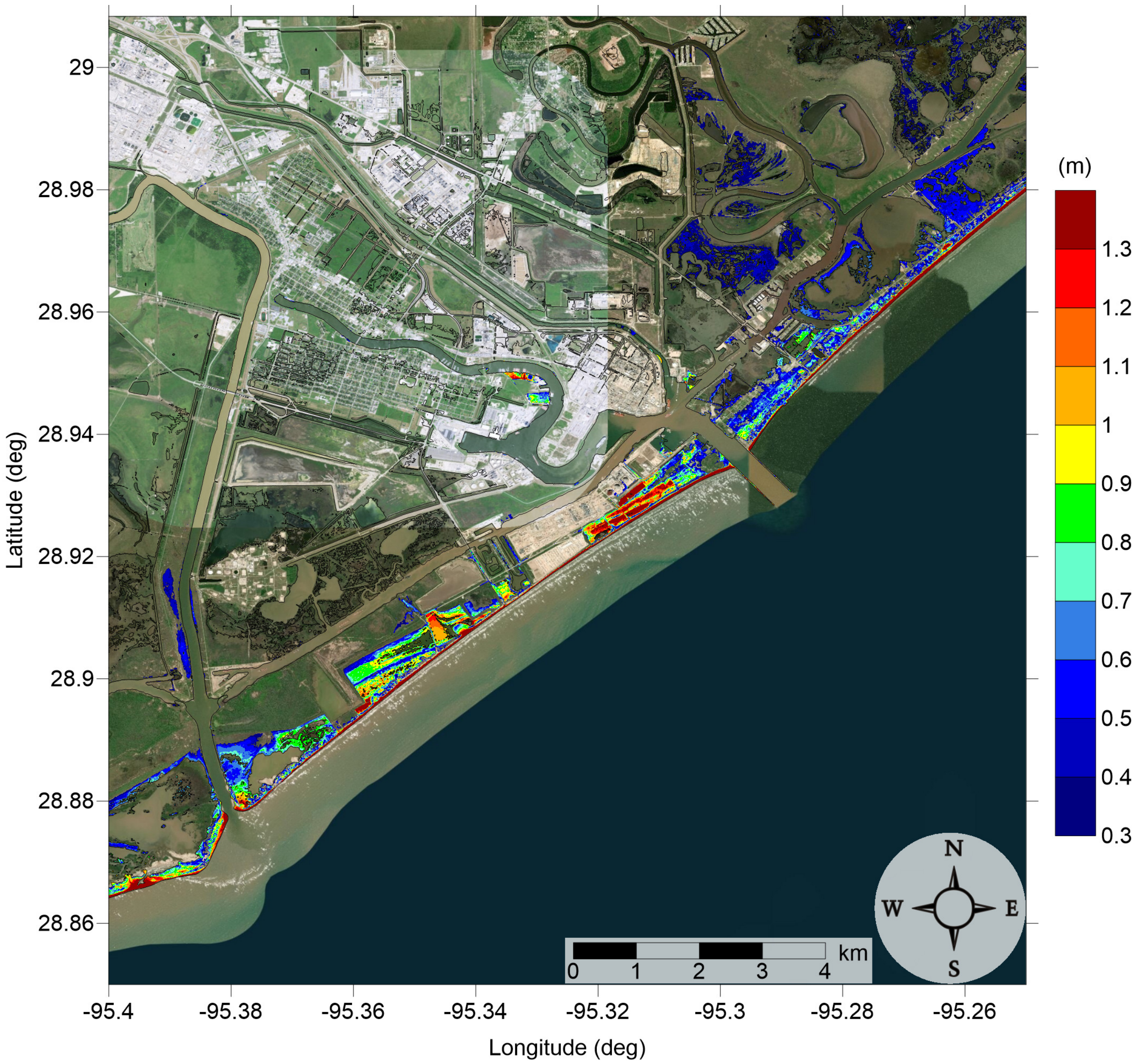

Figure 32: Maximum inundation depth (m) caused by the Probabilistic Submarine Landslide B1 in Freeport, TX. Contour drawn is the zero-meter contour for land elevation.

San Luis Pass, TX
Probabilistic Submarine Landslide B1
Maximum Inundation Depth

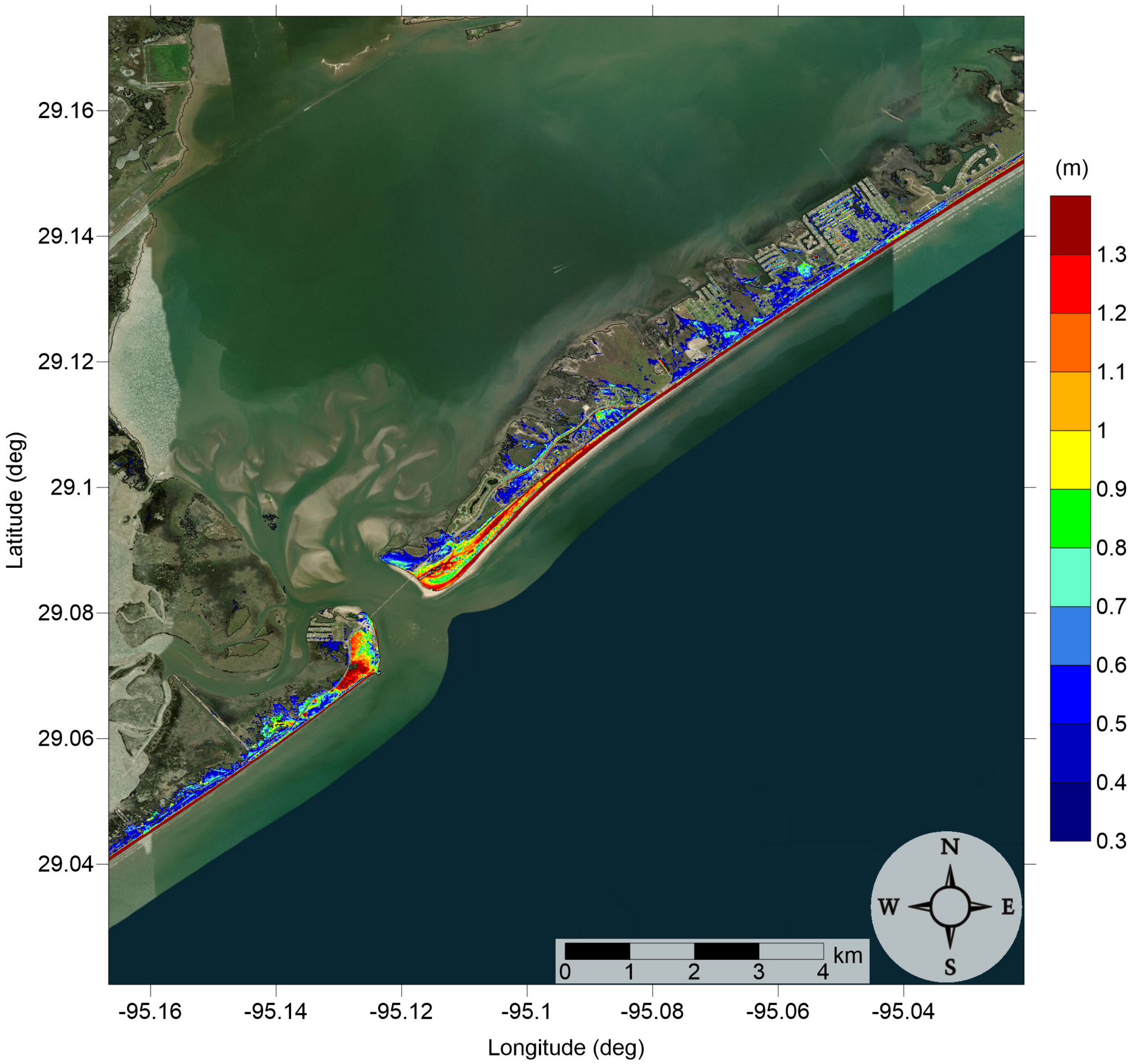

Figure 33: Maximum inundation depth (m) caused by the Probabilistic Submarine Landslide B1 in San Luis Pass, TX. Contour drawn is the zero-meter contour for land elevation.

Freeport, TX
Probabilistic Submarine Landslide B2
Maximum Momentum Flux

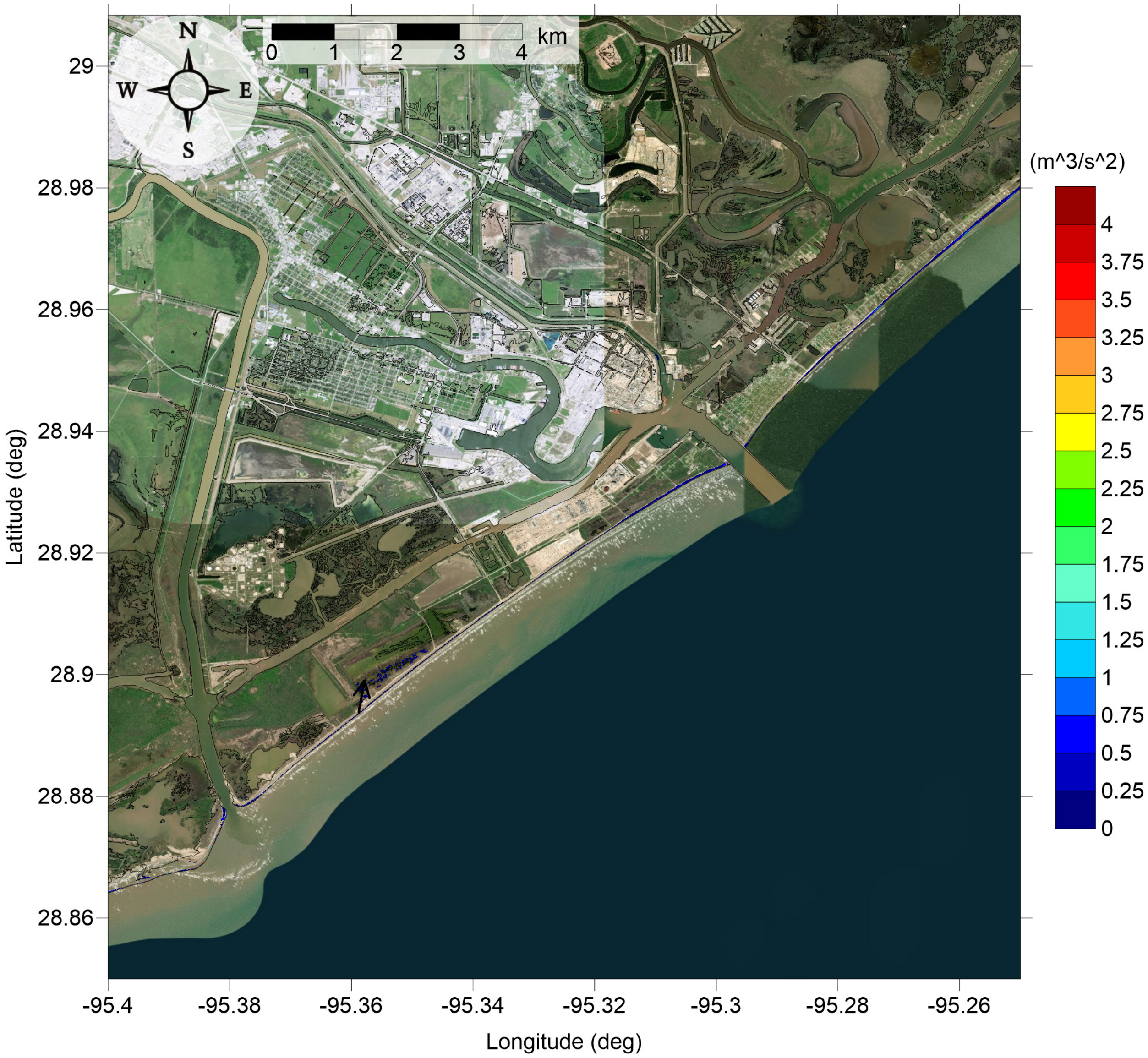

Figure 34: Maximum momentum flux (m^3/s^2) caused by the Probabilistic Submarine Landslide B2 in Freeport, TX. Arrows represent direction of maximum momentum flux. Contour drawn is the zero-meter contour for land elevation.

San Luis Pass, TX
Probabilistic Submarine Landslide B2
Maximum Momentum Flux

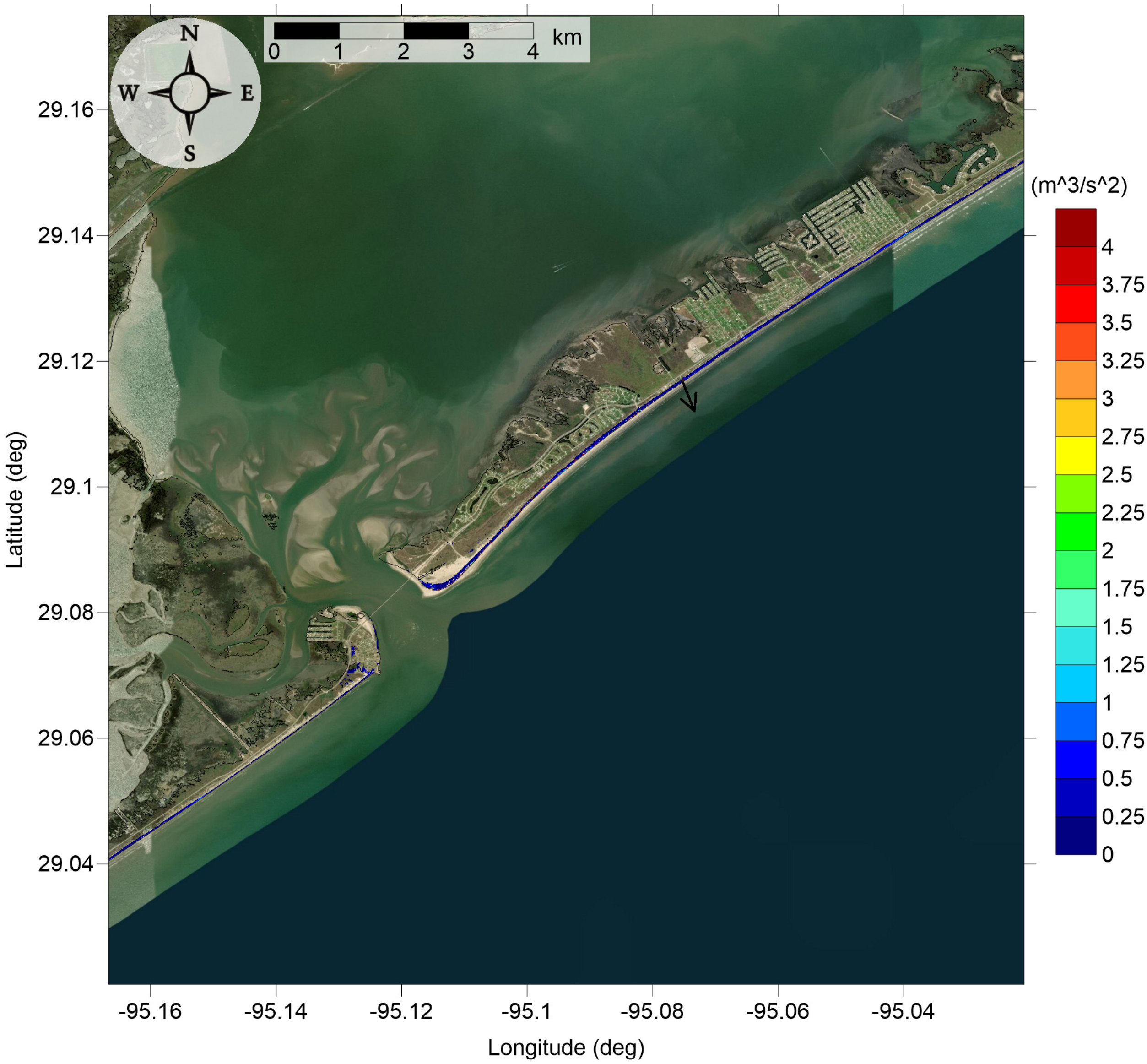

Figure 35: Maximum momentum flux (m^3/s^2) caused by the Probabilistic Submarine Landslide B2 in San Luis Pass, TX. Arrows represent direction of maximum momentum flux. Contour drawn is the zero-meter contour for land elevation.

Freeport, TX
Probabilistic Submarine Landslide B2
Maximum Inundation Depth

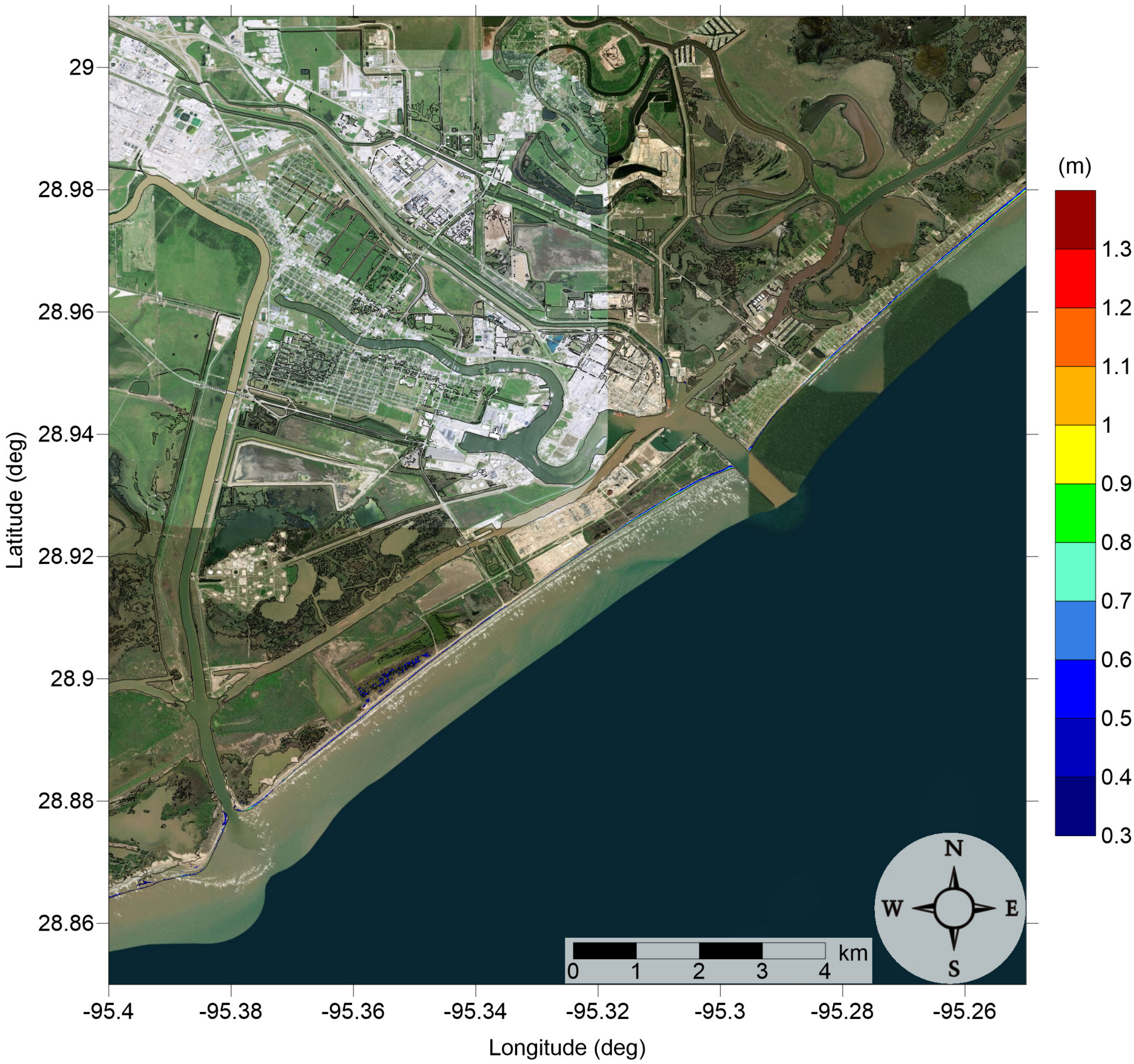

Figure 36: Maximum inundation depth (m) caused by the Probabilistic Submarine Landslide B2 in Freeport, TX. Contour drawn is the zero-meter contour for land elevation.

San Luis Pass, TX
Probabilistic Submarine Landslide B2
Maximum Inundation Depth

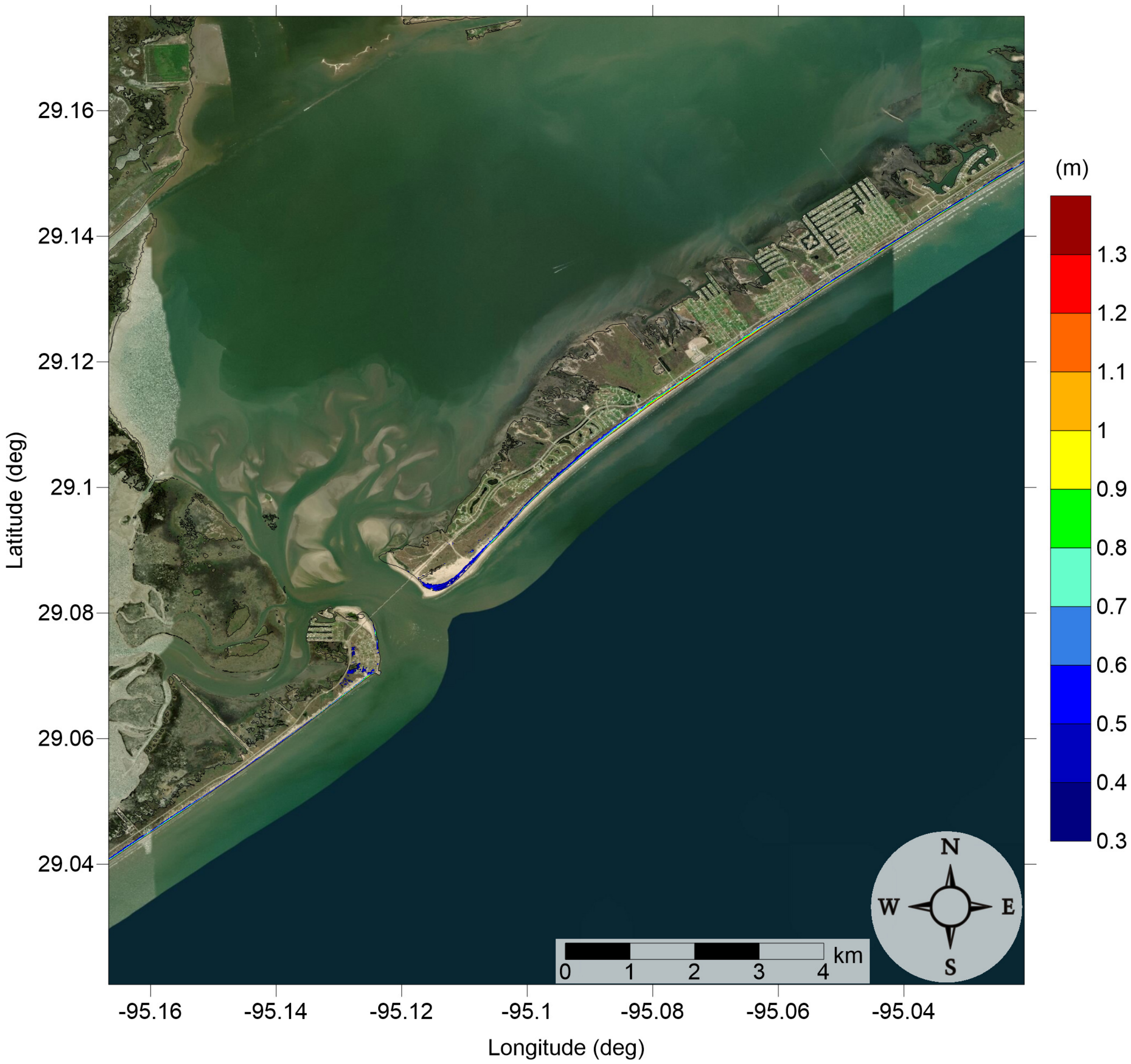

Figure 37: Maximum inundation depth (m) caused by the Probabilistic Submarine Landslide B2 in San Luis Pass, TX. Contour drawn is the zero-meter contour for land elevation.

Freeport, TX
Mississippi Canyon submarine landslide
Maximum Momentum Flux

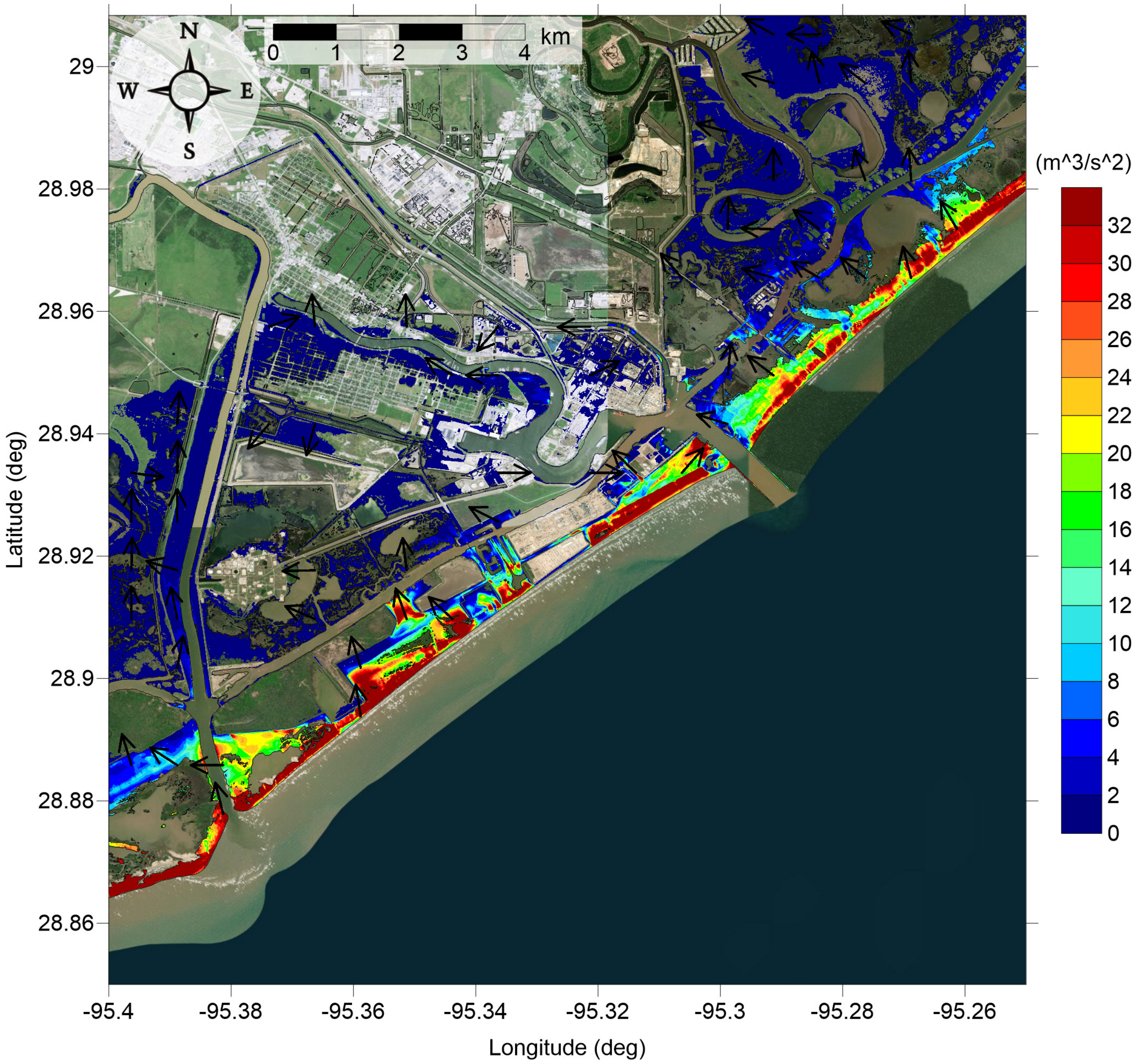

Figure 38: Maximum momentum flux (m^3/s^2) caused by the Mississippi Canyon submarine landslide in Freeport, TX. Arrows represent direction of maximum momentum flux. Contour drawn is the zero-meter contour for land elevation.

San Luis Pass, TX
Mississippi Canyon submarine landslide
Maximum Momentum Flux

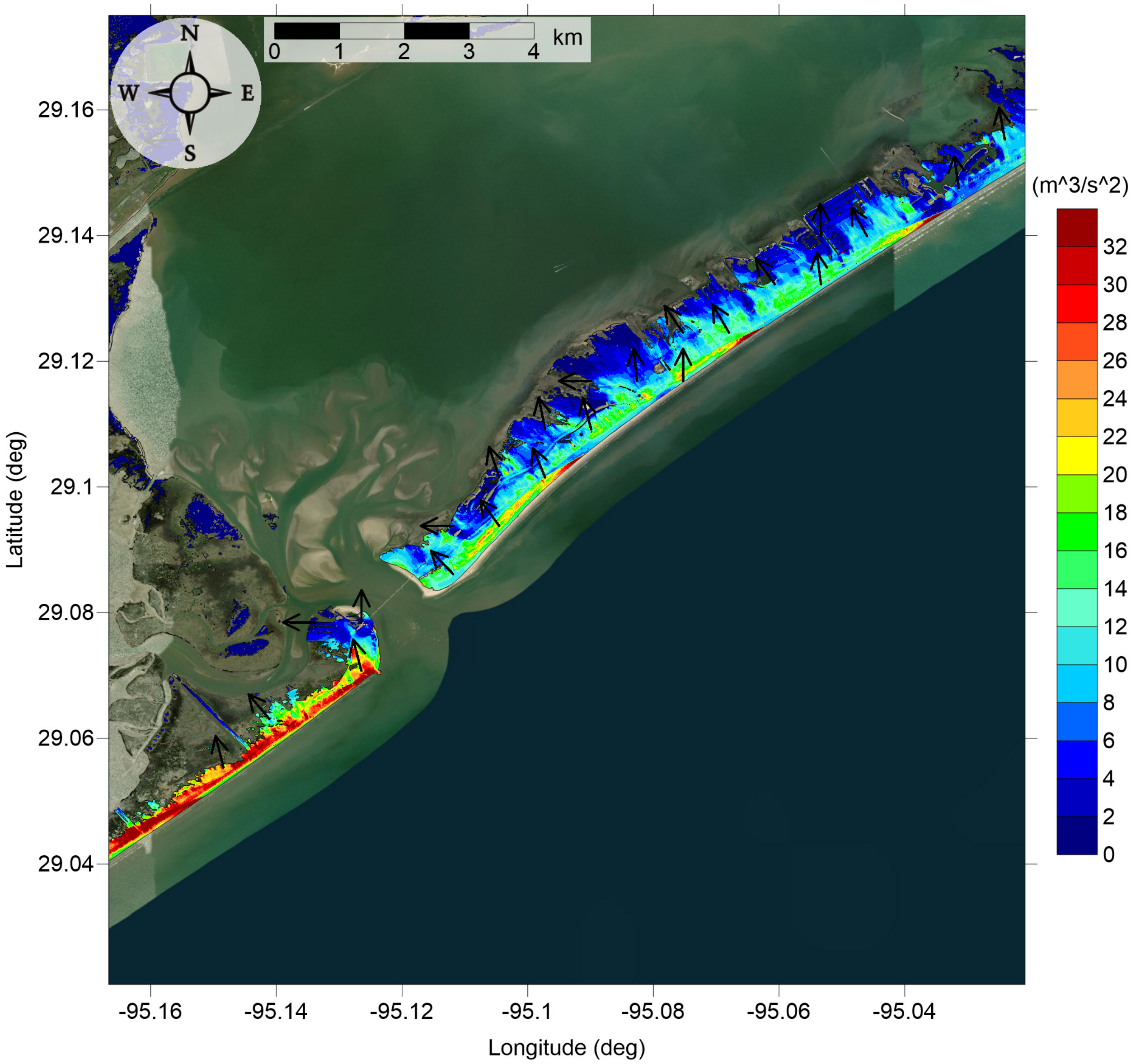

Figure 39: Maximum momentum flux (m^3/s^2) caused by the Mississippi Canyon submarine landslide in San Luis Pass, TX. Arrows represent direction of maximum momentum flux. Contour drawn is the zero-meter contour for land elevation.

Freeport, TX
Mississippi Canyon submarine landslide
Maximum Inundation Depth

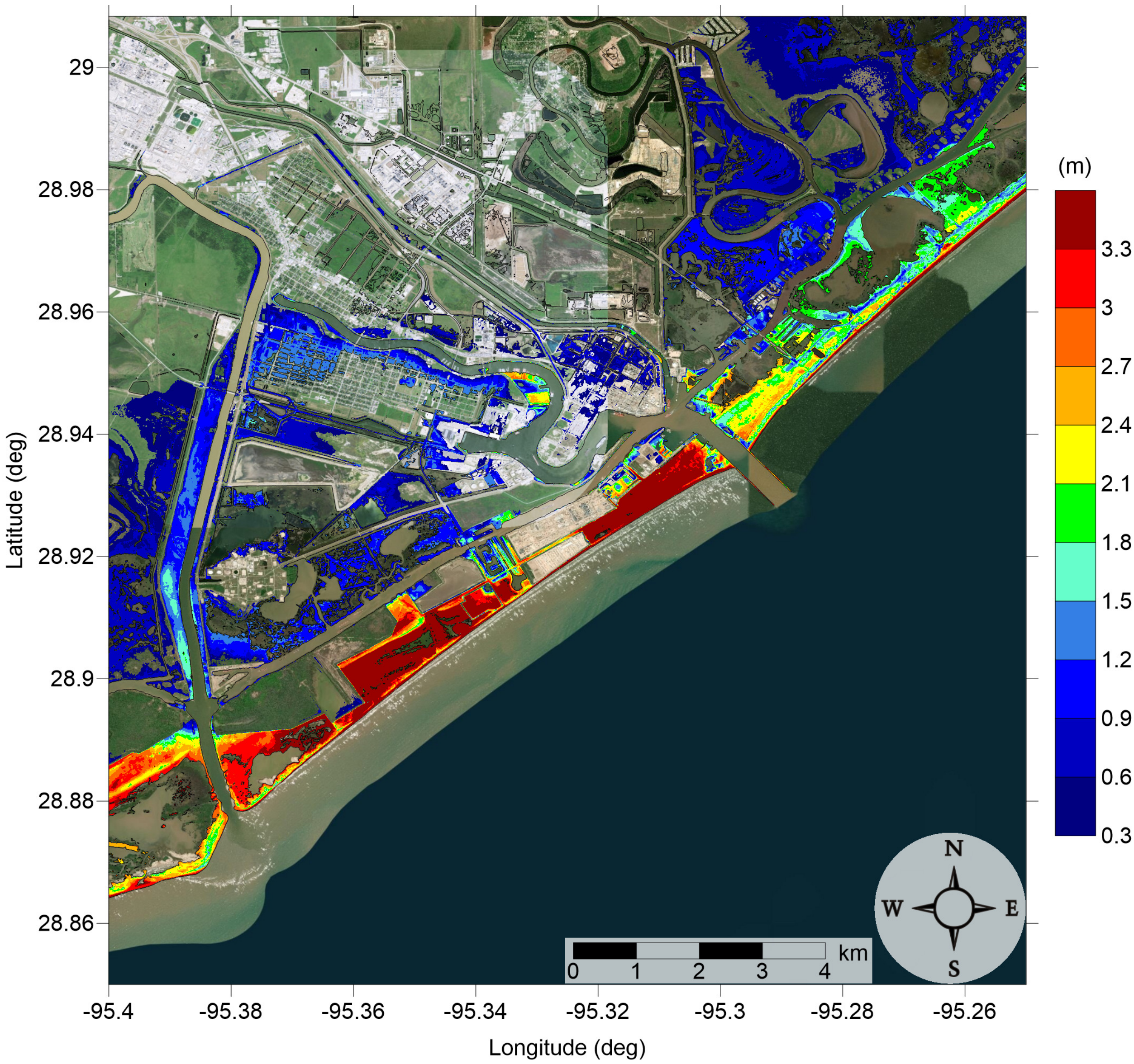

Figure 40: Maximum inundation depth (m) caused by the Mississippi Canyon submarine landslide in Freeport, TX. Contour drawn is the zero-meter contour for land elevation.

San Luis Pass, TX
Mississippi Canyon submarine landslide
Maximum Inundation Depth

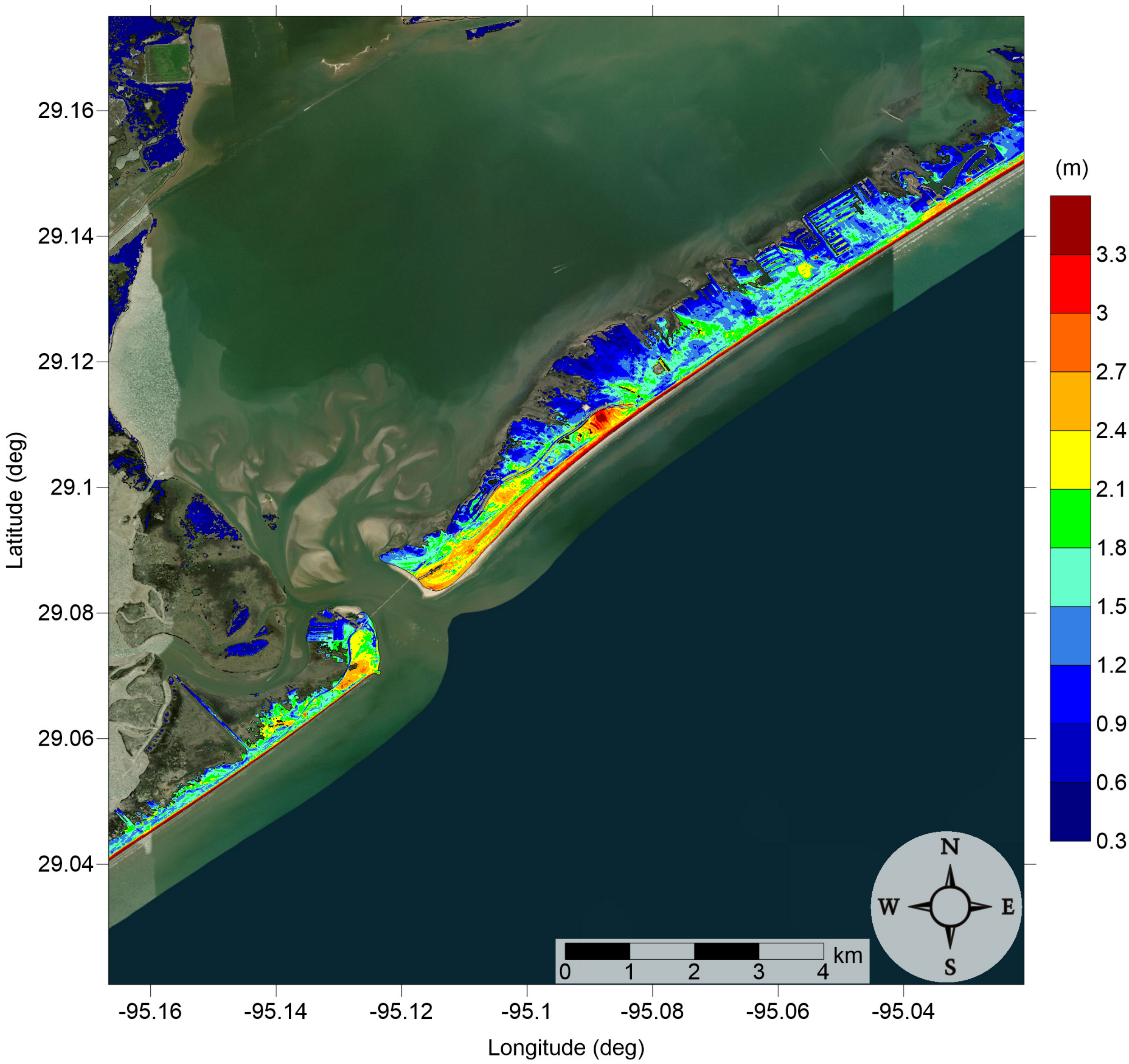

Figure 41: Maximum inundation depth (m) caused by the Mississippi Canyon submarine landslide in San Luis Pass, TX. Contour drawn is the zero-meter contour for land elevation.

Freeport, TX
Probabilistic Submarine Landslide C
Maximum Momentum Flux

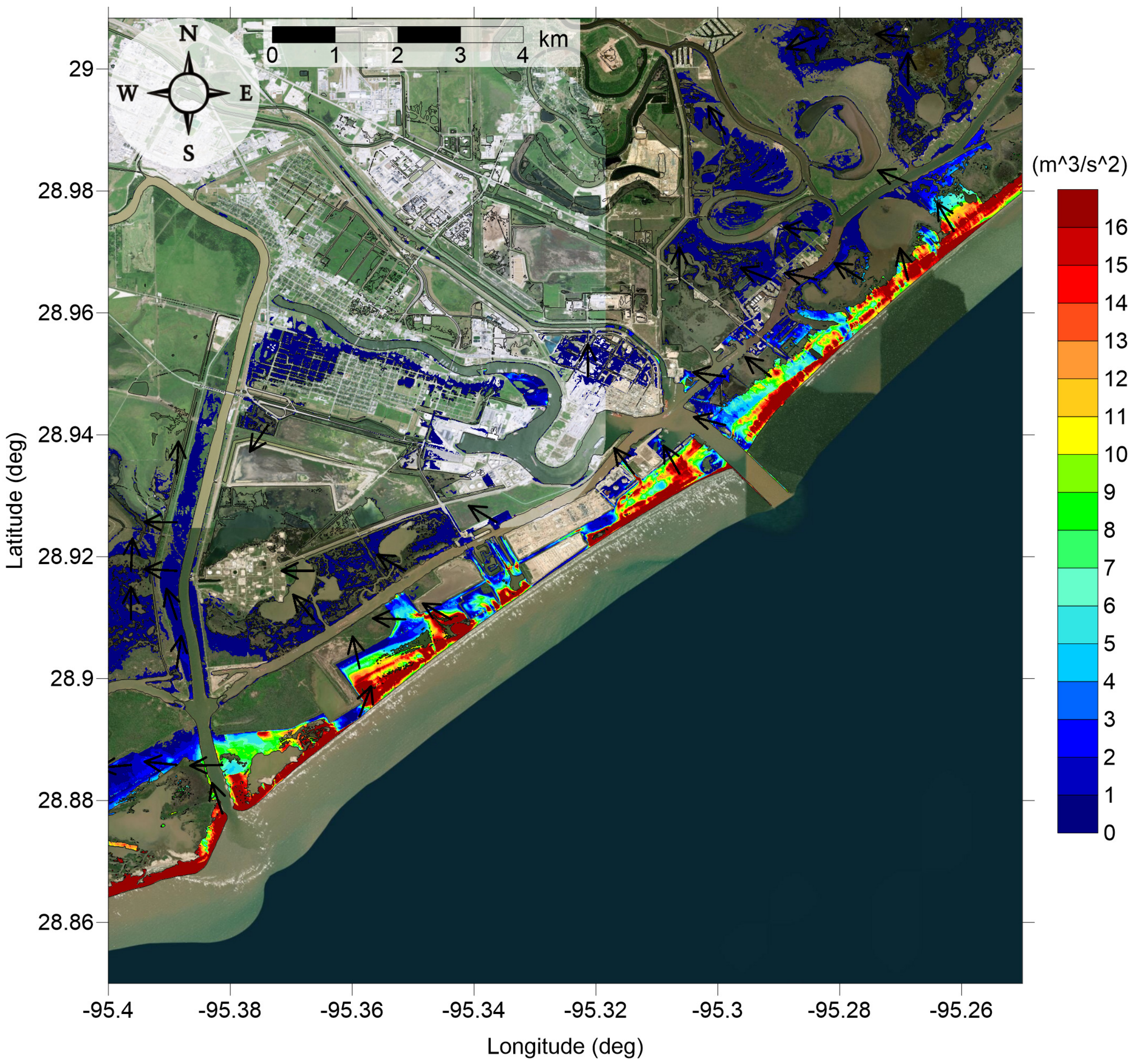

Figure 42: Maximum momentum flux (m^3/s^2) caused by the Probabilistic Submarine Landslide C in Freeport, TX. Arrows represent direction of maximum momentum flux. Contour drawn is the zero-meter contour for land elevation.

San Luis Pass, TX
Probabilistic Submarine Landslide C
Maximum Momentum Flux

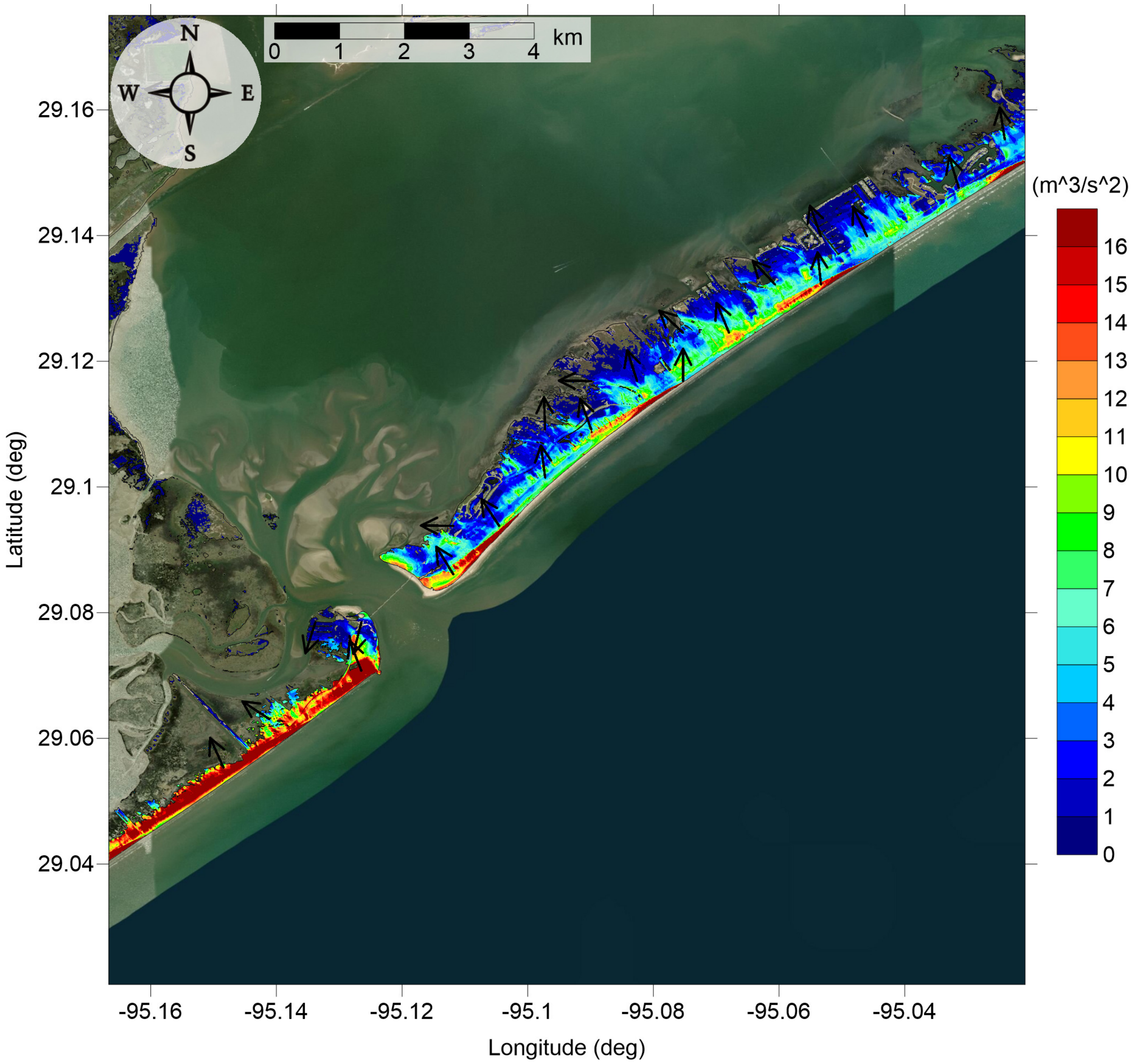

Figure 43: Maximum momentum flux (m^3/s^2) caused by the Probabilistic Submarine Landslide C in San Luis Pass, TX. Arrows represent direction of maximum momentum flux. Contour drawn is the zero-meter contour for land elevation.

Freeport, TX
Probabilistic Submarine Landslide C
Maximum Inundation Depth

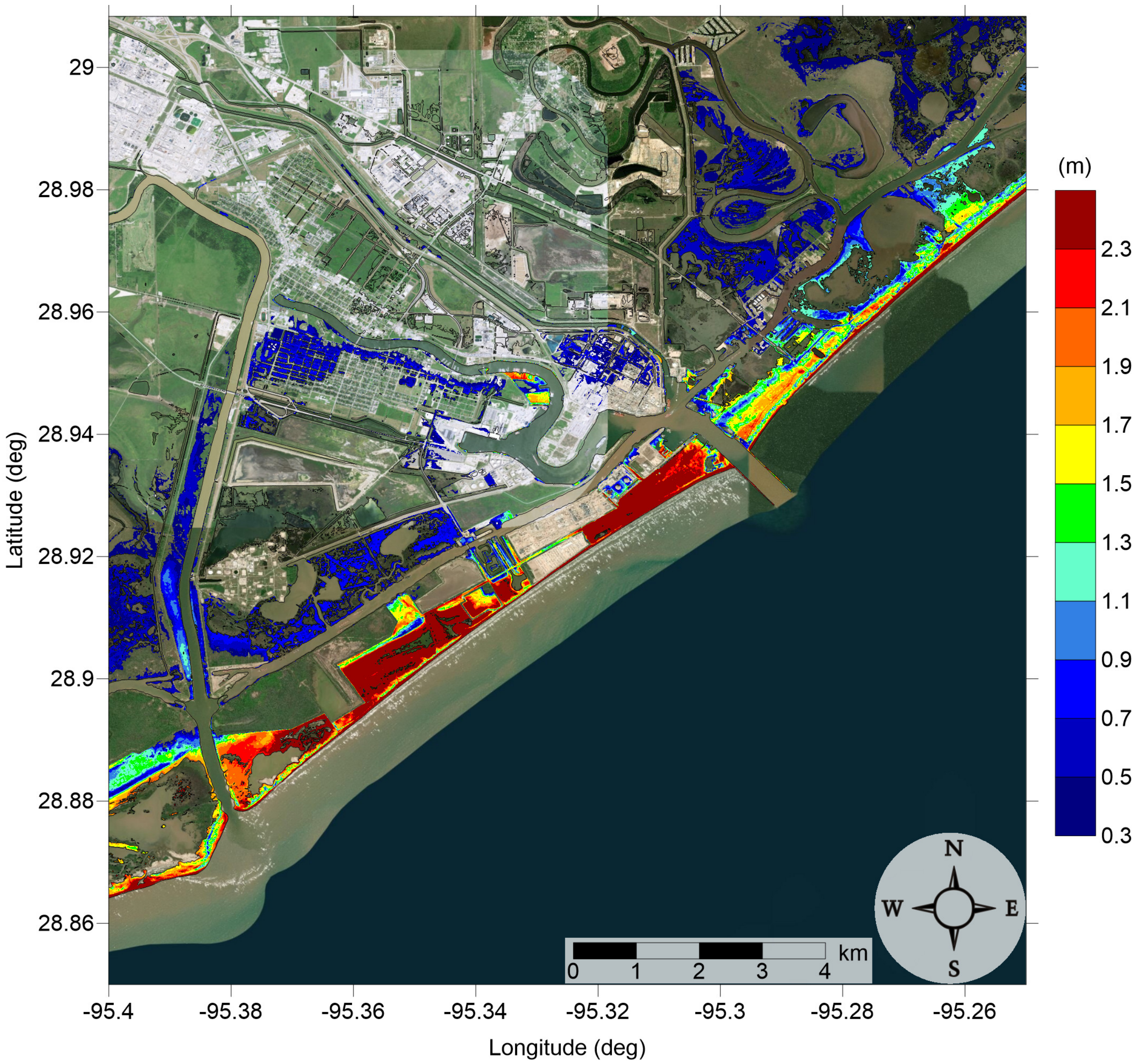

Figure 44: Maximum inundation depth (m) caused by the Probabilistic Submarine Landslide C in Freeport, TX. Contour drawn is the zero-meter contour for land elevation.

San Luis Pass, TX
Probabilistic Submarine Landslide C
Maximum Inundation Depth

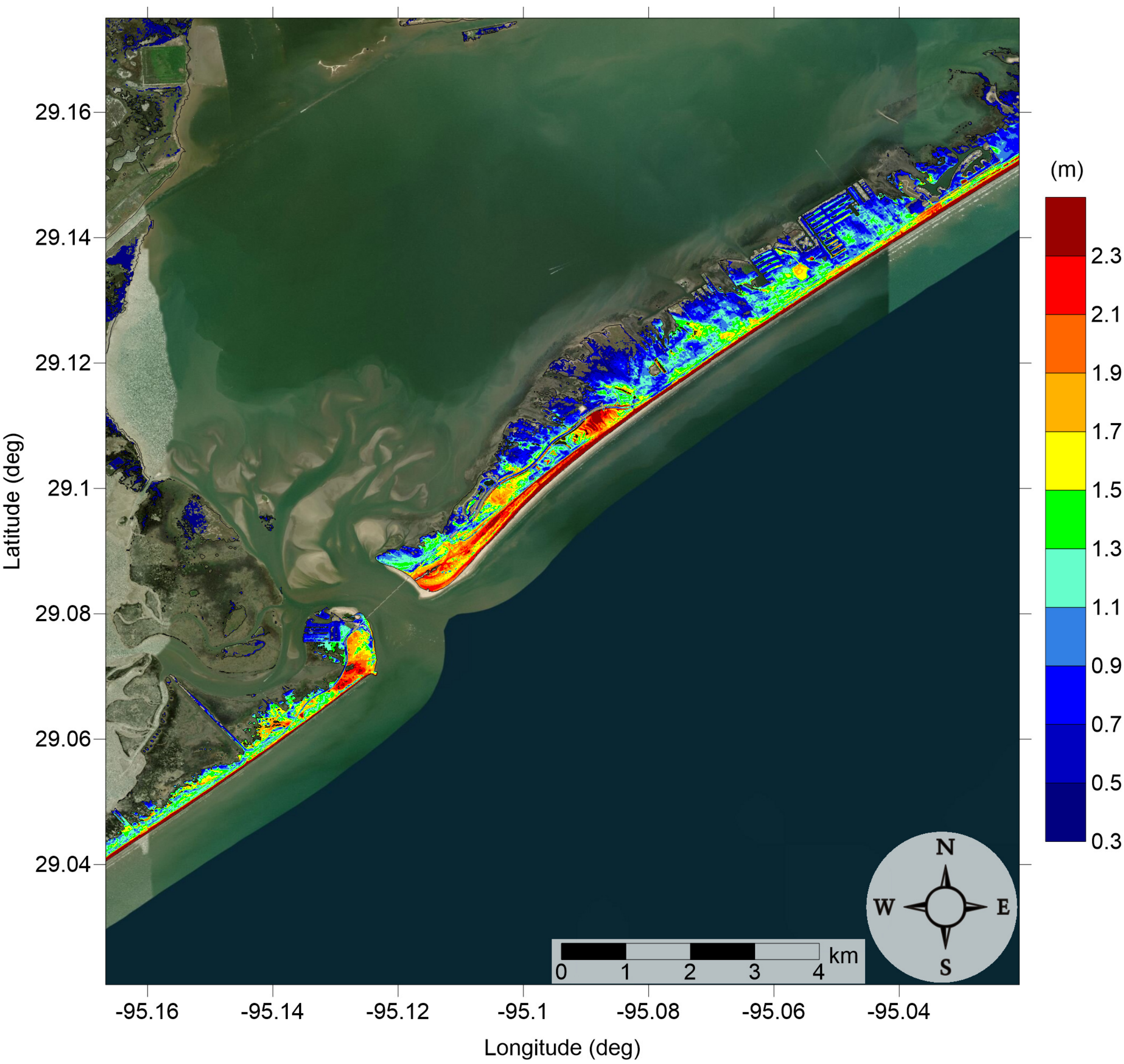

Figure 45: Maximum inundation depth (m) caused by the Probabilistic Submarine Landslide C in San Luis Pass, TX. Contour drawn is the zero-meter contour for land elevation.

Freeport, TX
West Florida submarine landslide
Maximum Momentum Flux

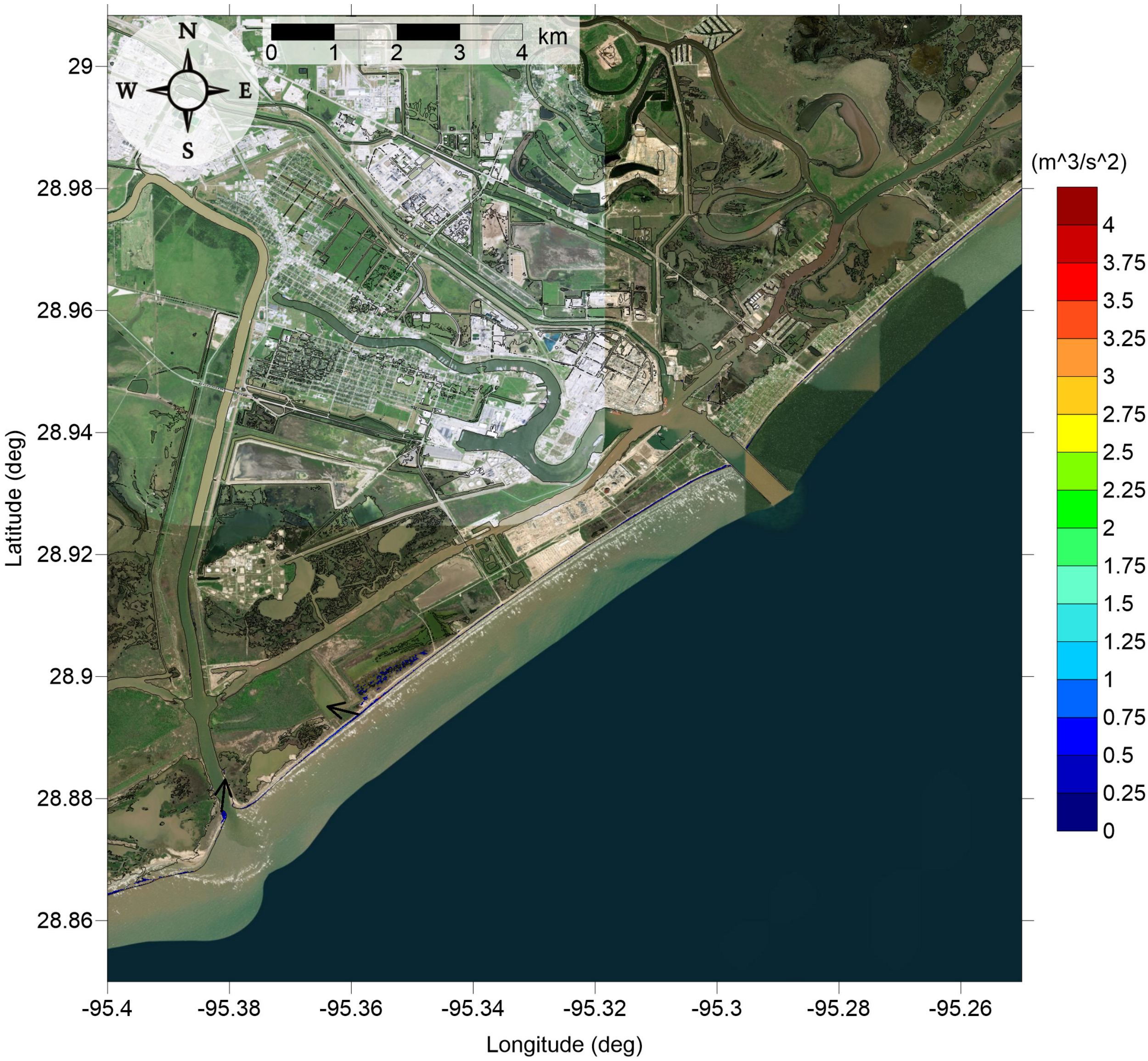

Figure 46: Maximum momentum flux (m^3/s^2) caused by the West Florida submarine landslide in Freeport, TX. Arrows represent direction of maximum momentum flux. Contour drawn is the zero-meter contour for land elevation.

San Luis Pass, TX
West Florida submarine landslide
Maximum Momentum Flux

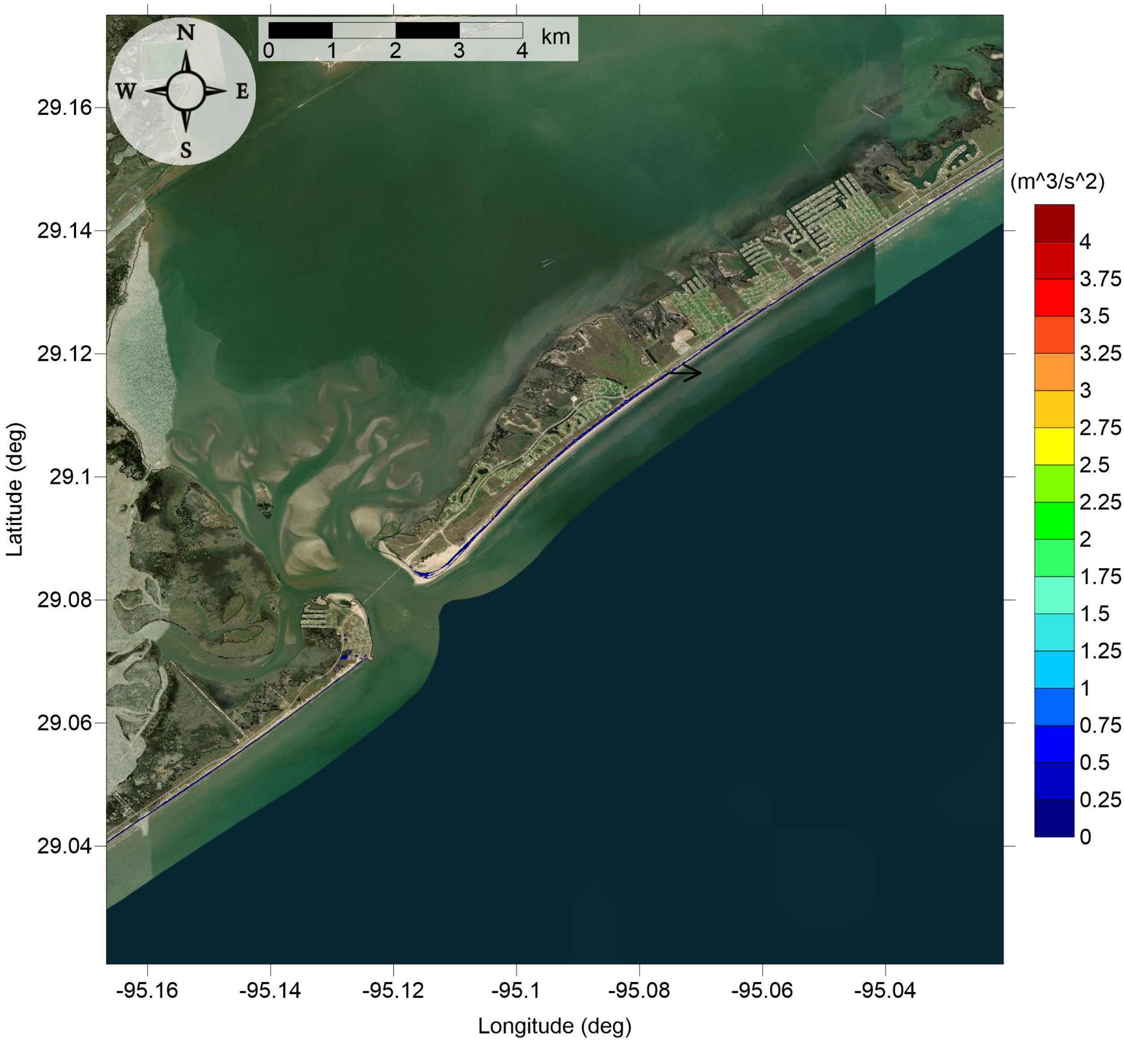

Figure 47: Maximum momentum flux (m^3/s^2) caused by the West Florida submarine landslide in San Luis Pass, TX. Arrows represent direction of maximum momentum flux. Contour drawn is the zero-meter contour for land elevation.

Freeport, TX
West Florida submarine landslide
Maximum Inundation Depth

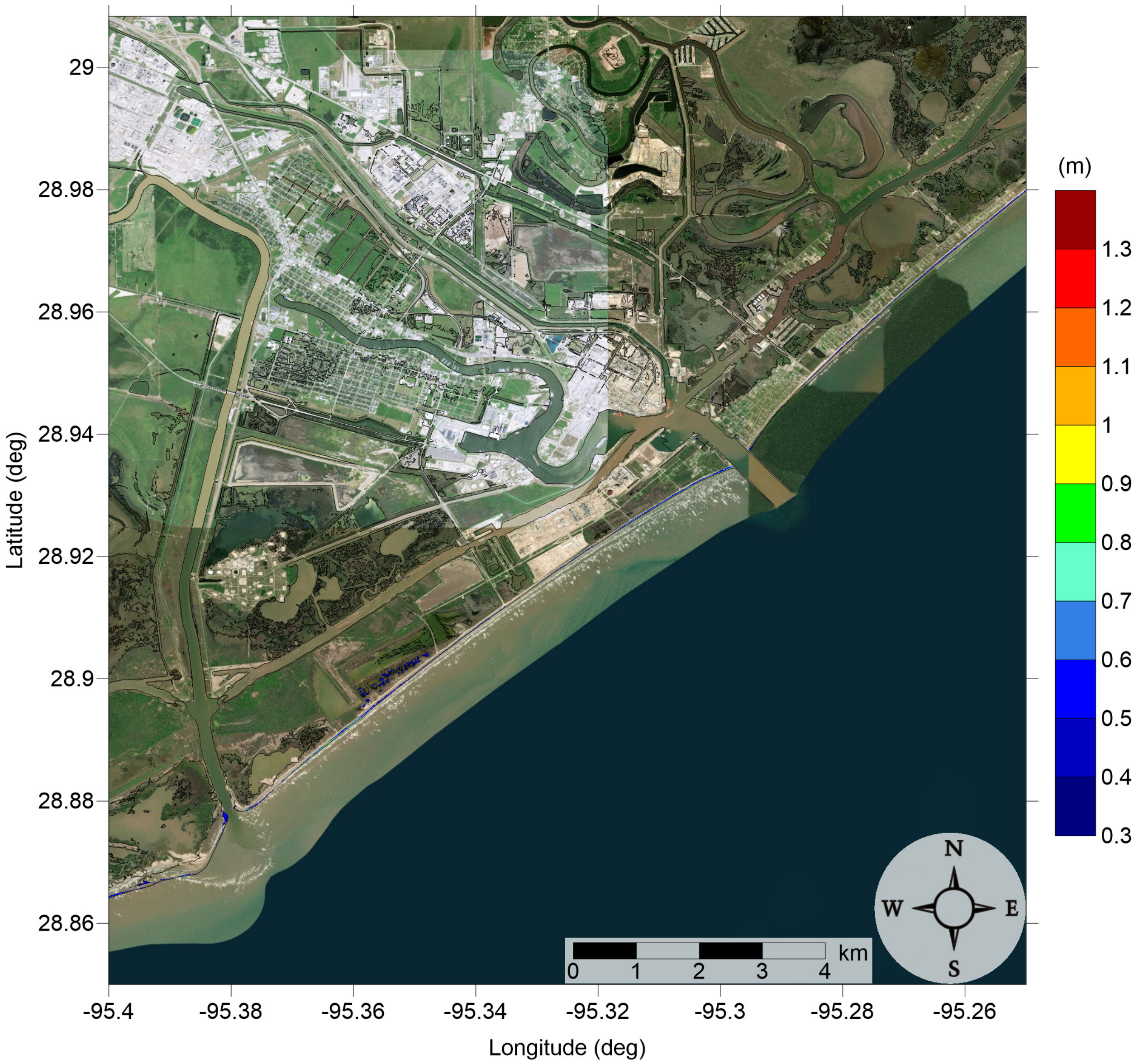

Figure 48: Maximum inundation depth (m) caused by the West Florida submarine landslide in Freeport, TX. Contour drawn is the zero-meter contour for land elevation.

San Luis Pass, TX
West Florida submarine landslide
Maximum Inundation Depth

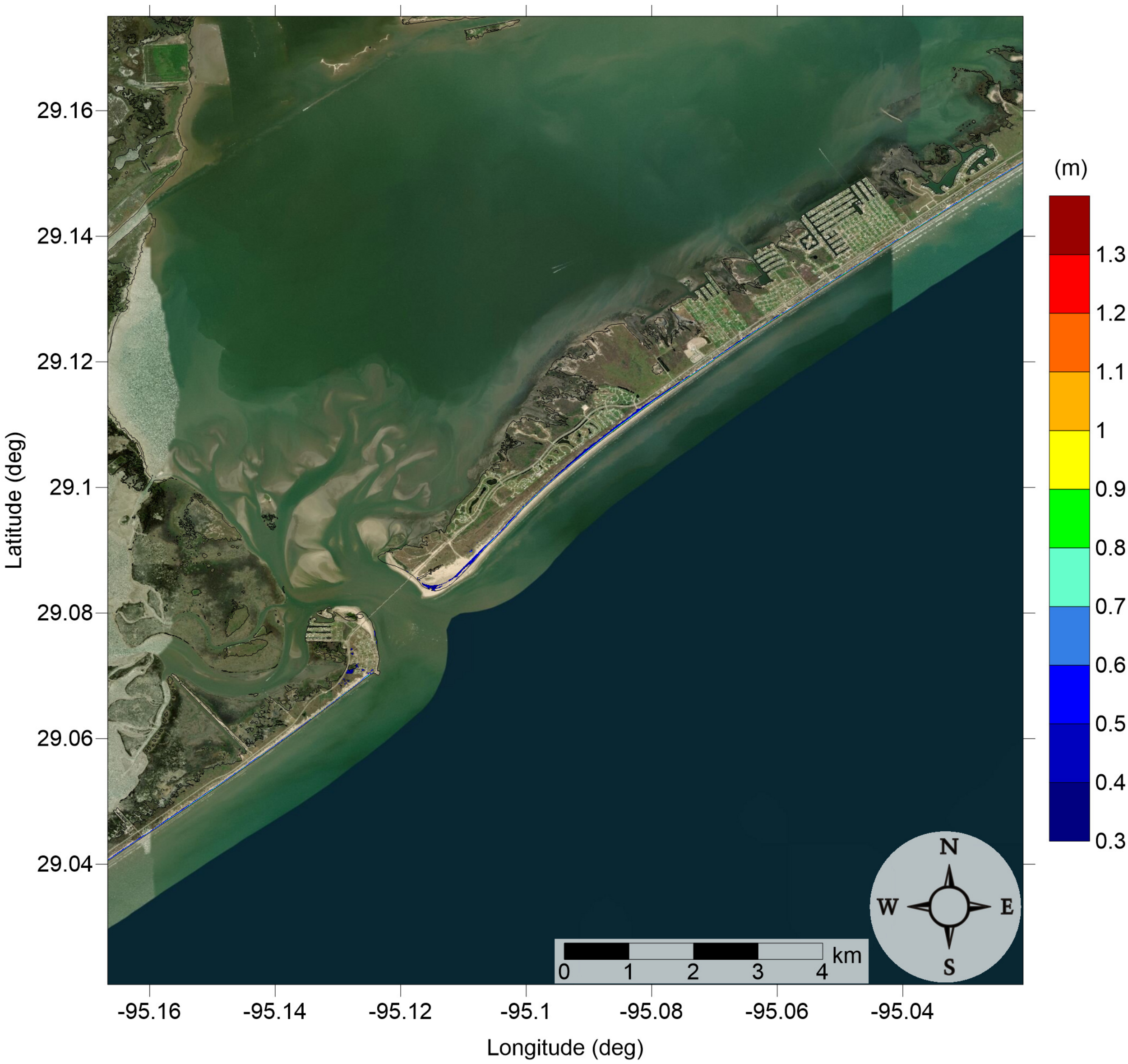

Figure 49: Maximum inundation depth (m) caused by the West Florida submarine landslide in San Luis Pass, TX. Contour drawn is the zero-meter contour for land elevation.

Freeport, TX
Yucatán 3 submarine landslide
Maximum Momentum Flux

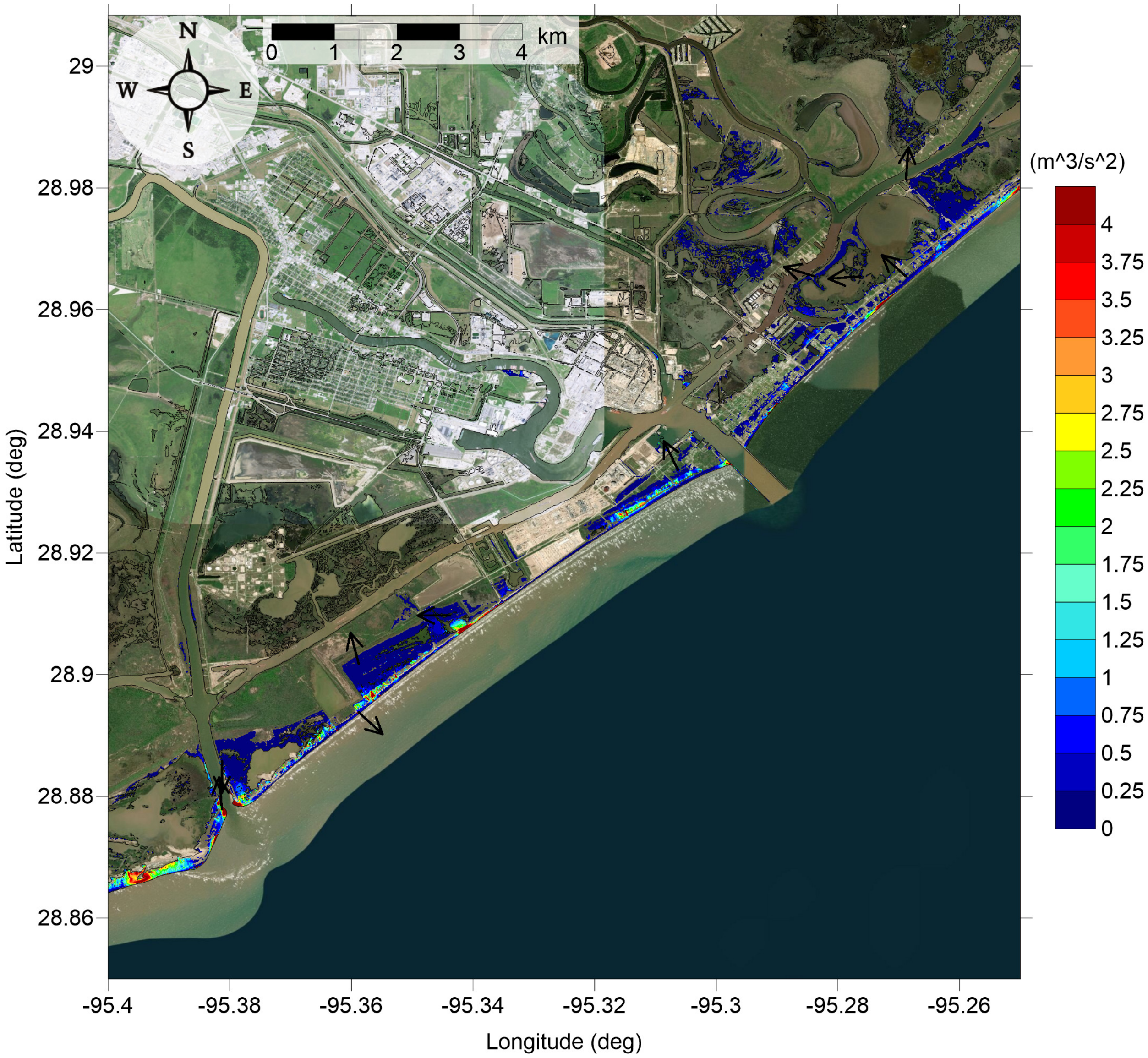

Figure 50: Maximum momentum flux (m^3/s^2) caused by the Yucatán 3 submarine landslide in Freeport, TX. Arrows represent direction of maximum momentum flux. Contour drawn is the zero-meter contour for land elevation.

San Luis Pass, TX
Yucatán 3 submarine landslide
Maximum Momentum Flux

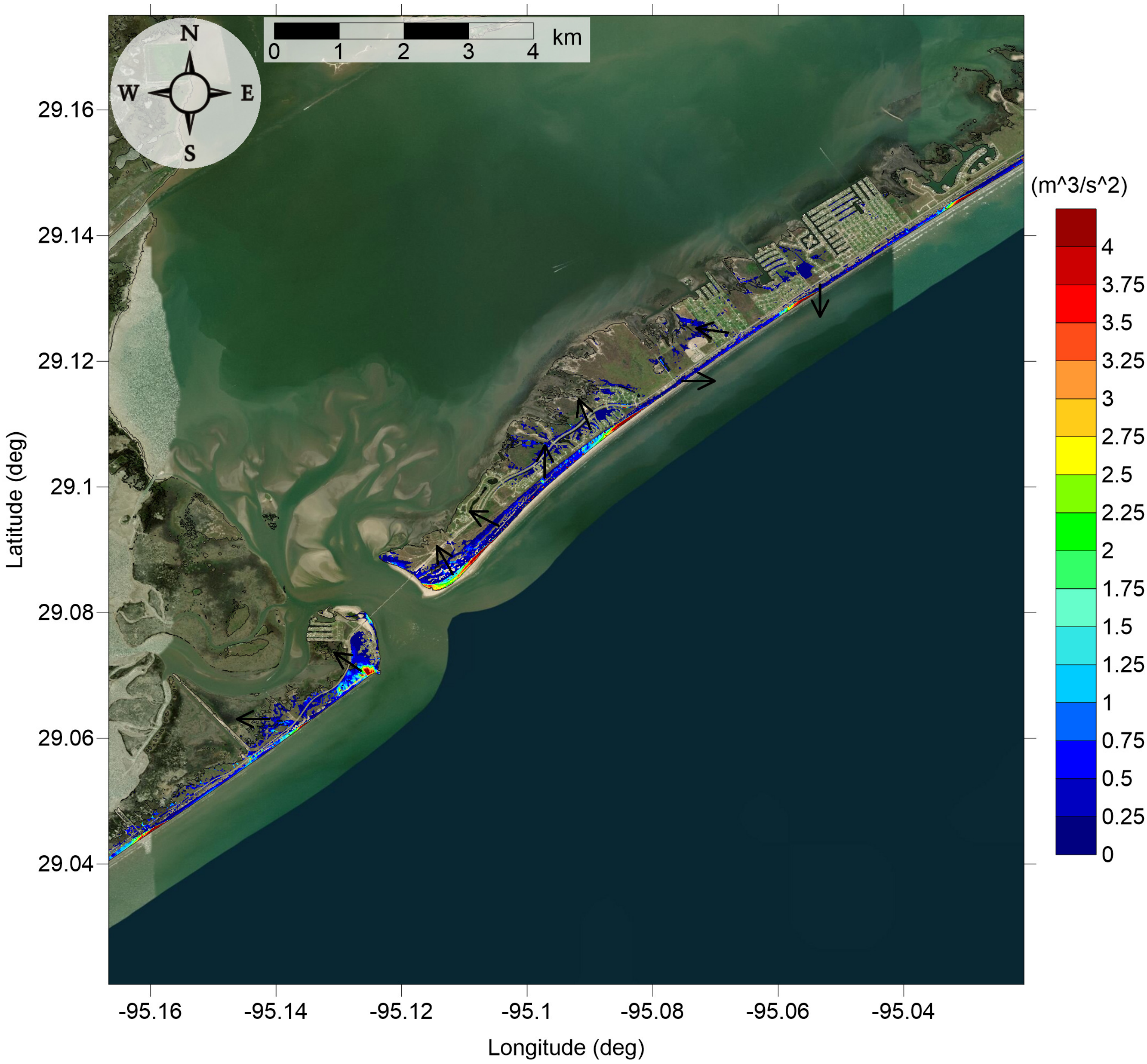

Figure 51: Maximum momentum flux (m^3/s^2) caused by the Yucatán 3 submarine landslide in San Luis Pass, TX. Arrows represent direction of maximum momentum flux. Contour drawn is the zero-meter contour for land elevation.

Freeport, TX
Yucatán 3 submarine landslide
Maximum Inundation Depth

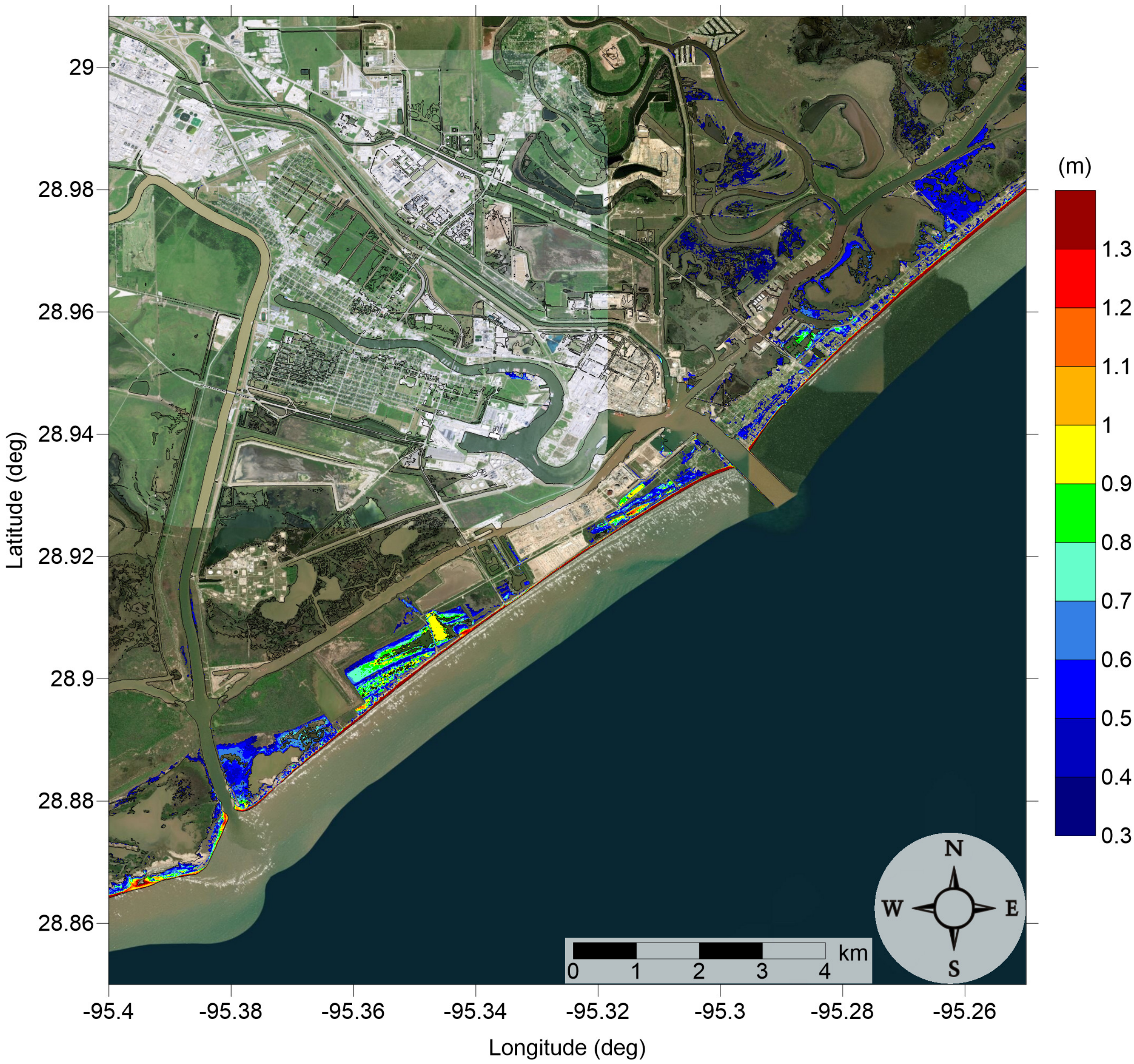

Figure 52: Maximum inundation depth (m) caused by the Yucatán 3 submarine landslide in Freeport, TX. Contour drawn is the zero-meter contour for land elevation.

San Luis Pass, TX
Yucatán 3 submarine landslide
Maximum Inundation Depth

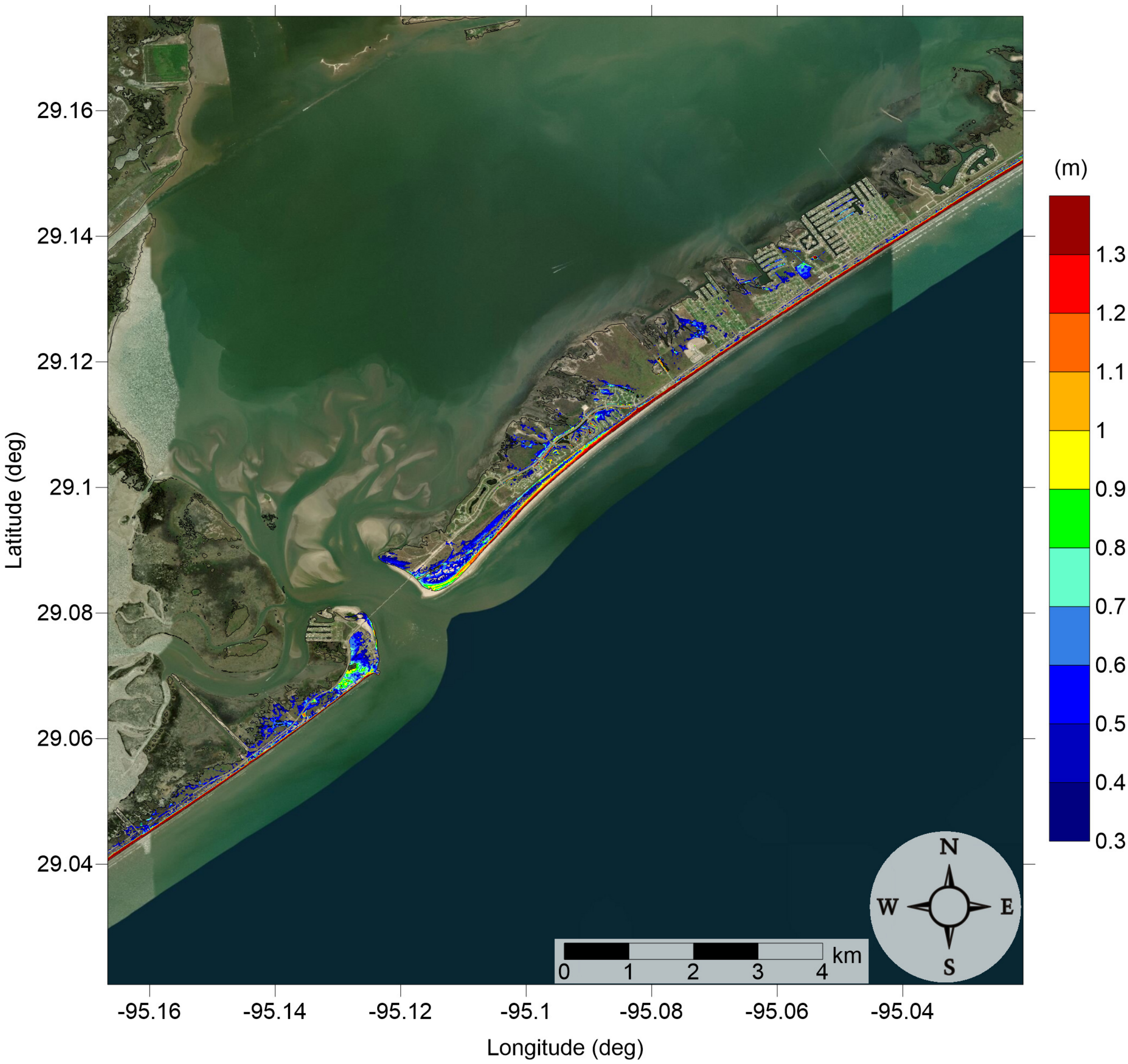

Figure 53: Maximum inundation depth (m) caused by the Yucatán 3 submarine landslide in San Luis Pass, TX. Contour drawn is the zero-meter contour for land elevation.

Freeport, TX
Yucatán 5 submarine landslide
Maximum Momentum Flux

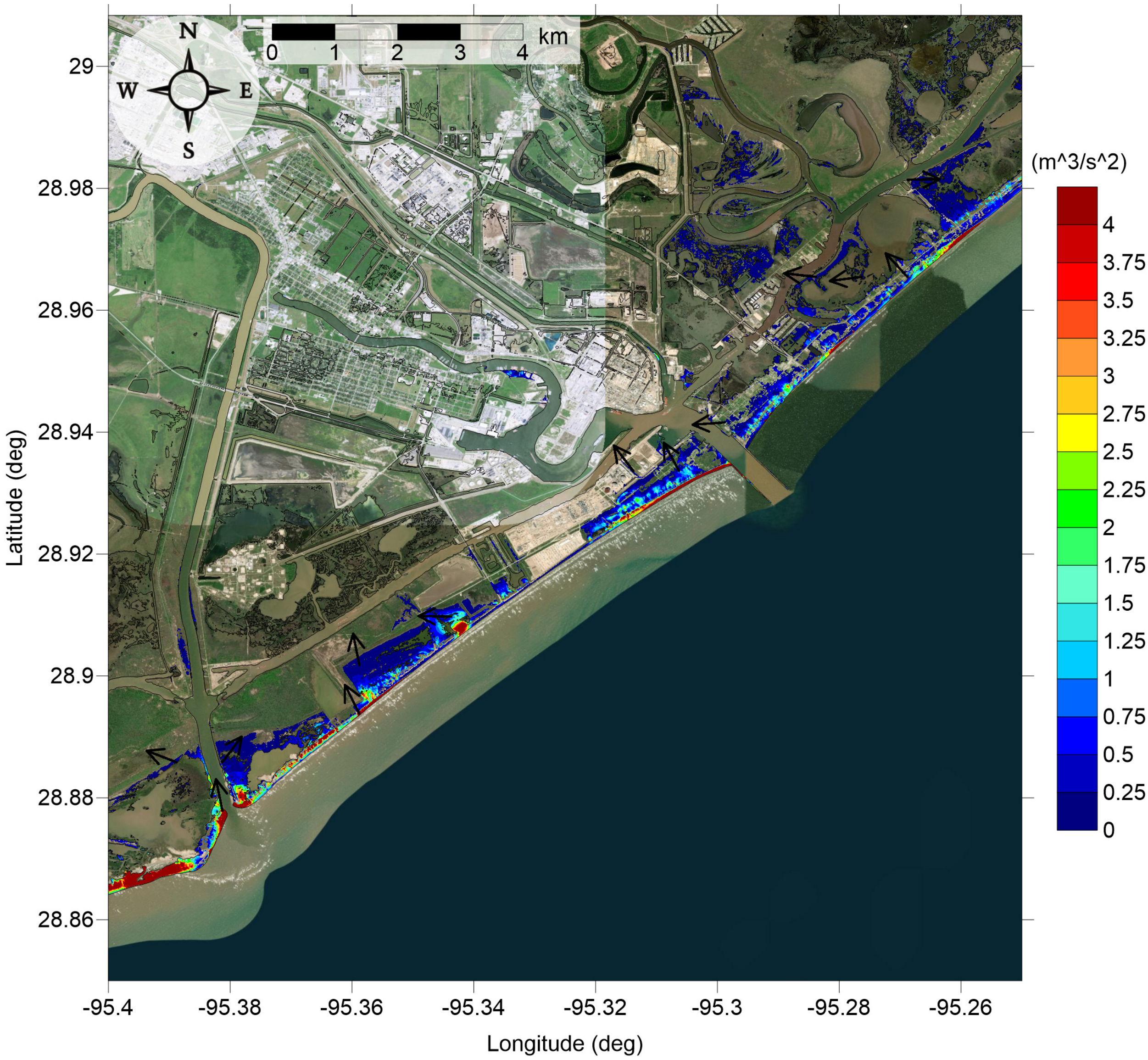

Figure 54: Maximum momentum flux (m^3/s^2) caused by the Yucatán 5 submarine landslide in Freeport, TX. Arrows represent direction of maximum momentum flux. Contour drawn is the zero-meter contour for land elevation.

San Luis Pass, TX
Yucatán 5 submarine landslide
Maximum Momentum Flux

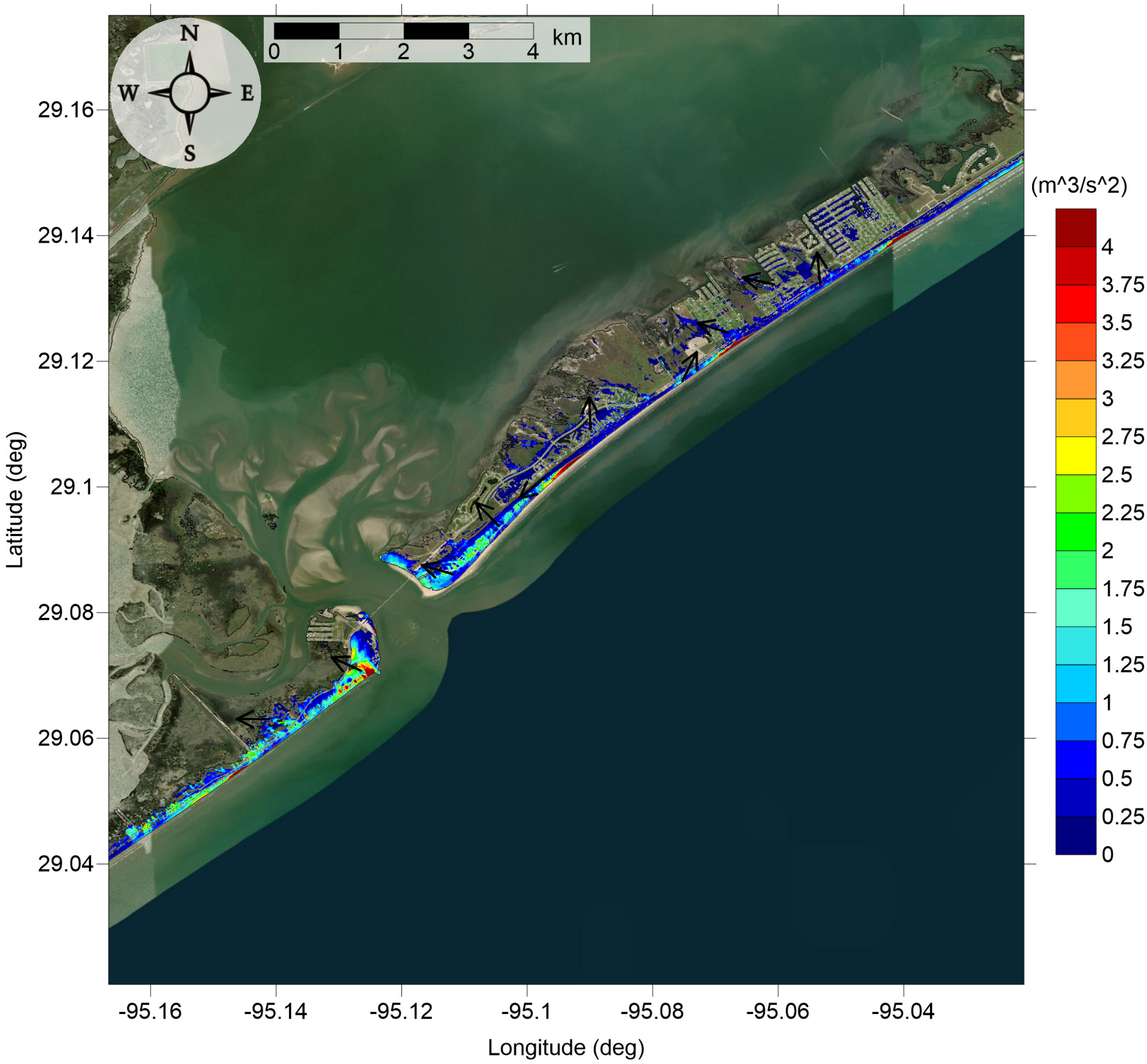

Figure 55: Maximum momentum flux (m^3/s^2) caused by the Yucatán 5 submarine landslide in San Luis Pass, TX. Arrows represent direction of maximum momentum flux. Contour drawn is the zero-meter contour for land elevation.

Freeport, TX
Yucatán 5 submarine landslide
Maximum Inundation Depth

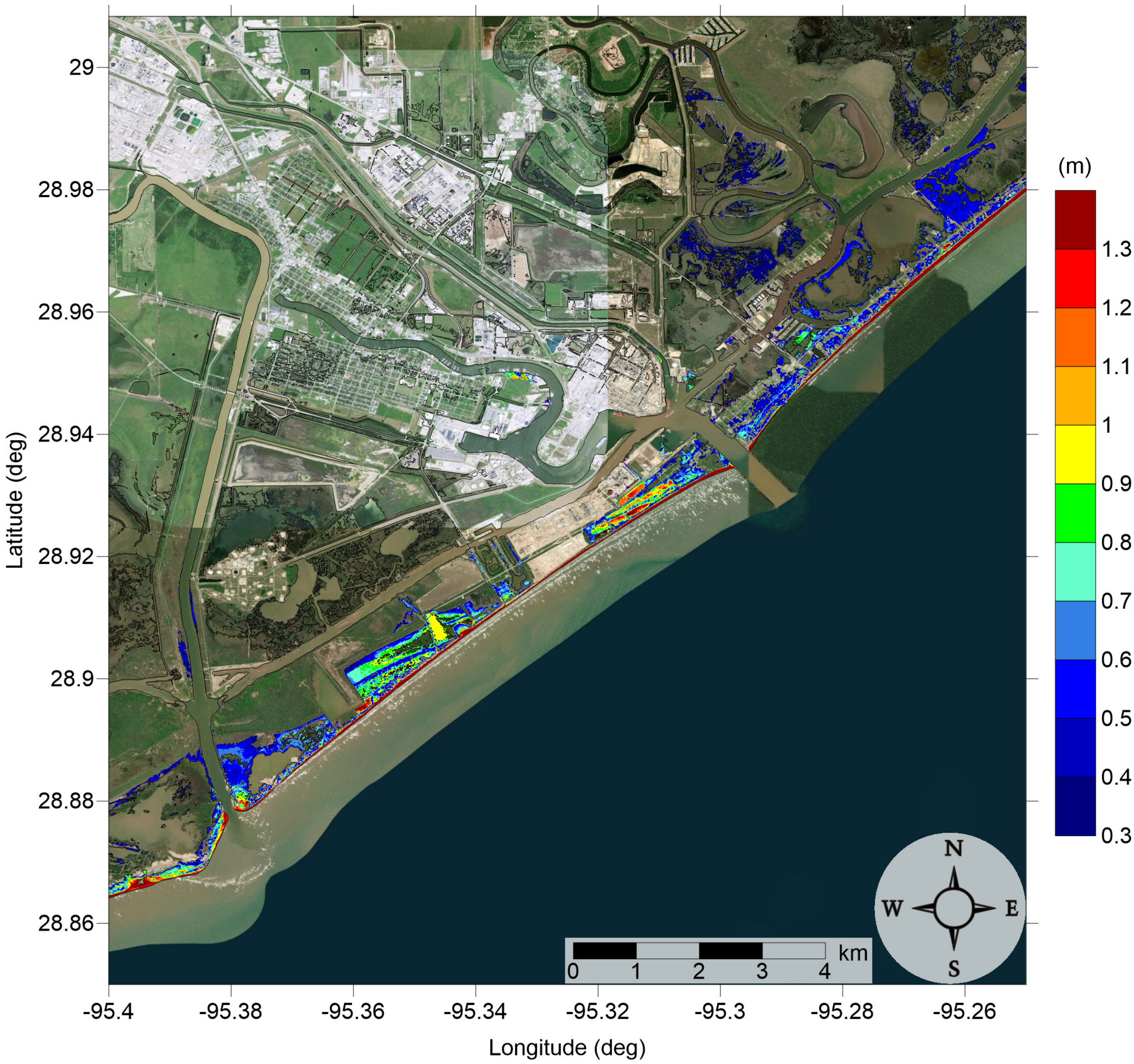

Figure 56: Maximum inundation depth (m) caused by the Yucatán 5 submarine landslide in Freeport, TX. Contour drawn is the zero-meter contour for land elevation.

San Luis Pass, TX
Yucatán 5 submarine landslide
Maximum Inundation Depth

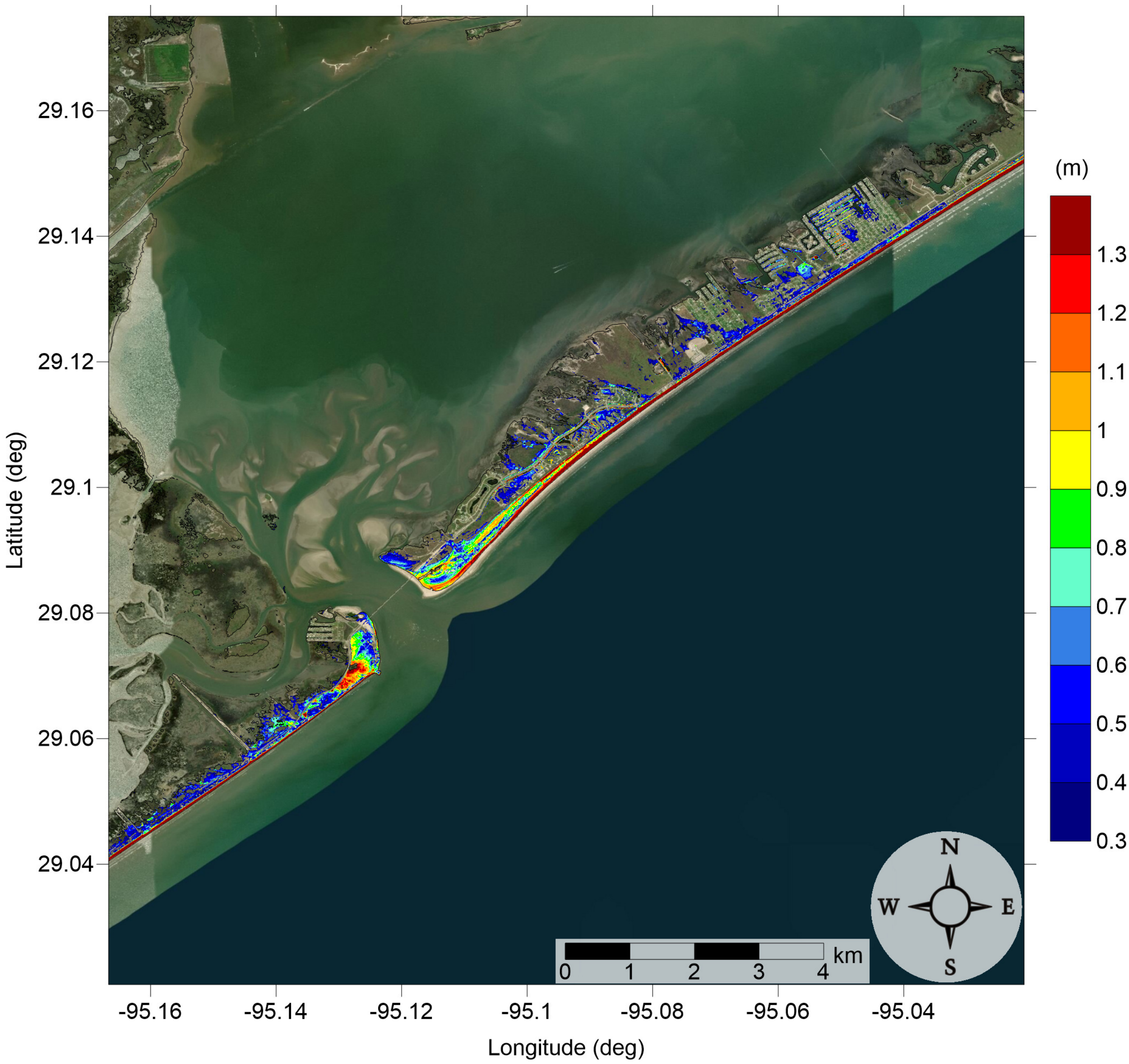

Figure 57: Maximum inundation depth (m) caused by the Yucatán 5 submarine landslide in San Luis Pass, TX. Contour drawn is the zero-meter contour for land elevation.

Freeport, TX
All Sources
Maximum of Maximum Inundation Depth

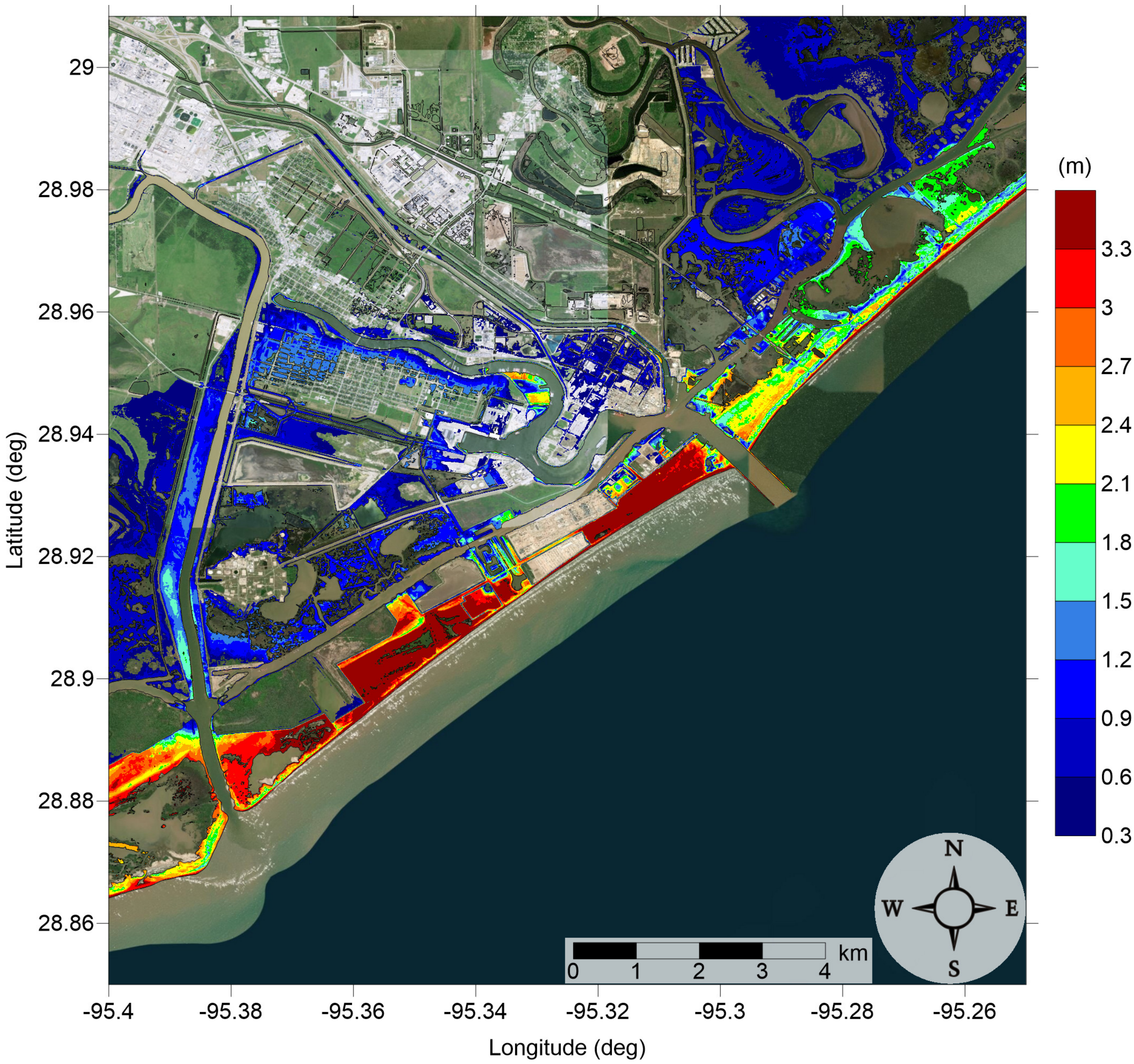

Figure 58: Maximum of maximums inundation depth (m) in Freeport, TX, calculated as the maximum inundation depth in each grid cell from an ensemble of all tsunami sources considered. Contour drawn is the zero-meter contour for land elevation.

Freeport, TX
All Sources
Maximum of Maximum Inundation Depth

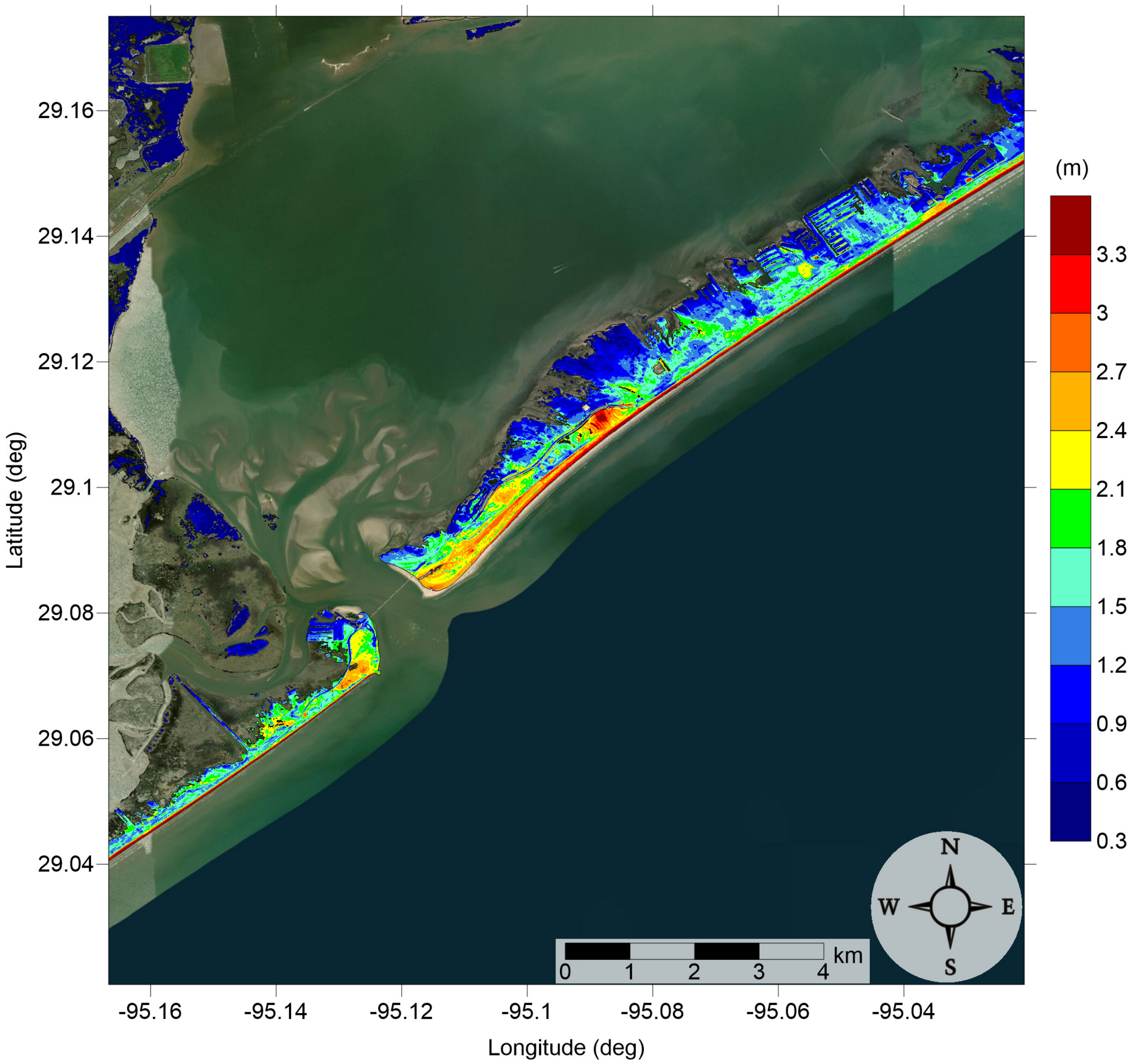

Figure 59: Maximum of maximums inundation depth (m) in San Luis Pass, TX, calculated as the maximum inundation depth in each grid cell from an ensemble of all tsunami sources considered. Contour drawn is the zero-meter contour for land elevation.

Freeport, TX
All Sources
Maximum Inundation Depth by Source

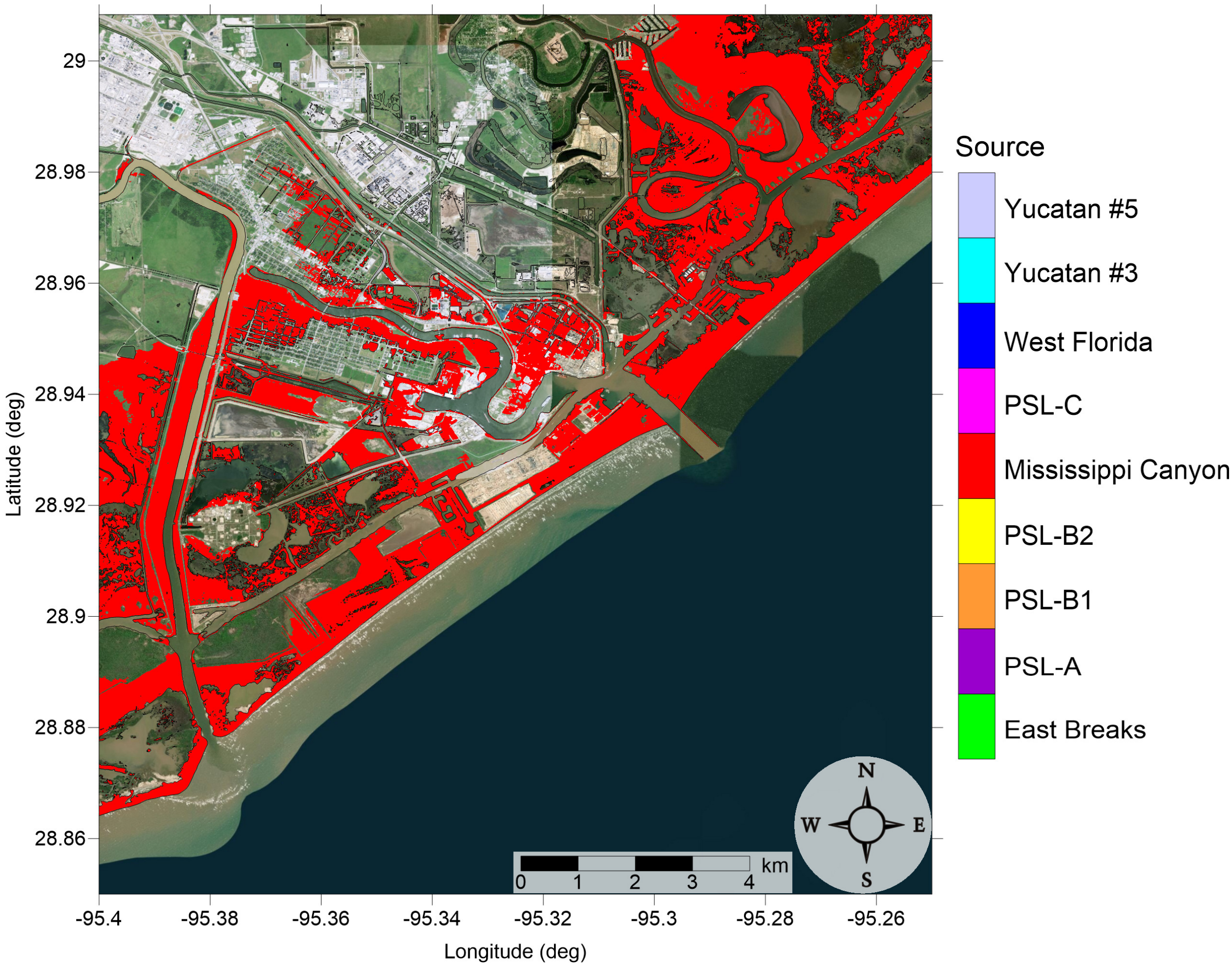

Figure 60: Indication of the tsunami source which causes the maximum of maximums inundation depth (m) in each grid cell from an ensemble of all tsunami sources in Freeport, TX. Contour drawn is the zero-meter contour for land elevation.

Freeport, TX
All Sources
Maximum Inundation Depth by Source

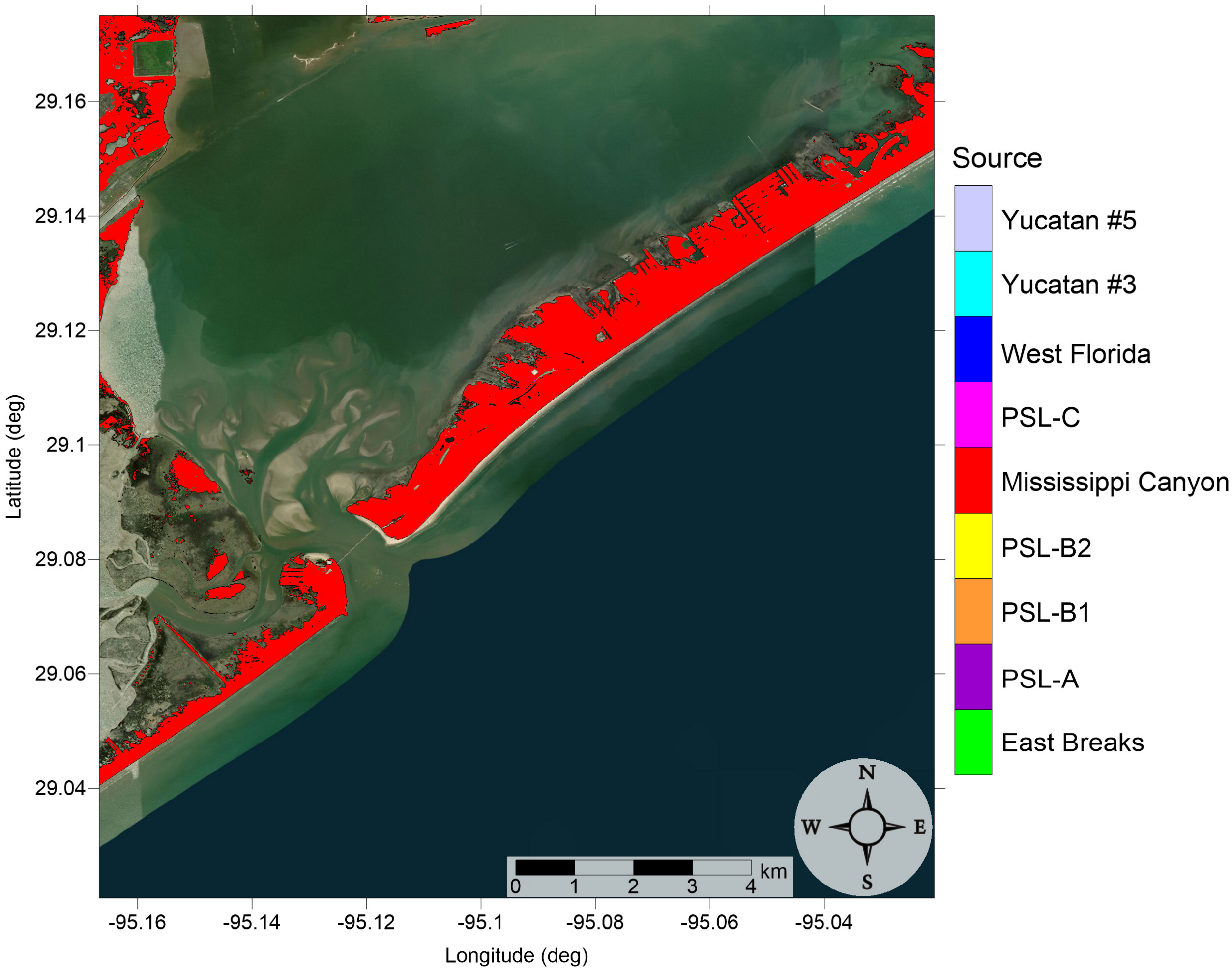

Figure 61: Indication of the tsunami source which causes the maximum of maximums inundation depth (m) in each grid cell from an ensemble of all tsunami sources in San Luis Pass, TX. Contour drawn is the zero-meter contour for land elevation.

5 Tsunami and Hurricane Storm Surge Inundation

Due to the limitations on availability of high-resolution (1/3 arcsecond) DEMs, detailed inundation maps for all communities along the Gulf Coast are not yet possible. In an effort to develop a first-order estimate of potential tsunami inundation for those locations where detailed inundation maps have not yet been developed, we compare tsunami inundation modeled for the communities mentioned above to hurricane storm surge modeled data. The motivation for and implications of this approach are twofold. It provides a way to assess tsunami inundation in un-mapped communities based on existing storm surge flood data and also relates the level of tsunami hazard to that of another hazard that is better defined in this region. Tsunamis are not well-understood as a threat along the Gulf Coast, making tsunami hazard mitigation efforts somewhat difficult. However, hurricane is a relatively well-understood threat in this region, and hurricane preparedness approaches are well-developed. As a result, comparisons of tsunami and hurricane storm surge inundation levels provide a more understandable and accessible idea of the level of hazard presented by potential tsunami events and can serve as a basis for tsunami preparedness efforts.

The hurricane storm surge data used here is available from the Sea, Lake, and Overland Surges from Hurricanes (SLOSH) model (http://www.nhc.noaa.gov/surge/slosh.php). The SLOSH model was developed by the National Weather Service (NWS) to provide estimates of storm surge heights caused by historical, predicted, or hypothetical hurricanes based on different values for atmospheric pressure, hurricane size, forward speed, and track. It uses a polar, elliptical, or hyperbolic grid for computations, leading to higher resolutions near coastal areas of interest. Some limitations of the SLOSH model should be acknowledged. Resolution of the model varies from tens of meters to a kilometer or more. Near the coastal communities of interest here, resolution is on the order of 1 km. Sub-grid scale water and topographic features such as channels, rivers, levees, and roads, are parameterized instead of being explicitly modeled. Despite these limitations, the hurricane storm surge data from the SLOSH model is currently the best data publicly available for our purposes, and efforts have been made to ensure the validity of the SLOSH data in performing comparisons with tsunami inundation.

The SLOSH MOM results provide the worst-case storm surge for a given hurricane category and initial tide level based on a set of model runs with various combinations of parameters such as forward speed, trajectory, and landfall location. To perform the storm surge and tsunami comparisons, SLOSH storm surge elevation data was first converted to meters and adjusted from the NAVD88 to the MHW vertical datum using NOAA's VDatum tool (http://vdatum.noaa.gov/). Due to the relatively low resolution of the SLOSH data as compared to the DEMs used for tsunami modeling, the SLOSH data was interpolated to 1/3 arcsecond (10 m) resolution using a kriging method. Inundation was then determined by subtracting land elevation from the storm surge elevation.

Here, an initial high tide level is used for the SLOSH MOM results in order to compare the worst-case tsunami inundation with a worst-case storm surge scenario. The high tide SLOSH MOM data includes effects of the highest predicted tide level at each location. In comparison, water elevations in the tsunami modeling are based on the MHW datum, which averages the high water levels over the National Tidal Datum Epoch (NTDE). Within the

GOM, tidal ranges are relatively small, with diurnal ranges on the order of 1.5 ft (0.5 m) for most of the communities studied here, and slightly higher at around 2.5 ft (0.8 m) for the west coast of Florida. Thus, differences between highest tide levels and the mean of the highest tide levels are expected to be relatively small, though local bathymetric effects combined with tidal effects can still be significant.

It should be noted that the updated Saffir-Simpson Hurricane Wind Scale which delineates hurricane categories 1-5 does not include storm surge as a component of the measure of hurricane intensity and that other methods may capture the physics of hurricane severity and damage in a more appropriate manner (e.g. Kantha [2006], Basco and Klentzman [2006], Irish and Resio [2010]). However, the SLOSH MOM results take into account thousands of scenarios for a given hurricane category, resulting in a composite worst-case storm surge scenario for each Saffir-Simpson hurricane category. Thus, since hurricane preparedness, storm surge evacuation zones, and hazard mitigation efforts are based on hurricane category assignment, we aim to determine the hurricane category which produces MOM storm surge inundation ζ_h that is a best match to the tsunami MOM inundation ζ_t. That is, we determine the hurricane category which satisfies

$$min_c(|\zeta_{h_c} - \zeta_t|), \qquad c = \text{Cat1,..,Cat5} \tag{1}$$

for each grid cell. The inundation level for the best-match category is denoted $\zeta_{h_{min}}$. The actual difference between hurricane and tsunami inundation levels $\Delta\zeta = \zeta_{h_{min}} - \zeta_t$ then indicates how close of a match the best-match category actually is. Thus, positive values of $\Delta\zeta$ indicate where hurricane storm surge inundation is higher than tsunami inundation, and negative values indicate where tsunami inundation is higher. A common local practice in tsunami modeling is to only consider inundation above a threshold of 0.3 m (1 ft) [Horrillo et al., 2011, 2015]. This is due to the extensive flat and low-lying elevation found along the Gulf Coast. All depths are calculated for tsunami inundation modeling, but inundation less than 0.3 m (1 ft) is considered negligible here for inundation mapping purposes. Thus, comparisons are only made where either the tsunami or hurricane MOM inundation is at least 0.3 m (1 ft). Results for the two selected Gulf Coast communities are given in the following subsections. It is possible that tsunami inundation zone has no hurricane flooding, therefore matching with hurricane category cannot be made.

5.1 Grand Isle, LA

Fig. 20 shows the MOM tsunami inundation affecting Grand Isle, LA. Tsunami completely inundates the whole Fifi Island, Grand Terre Islands, Beauregard Island, and the islands surrouding Raccoon Lake. On Grand Isle, only the area roughly bounded between Anchor Dr. and Santiny Ln. longitudinally and between Louisiana Ave. and Jefferson Ave. is not flooded. Due to being just 60 km north of the Mississippi landslide source, nearly two thirds of the southern Grand Isle is inundated by water over 6 m on average, and inundation diminishes toward the north to over 3 m around Bayou Rigaud. Inundation at Grand Terre Islands and Beauregard Island is generally between 4 and 6 m, while islands surrounding Raccoon Lake and Bay Joyeux is between 3 and 4.5 m. Mississippi Canyon landslide is responsible for the MOM inundation (see Fig. 21).

Fig. 62 shows the hurricane category which best matches the tsunami inundation in Grand Isle, LA. Fig. 63 shows $\Delta\zeta$ for the best-match hurricane category satisfying equation 1 and shown in Fig. 62. The hurricane category that best matches tsunami inundation for the previously mapped communities usually closely follow the MOM tsunami inundation trend, however, because of the close Mississippi landslide source, Grand Isle tsunami inundation exceeds Category 5 by as high as 4 m except for the islands northwest of Bay Joyeux where it is Category 4. Since tsunami inundation exceeds Category 5 hurricane inundation, this indicates that tsunami produces significantly higher water depth even when comparing to the most severe hurricane.

Grand Isle, LA
All Sources
SLOSH Storm Surge and MOM Tsunami Inundation Comparison

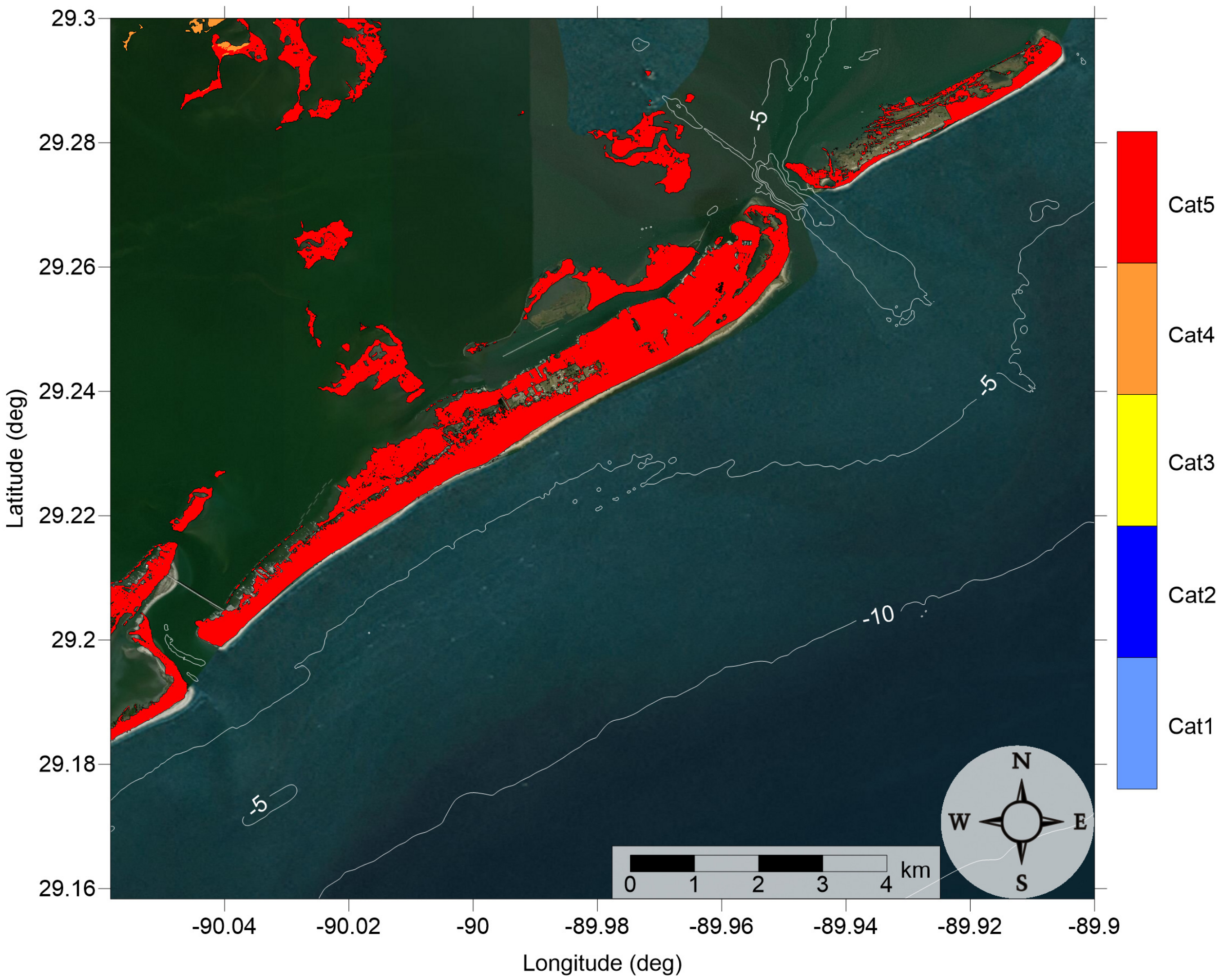

Figure 62: Hurricane category which produces inundation at high tide that best matches the MOM tsunami inundation shown in Figure 20 for Grand Isle, LA. The contours drawn and labeled are at -5 m, -10 m, and -15 m levels.

Grand Isle, LA
All Sources
SLOSH Storm Surge and MOM Tsunami Inundation Comparison

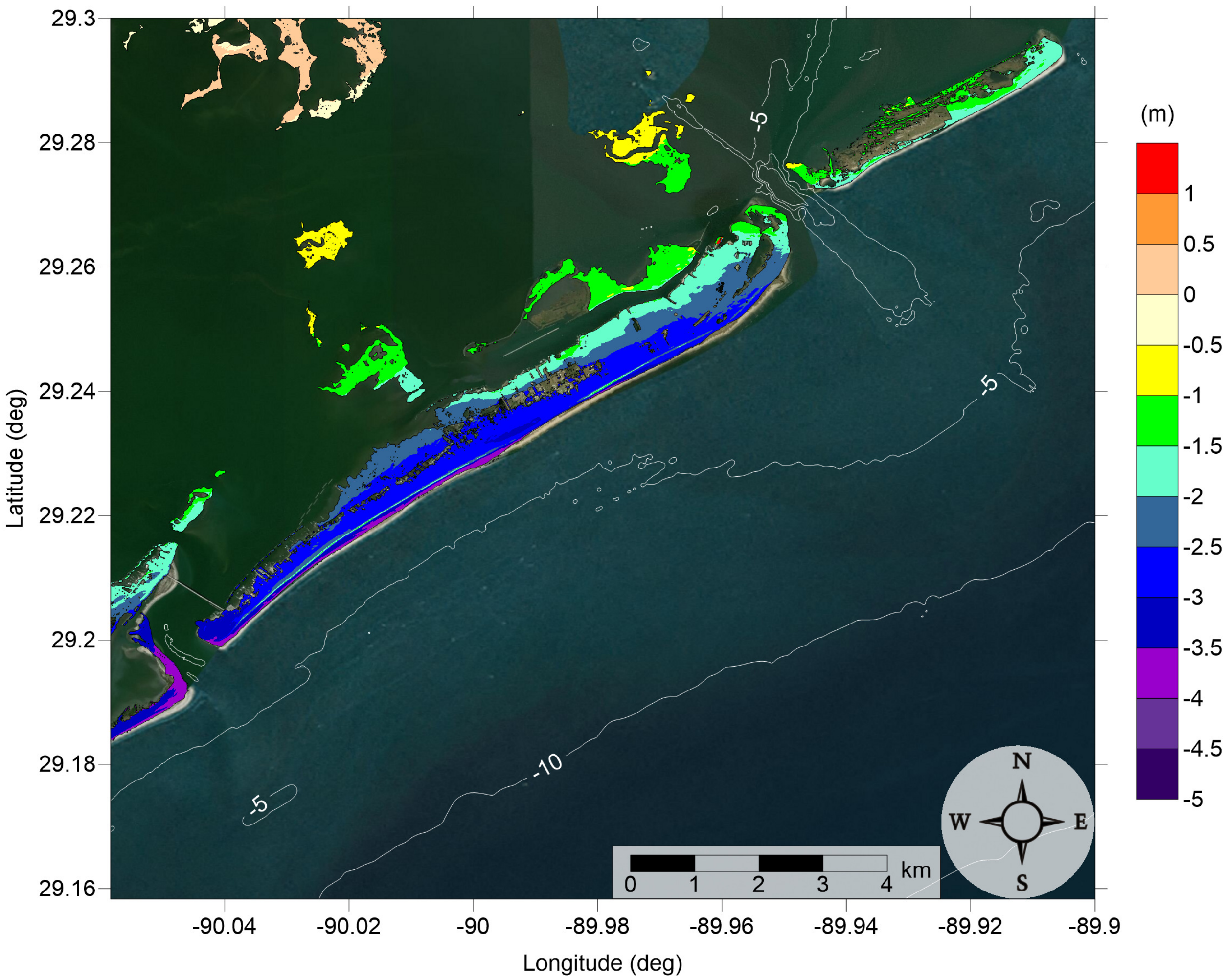

Figure 63: Actual difference $\Delta\zeta$ (in meters) between SLOSH MOM storm surge inundation and MOM tsunami inundation for the best-match hurricane category shown in Figure 62 for Grand Isle, LA. Note that negative values indicate where tsunami inundation is higher than hurricane inundation, and pale colors indicate relatively good agreement between tsunami and storm surge inundation, i.e. $|\Delta\zeta| \leq 0.5$ m. The contours drawn and labeled are at -5 m, -10 m, and -15 m levels.

5.2 Freeport, TX

Freeport, TX

Fig. 58 shows the MOM tsunami inundation affecting Freeport, TX. Overall the barrier island provides nice protection for the mainland against tsunami inundation. While inundation depth at the barrier island ranges from 1 to over 3 m, the mainland is mostly less than 2 m. West of the Freeport jetty, Quintana Beach area is completely inundated by over 3 m water. North of County Rd 723 on the island, the two small communities at Compass Ct. and Deep Sea Dr and Freeport LNG pretreatment facility are flooded with water less than 2 m high. However the roads surrounding these areas are severely flooded with water deeper than 2 m. East of the Freeport jetty, Surfside Beach suffered greater than 3 m water while protecting its residential area where tsunami inundation is generally less than 2 m. Although in general the barrier island is severely inundated as well as its internal roads, the FM 1495 and TX 332, which connect the islands west and east of Freeport jetty respectively, are much less flooded. Over at the mainland, the only area experiencing greater than 2 m inundation is on the west bank of the bend in the Freeport Harbor Channel where Freeport Launch Services is located. The large residential communities surrounding the channel is well protected, except for the area adjacent to the southeast bank of the channel where inundation is generally less than 1.5 m. The Mississippi Canyon landslide is responsible for the MOM inundation (see Fig. 60).

Fig. 64 shows the hurricane category which best matches the tsunami inundation in Freeport, TX. Fig. 65 shows $\Delta\zeta$ for the best-match hurricane category satisfying equation 1 and shown in Fig. 64.

The matching hurricane category distribution closely reflects that of tsunami inundation. West of the Freeport jetty, it is dominated by Category 3 and 4, and Category 2 appears around the two small communities at Compass Ct. and Deep Sea Dr. Category 5 only appears on few scattered spots at the beach. On the east side of the jetty, beachfront corresponds to Category 3 while other parts of the barrier island Category 2. Over at the mainland, the majority of the inundated area corresponds to Category 1, with the exception of two locations. The first area is bounded by W 2nd St and W 9th St, and Levee Rd and Locust St, that corresponds to Category 3. The second is the channel bend at Freeport Launch Services that is Category 2. The difference between hurricane flooding and tsunami inundation $\Delta\zeta$ is generally within $\pm$ 0.5 m.

San Luis Pass, TX

Fig. 59 shows the MOM tsunami inundation affecting San Luis Pass, TX. San Luis Pass is also significantly impacted. The inundation pattern is similar to Surfside Beach, where the immediate beachfront has 3 m water depth and it tapers toward the bay. On the west end of the Galveston barrier island up to Salt Cedar Dr, it is more inundated due to San Luis Pass Rd making a turn and the high elevation of the road. The Mississippi Canyon landslide is also responsible for the MOM inundation (see Fig. 61). The marsh of Inner Clam Bay is flooded with water depth greater than 2 m, but this area is not populated.

Fig. 66 shows the hurricane category which best matches the tsunami inundation in San

Luis Pass, TX. Fig. 67 shows $\Delta\zeta$ for the best-match hurricane category satisfying equation 1 and shown in Fig. 66.

The San Luis Pass area is clearly divided into three tiers following the inundation pattern. South of San Luis Pass Rd is dominated by Category 3, and it transitioned into Category 2 on the other side of the road and finally to Category 1 at the bayside barrier island coast. The difference between hurricane flooding and tsunami inundation is larger than 1 m (hurricane $>$ tsunami) around the Chocolate Bay, and less than 0.5 m (absolute value) at the barrier island.

Freeport, TX
All Sources
SLOSH Storm Surge and MOM Tsunami Inundation Comparison

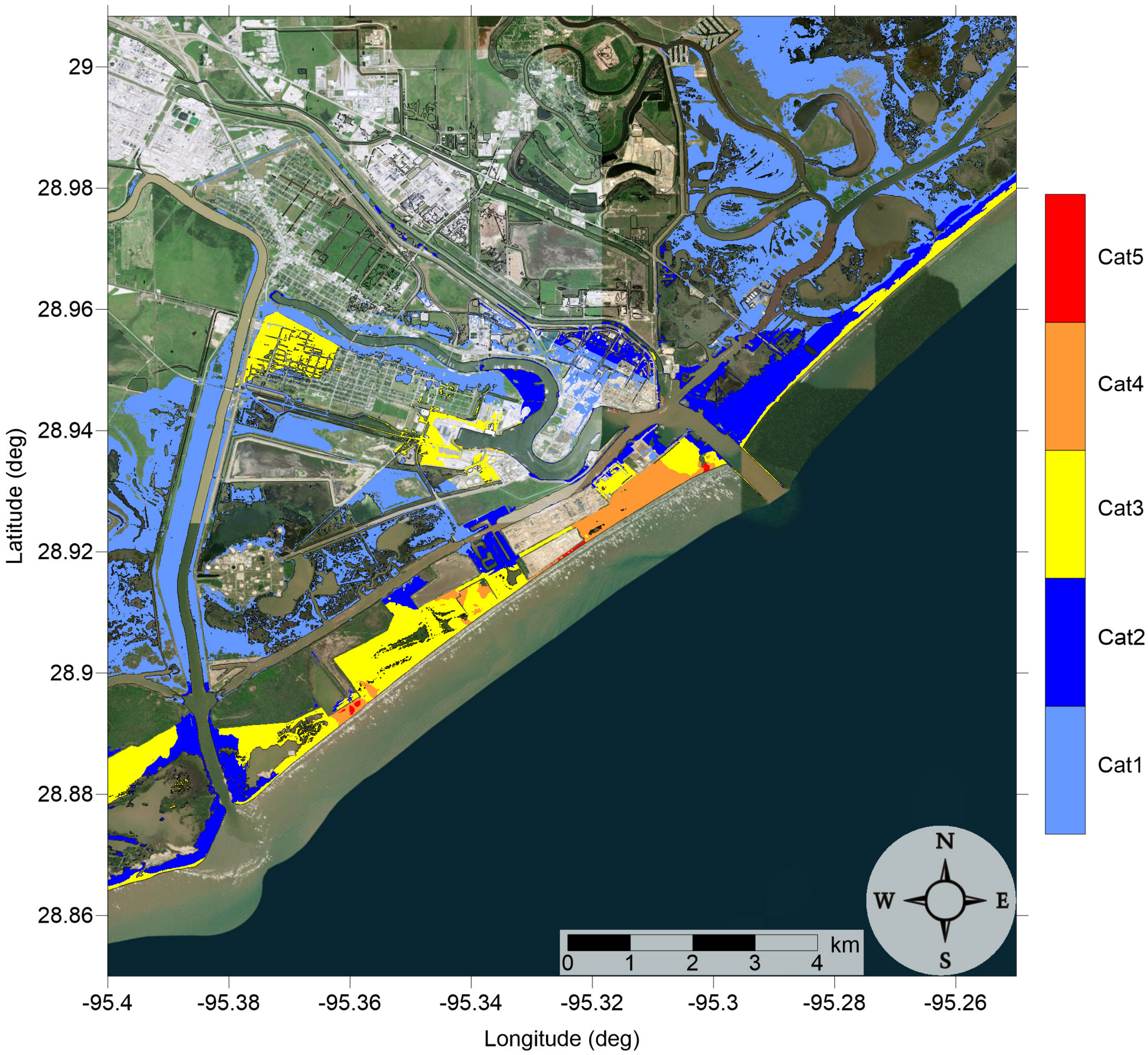

Figure 64: Hurricane category which produces inundation at high tide that best matches the MOM tsunami inundation shown in Figure 58 for Freeport, TX. The contours drawn and labeled are at -5 m, -10 m, and -15 m levels.

Freeport, TX
All Sources
SLOSH Storm Surge and MOM Tsunami Inundation Comparison

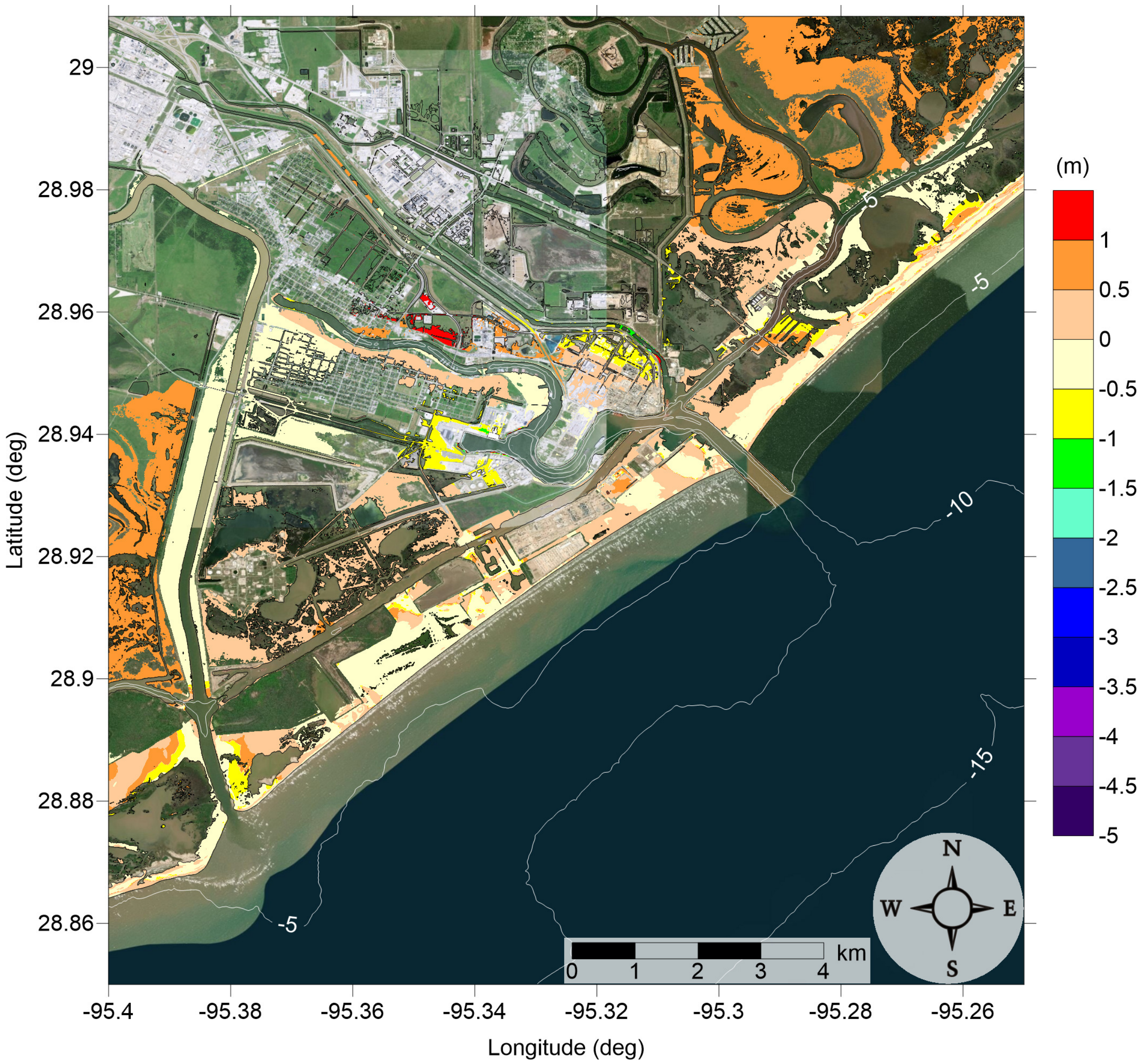

Figure 65: Actual difference $\Delta\zeta$ (in meters) between SLOSH MOM storm surge inundation and MOM tsunami inundation for the best-match hurricane category shown in Figure 64 for Freeport, TX. Note that negative values indicate where tsunami inundation is higher than hurricane inundation, and pale colors indicate relatively good agreement between tsunami and storm surge inundation, i.e. $|\Delta\zeta| \leq 0.5$ m. The contours drawn and labeled are at -5 m, -10 m, and -15 m levels.

San Luis Pass, TX
All Sources
SLOSH Storm Surge and MOM Tsunami Inundation Comparison

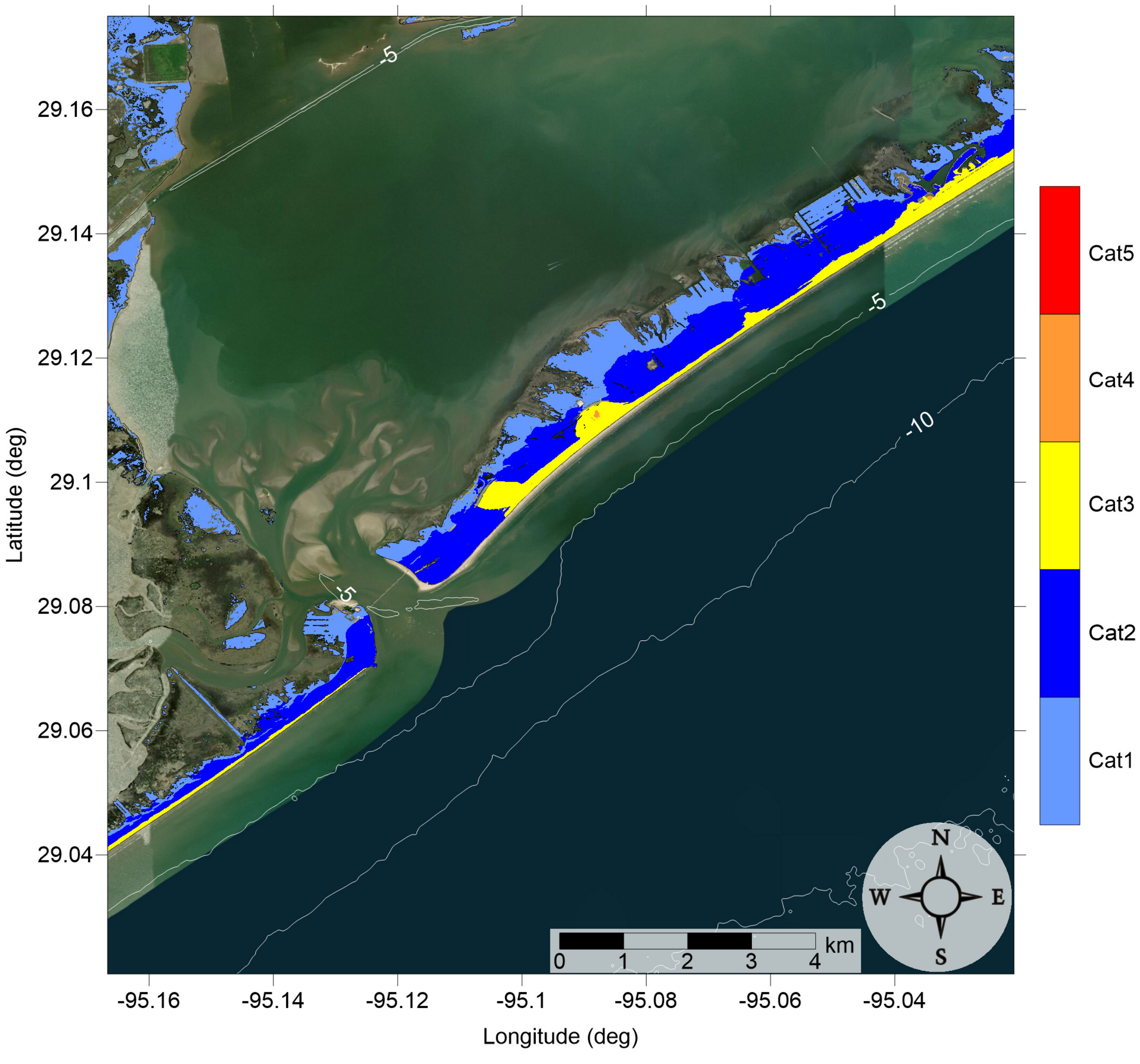

Figure 66: Hurricane category which produces inundation at high tide that best matches the MOM tsunami inundation shown in Figure 59 for San Luis Pass, TX. The contours drawn and labeled are at -5 m, -10 m, and -15 m levels.

San Luis Pass, TX
All Sources
SLOSH Storm Surge and MOM Tsunami Inundation Comparison

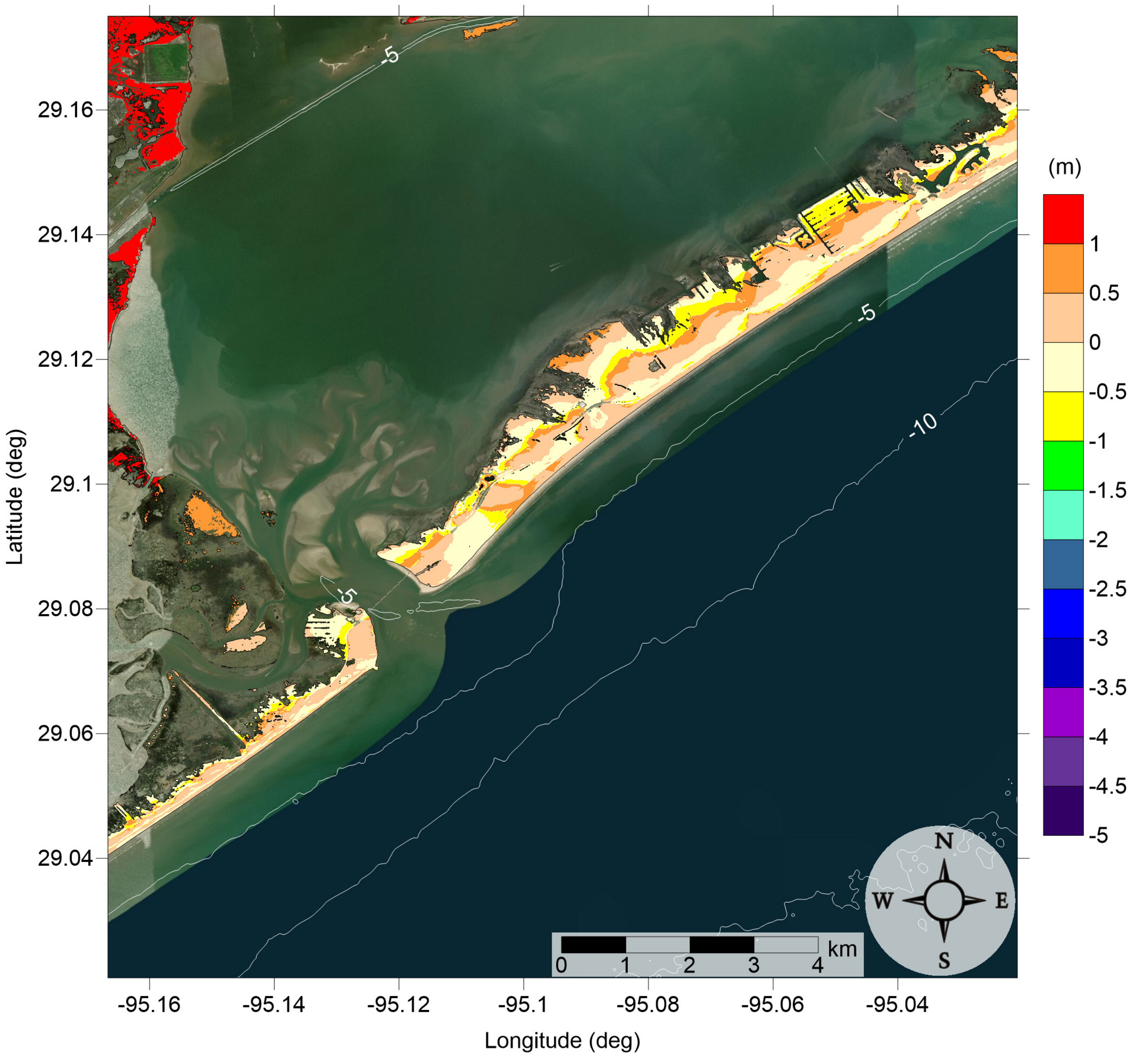

Figure 67: Actual difference $\Delta\zeta$ (in meters) between SLOSH MOM storm surge inundation and MOM tsunami inundation for the best-match hurricane category shown in Figure 66 for San Luis Pass, TX. Note that negative values indicate where tsunami inundation is higher than hurricane inundation, and pale colors indicate relatively good agreement between tsunami and storm surge inundation, i.e. $|\Delta\zeta| \leq 0.5$ m. The contours drawn and labeled are at -5 m, -10 m, and -15 m levels.

6 Tsunami Maritime Products

Accurate estimates of tsunami wave amplitude do not necessarily equate to the prediction of localized damaging currents in a basin or harbor [Lynett et al., 2012]. Furthermore, damage potential in ports is strongly related to the current speed. Therefore, tsunami hazard mitigation products need to be advanced to predict damage potential in basins or harbors. Recent tsunamis have shown that the maritime community requires additional information and guidance about tsunami hazards and post-tsunami recovery [Wilson et al., 2012, 2013]. To accomplish mapping and modeling activities to meet NTHMP's planning/response purposes for the maritime community and port emergency management and other customer requirements, it is necessary to continue the process to include maritime products in our current inundation map development. These maritime products will help identify impact specifically on ship channels, bay inlets, harbors, marinas, and oil infrastructures (e.g., designated lightering and oil tanker waiting zones).

In this study, Grand Isle, LA and Freeport, TX are added to the maritime portfolio, where tsunami hazard maritime products such as tsunami current magnitude, vorticity, safe/hazard zones are included. This work is based on our pilot tsunami maritime study conducted in the Galveston Bay in Horrillo et al. [2016], and later extended to another nine locations, South Padre Island, TX, Mobile, AL, Panama City, FL, and Tampa, FL, Pensacola, FL, Key West, FL, Okaloosa County, FL, Santa Rosa County, FL and Mustang Island, TX, which were reported in Horrillo et al. [2017], and Osprey-Venice-Englewood, FL and Sanibel Island-Naples, FL in Horrillo et al. [2018].

Lynett et al. [2014] complied a general relationship between tsunami current speed and harbor damage based on observational data, in which the current speed is divided into four ranges of damaging potential, 0 - 3 knots means unharmful currents, 3 - 6 knots corresponds to minor-to-moderate damage, 6 - 9 knots moderate-to-major damage, and over 9 knots extreme damage. Since the extent of damage is very location-dependent, to make the text concise, we associate 0 - 3 knots to unharmful currents, 3 - 6 knots to minor damage, 6 - 9 knots to moderate damage, and finally over 9 knots to major damage. The four levels are denoted with white, blue, yellow and red colors, respectively, for all the velocity contour plots within our velocity maritime products.

Using this damage-to-speed relationship, we have plotted the maximum of maximum depth-averaged velocity for each computational subdomain of the two new communities. Fig. 68 shows the minimum offshore safe depth (approximately 200 m or 100 fathoms), and the maximum of maximum velocity magnitude contour plot across the entire Gulf of Mexico (15 arcsecond resolution) for all landslide scenarios (Eastbreaks, PSL-A, PSL-B1, PSL-B2, Mississippi Canyon, PSL-C, West Florida, Yucatántán #3 and Yucatántán #5). Potential damaging currents (> 3 knots, blue, yellow and red areas) tend to be present in most of the area shallower than the minimum offshore safe depth. However, damaging currents could reach areas deeper than 200 m close to most of the landslide generation regions. Major damaging currents (> 9 knots, red) can be expected in most of the landslide generation regions, in the continental shelf adjacent to Mississippi Canyon, offshore northwest Florida, and Yucatán shelf. Moderate (> 6 knots and < 9 knots, yellow) damaging current areas are scattered over the continental shelf, but mostly close to areas with major damage currents.

All locations
All Sources
Maximum of Maximum Velocity Magnitude

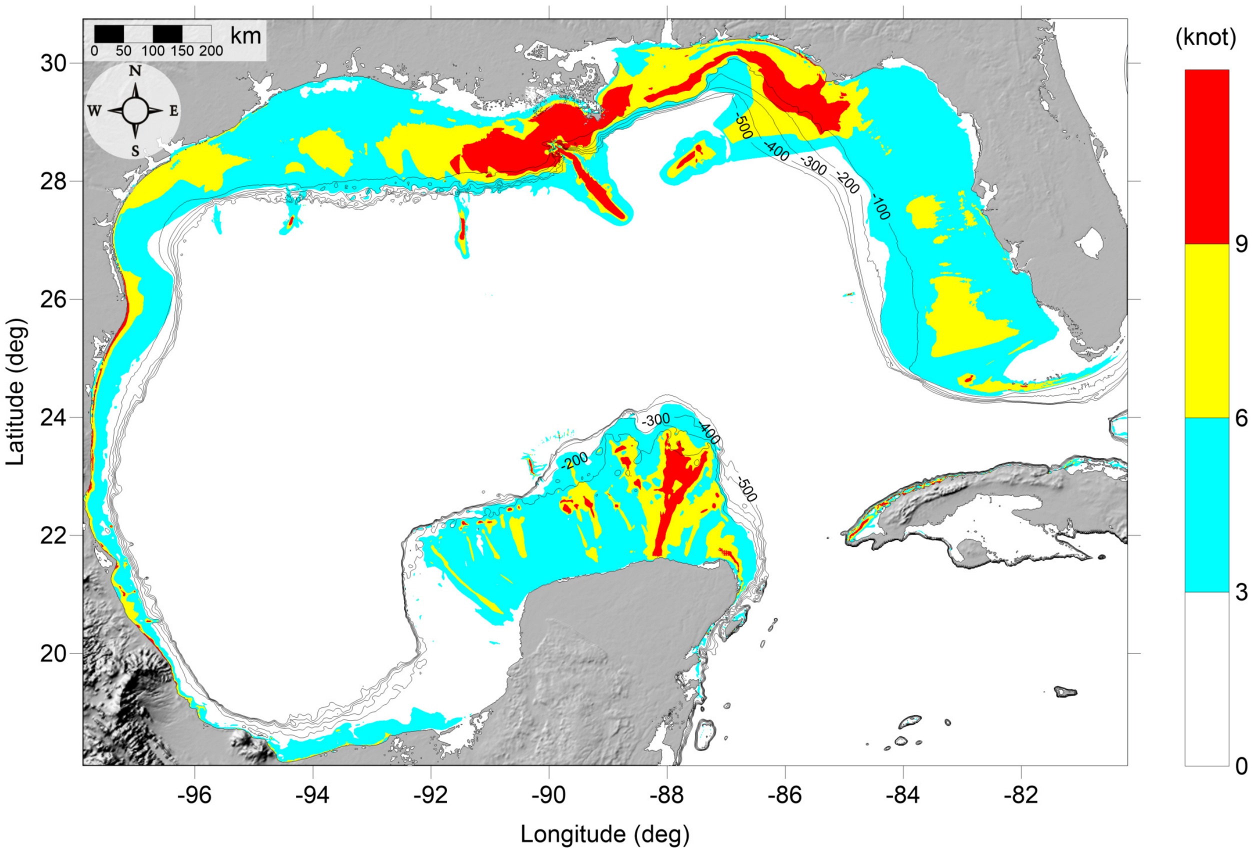

Figure 68: Maximum of maximum velocity magnitude contour in GOM for all landslide scenarios and all locations.

The MOM velocity magnitude (damaging potential) contour maps and the MOM vorticity magnitude contour maps for the finer computational subdomains of Grand Isle, LA and Freeport, TX are presented from Fig. 69 to Fig. 78.

General trends can be observed from the different domain levels of the MOM velocity for Grand Isle, LA. In the vicinity of the barrier island and the open ocean, there are mostly major damaging currents ($>$ 9 knots, red). Again the large area of major damaging currents is attributed to the nearby Mississippi landslide source. Current velocity decreases toward the mainland with contour lines following the orientation of the barrier islands.

In Freeport, TX, the situation is much less severe than Grand Isle, LA. Major damaging current area appears as a thin strip seaward of the barrier island and diminishes toward the gulf to minor currents. In the interior bays and channels, the tsunami currents are less severe which can be used as shelter to minimize tsunami impact.

6.1 Grand Isle, LA

Grand Isle, LA
All Sources
Maximum of Maximum Velocity Magnitude

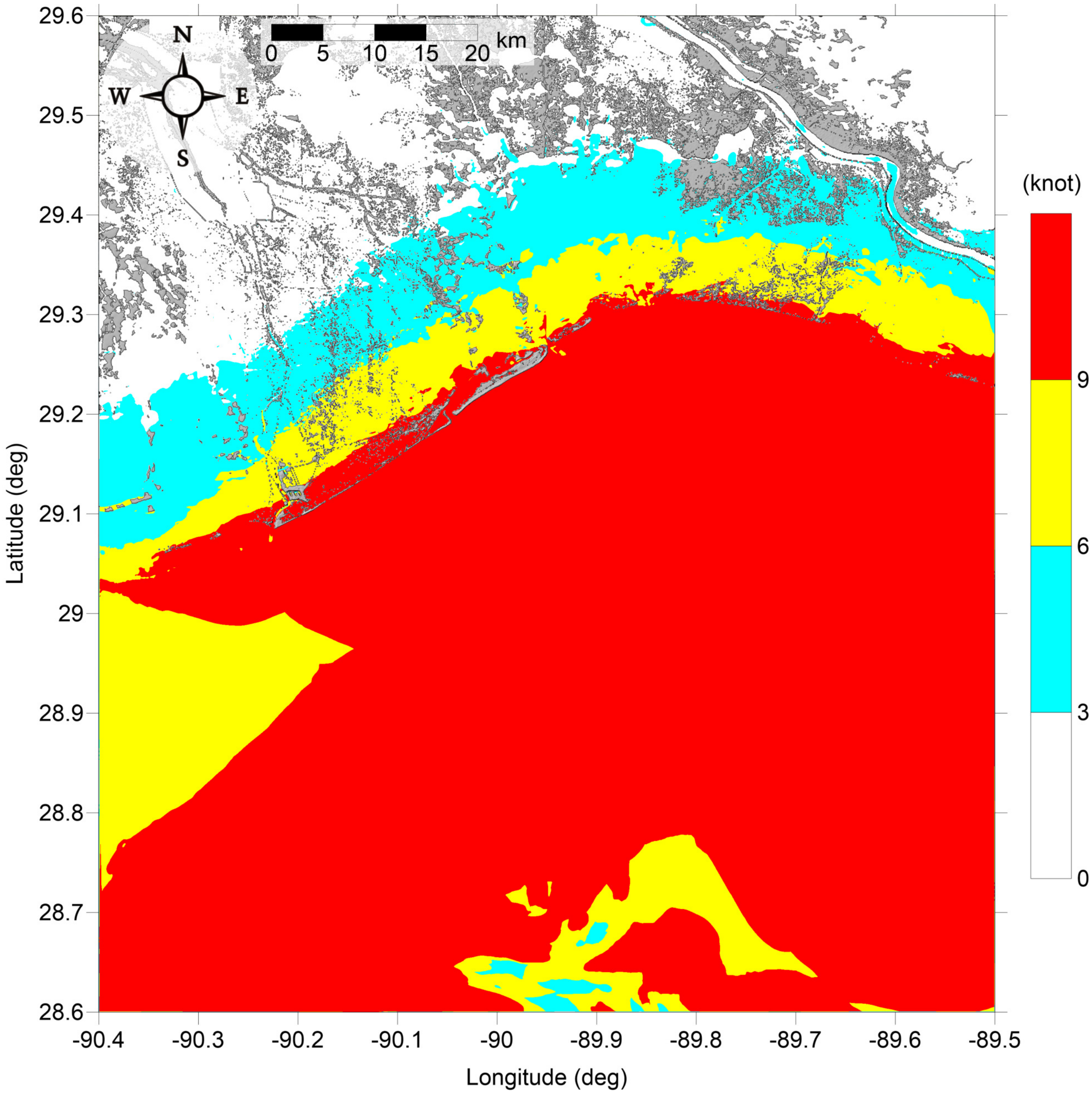

Figure 69: Maximum of maximum velocity magnitude contour in Grand Isle, LA (Grid 2 - 3 arcsecond) for all landslide scenarios.

Grand Isle, LA
All Sources
Maximum of Maximum Velocity Magnitude

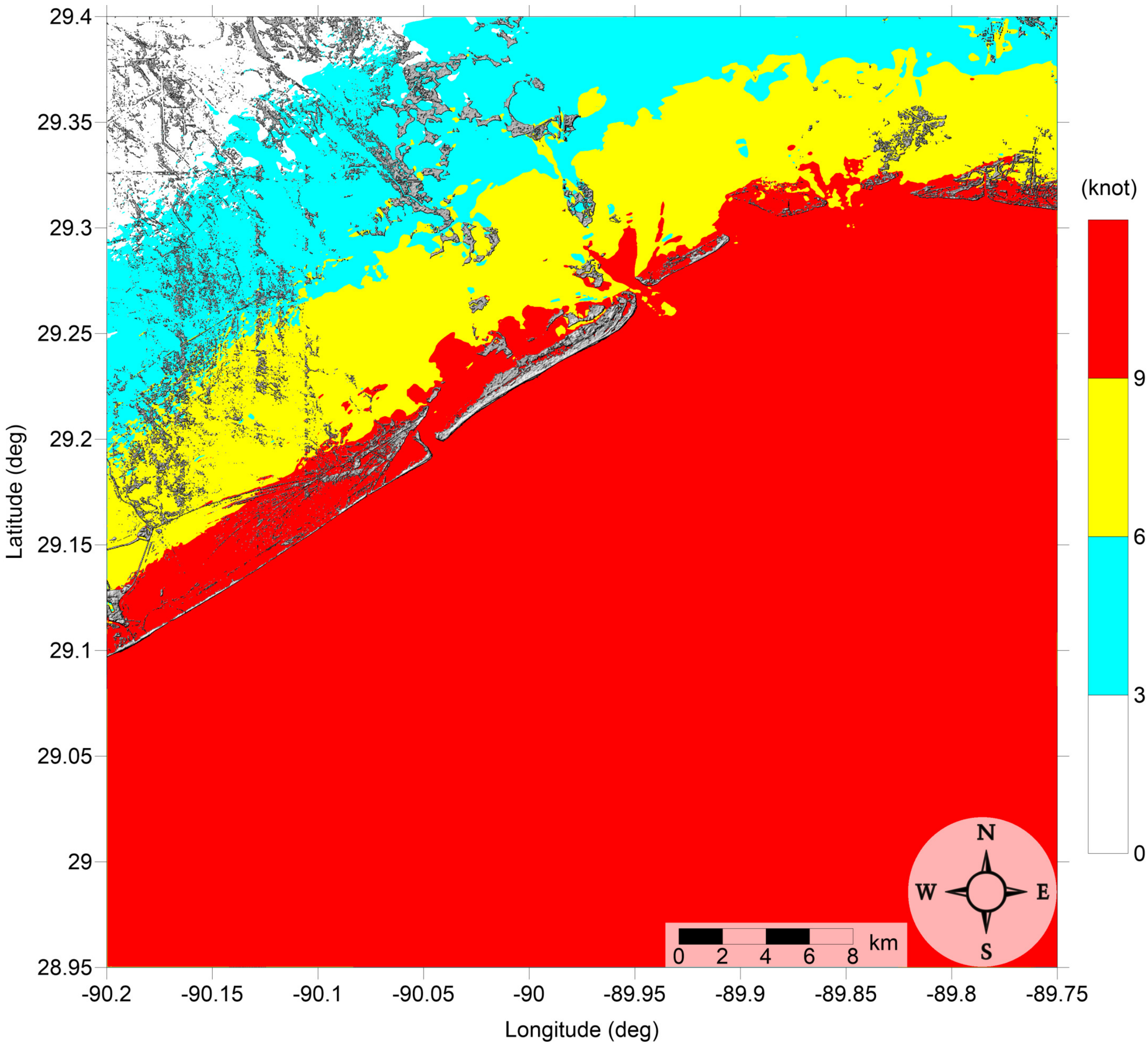

Figure 70: Maximum of maximum velocity magnitude contour in Grand Isle, LA (Grid 3 - 1 arcsecond) for all landslide scenarios.

Grand Isle, LA
All Sources
Maximum of Maximum Velocity Magnitude

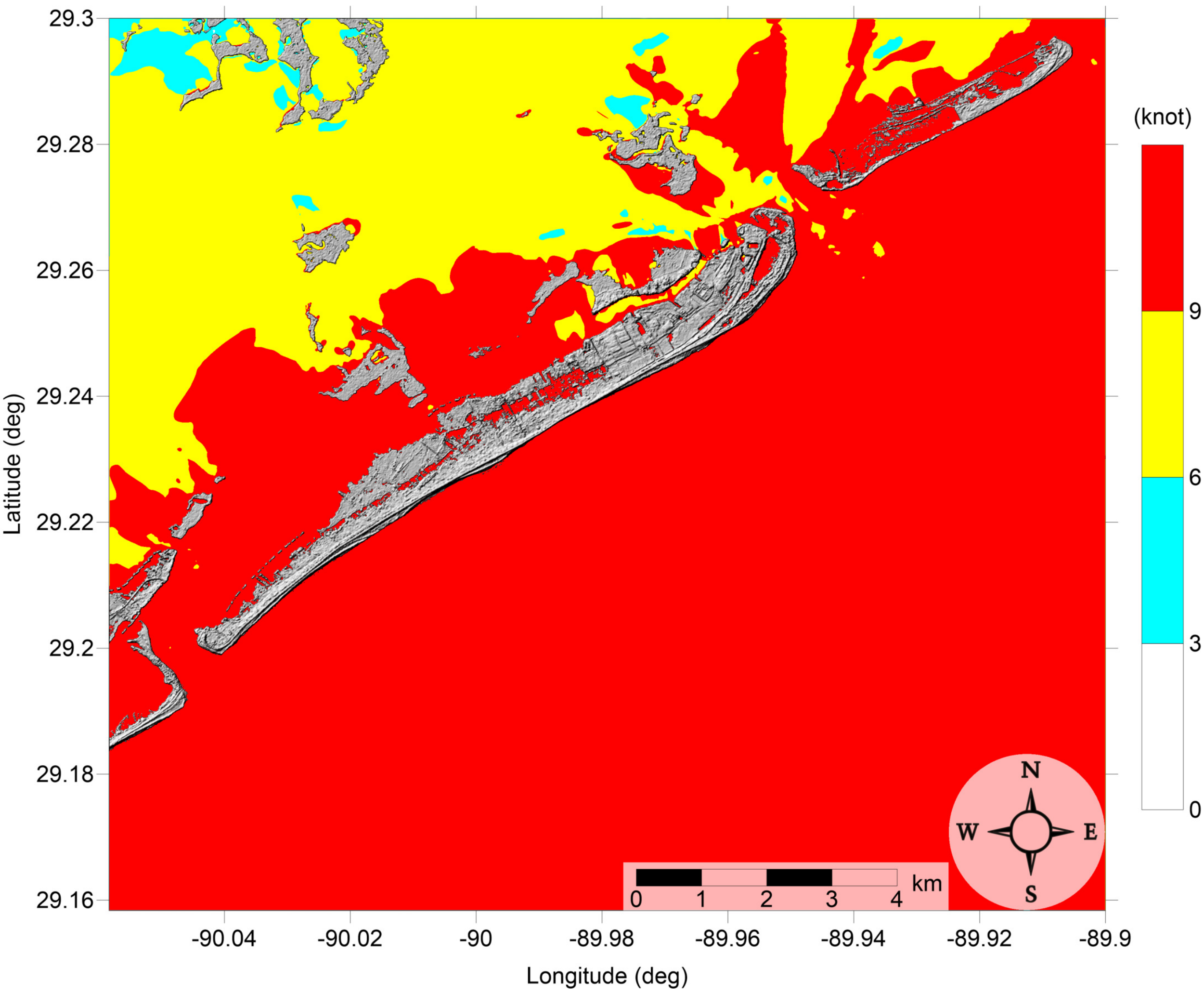

Figure 71: Maximum of maximum velocity magnitude contour in Grand Isle, LA (Grid 4 - 1/3 arcsecond) for all landslide scenarios.

Grand Isle, LA
All Sources
Maximum of Maximum Vorticity Magnitude

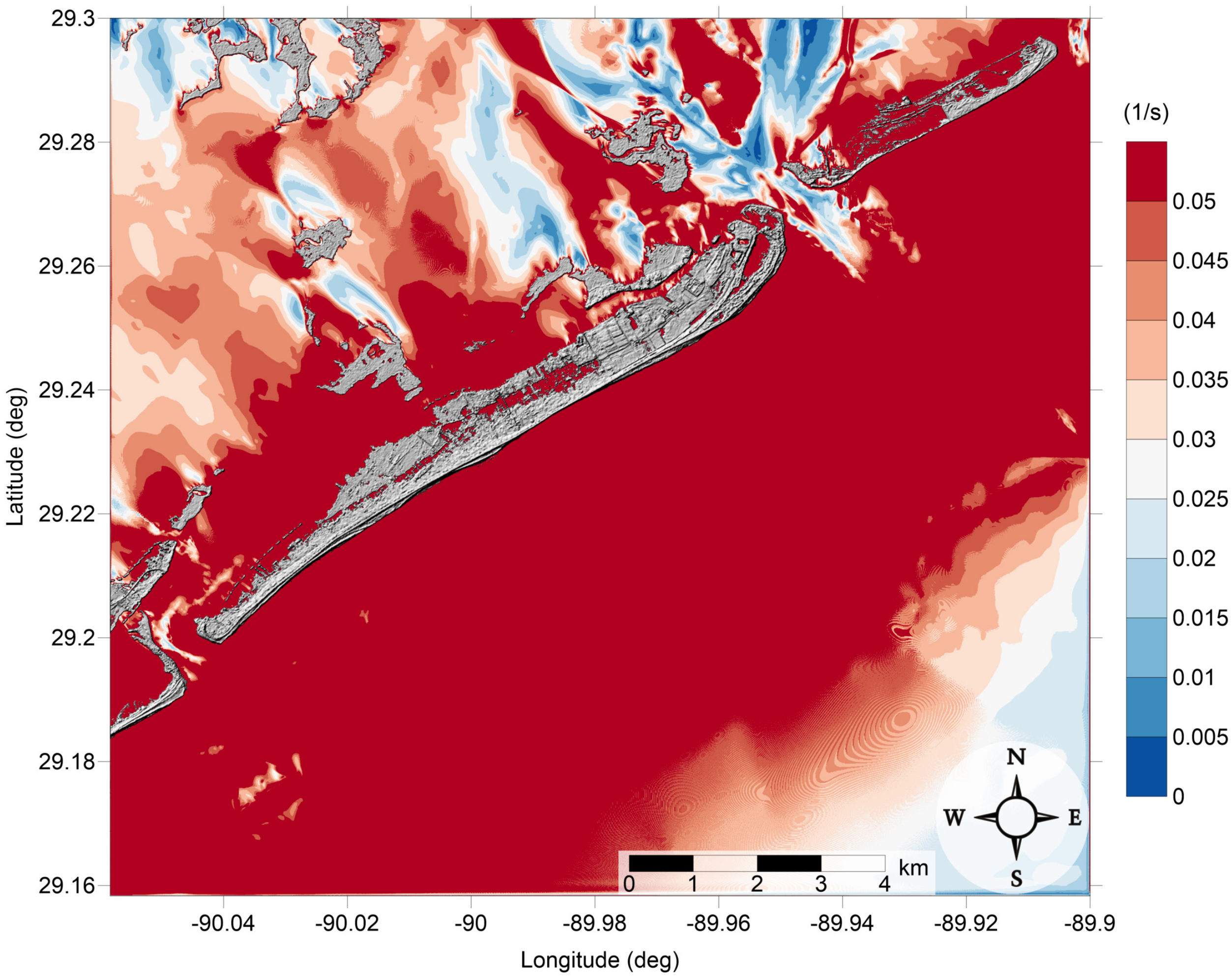

Figure 72: Maximum of maximum vorticity magnitude contour in Grand Isle, LA Grid 4 (1/3 arcsecond) for all landslide scenarios.

6.2 Freeport, TX

Freeport, TX
All Sources
Maximum of Maximum Velocity Magnitude

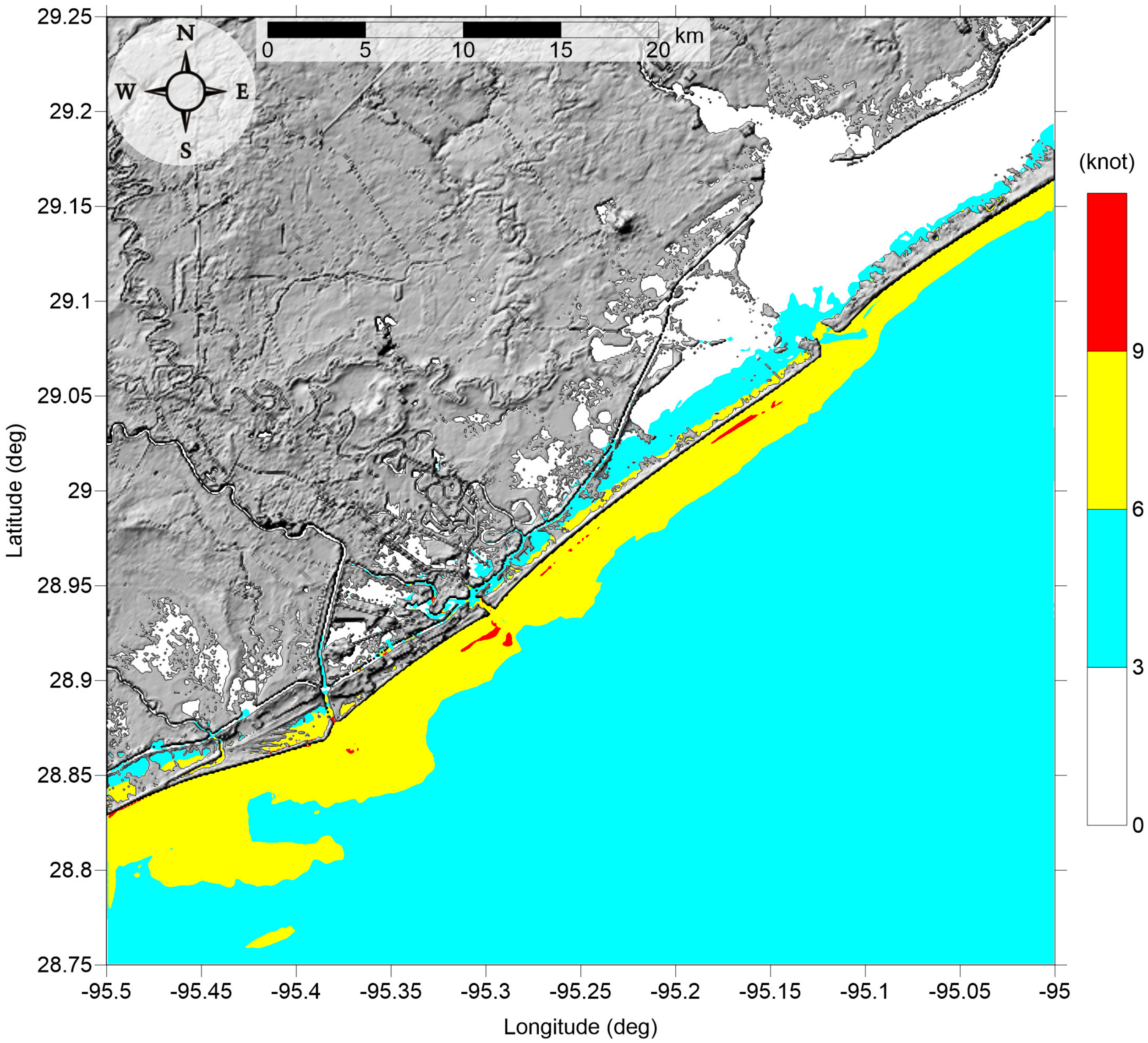

Figure 73: Maximum of maximum velocity magnitude contour in Freeport, TX (Grid 2 - 3 arcsecond) for all landslide scenarios.

Freeport, TX
All Sources
Maximum of Maximum Velocity Magnitude

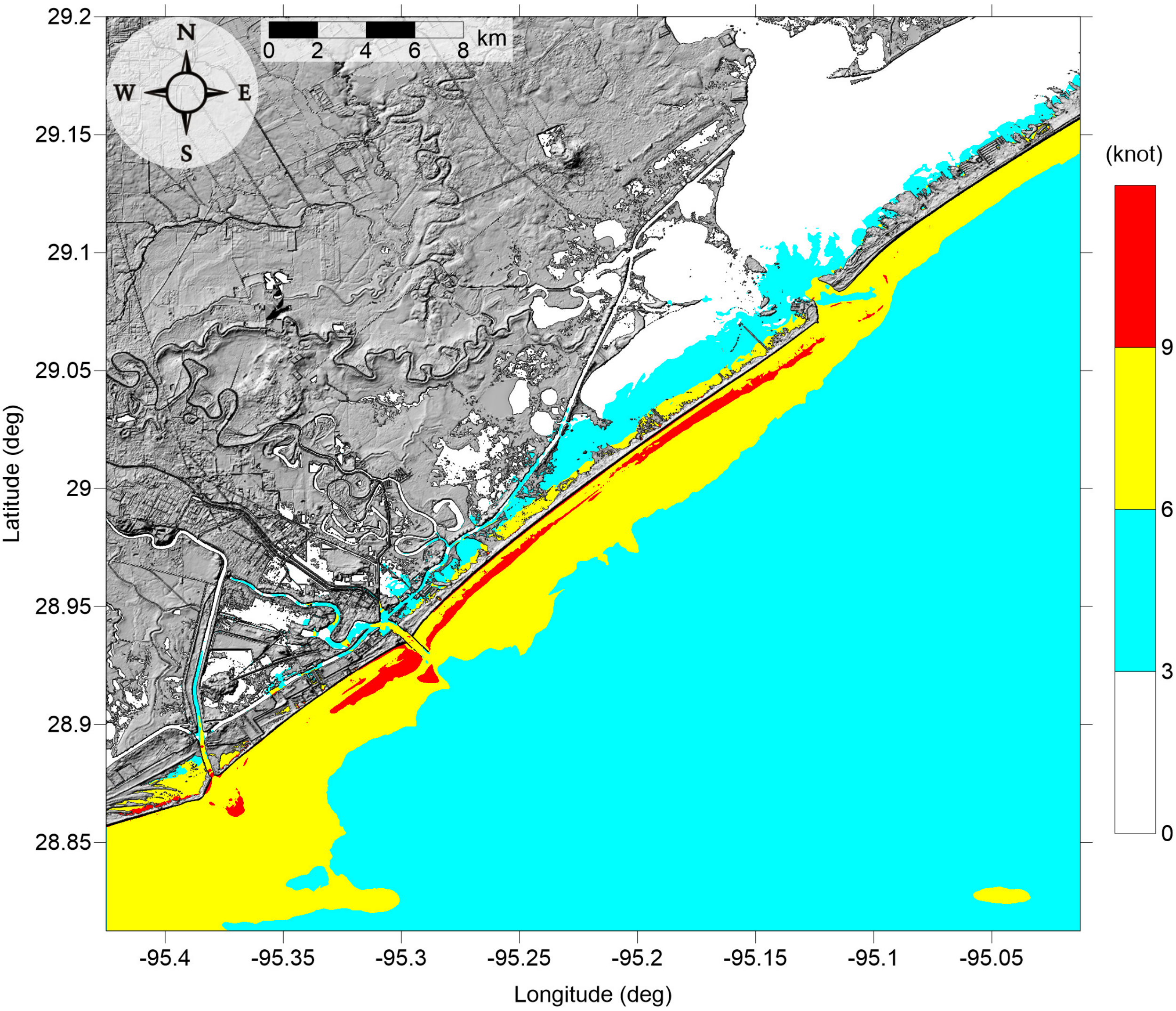

Figure 74: Maximum of maximum velocity magnitude contour in Freeport, TX (Grid 3 - 1 arcsecond) for all landslide scenarios.

Freeport, TX
All Sources
Maximum of Maximum Velocity Magnitude

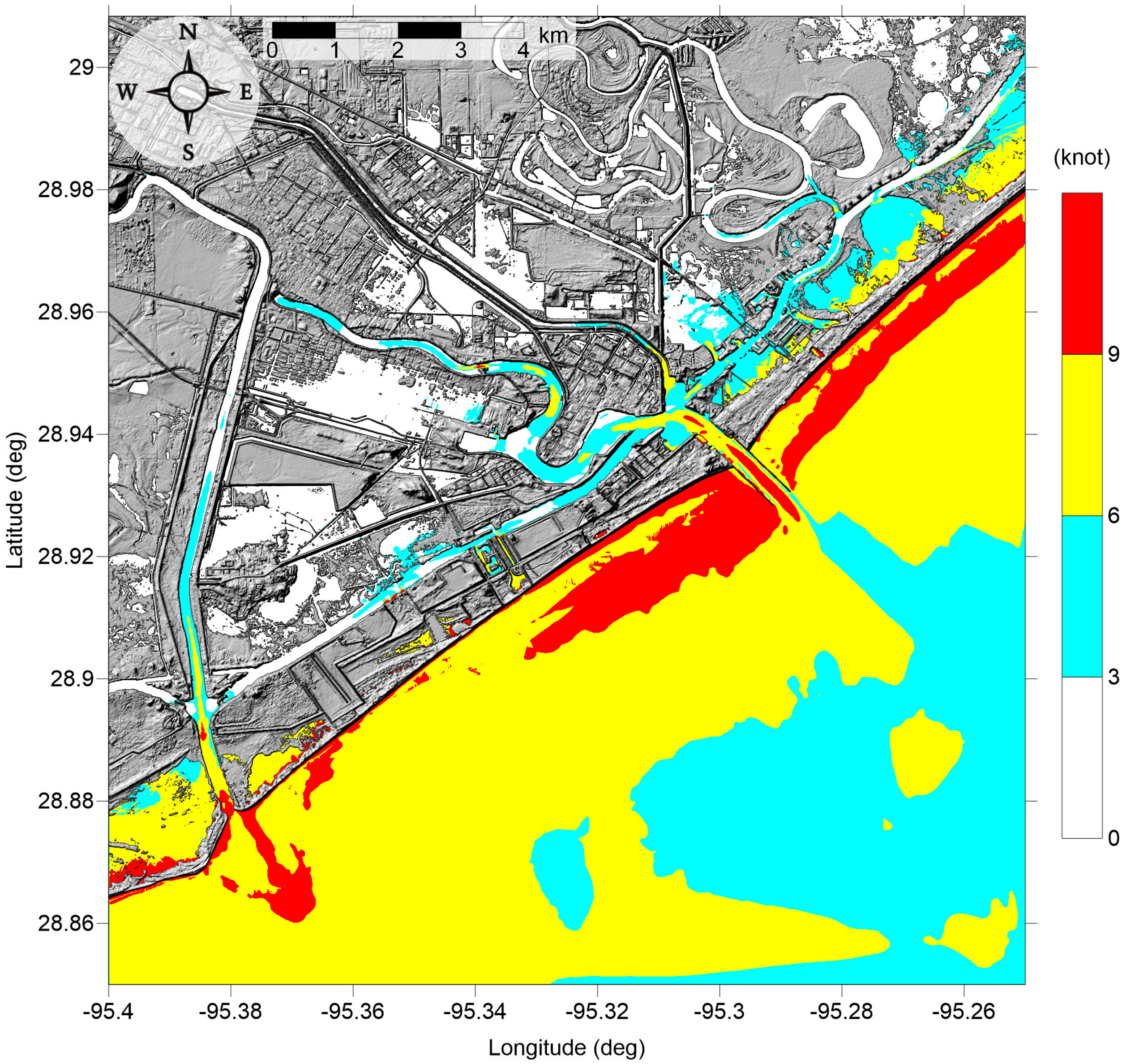

Figure 75: Maximum of maximum velocity magnitude contour in Freeport, TX (Grid 4 - 1/3 arcsecond) for all landslide scenarios.

San Luis Pass, TX
All Sources
Maximum of Maximum Velocity Magnitude

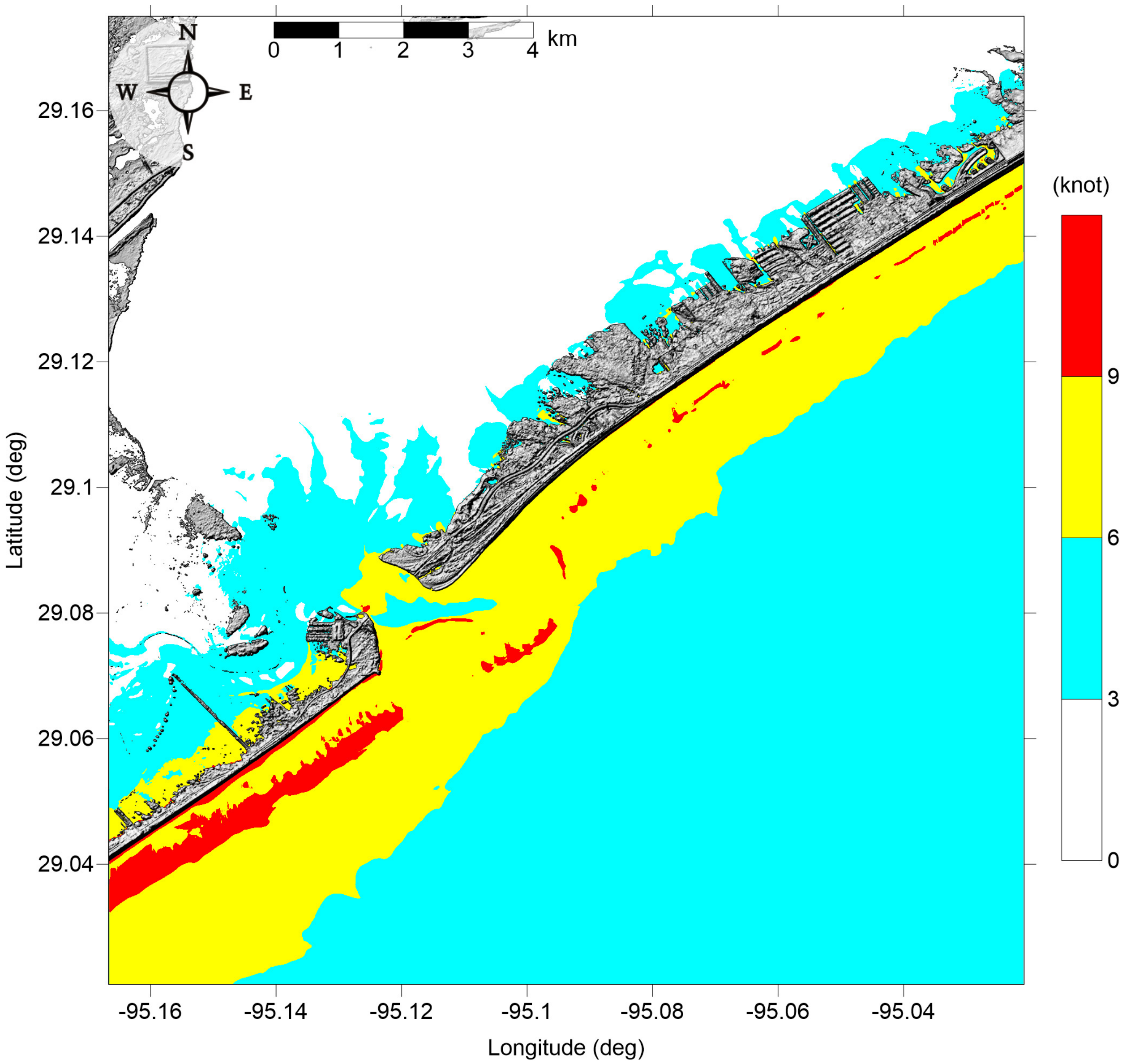

Figure 76: Maximum of maximum velocity magnitude contour in San Luis Pass, TX (Grid 5 - 1/3 arcsecond) for all landslide scenarios.

Freeport, TX
All Sources
Maximum of Maximum Vorticity Magnitude

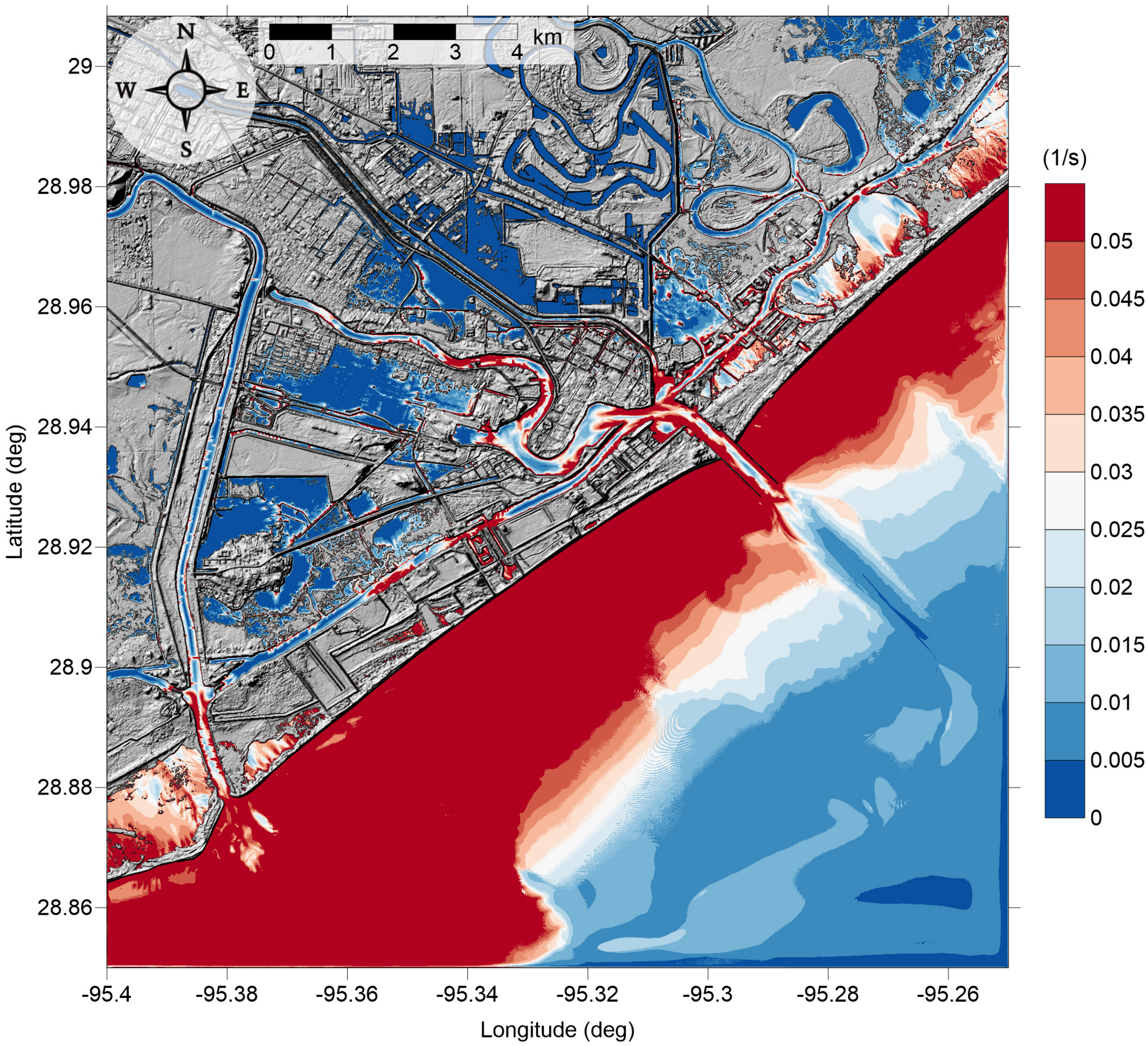

Figure 77: Maximum of maximum vorticity magnitude contour in Freeport, TX Grid 4 (1/3 arcsecond) for all landslide scenarios.

San Luis Pass, TX
All Sources
Maximum of Maximum Vorticity Magnitude

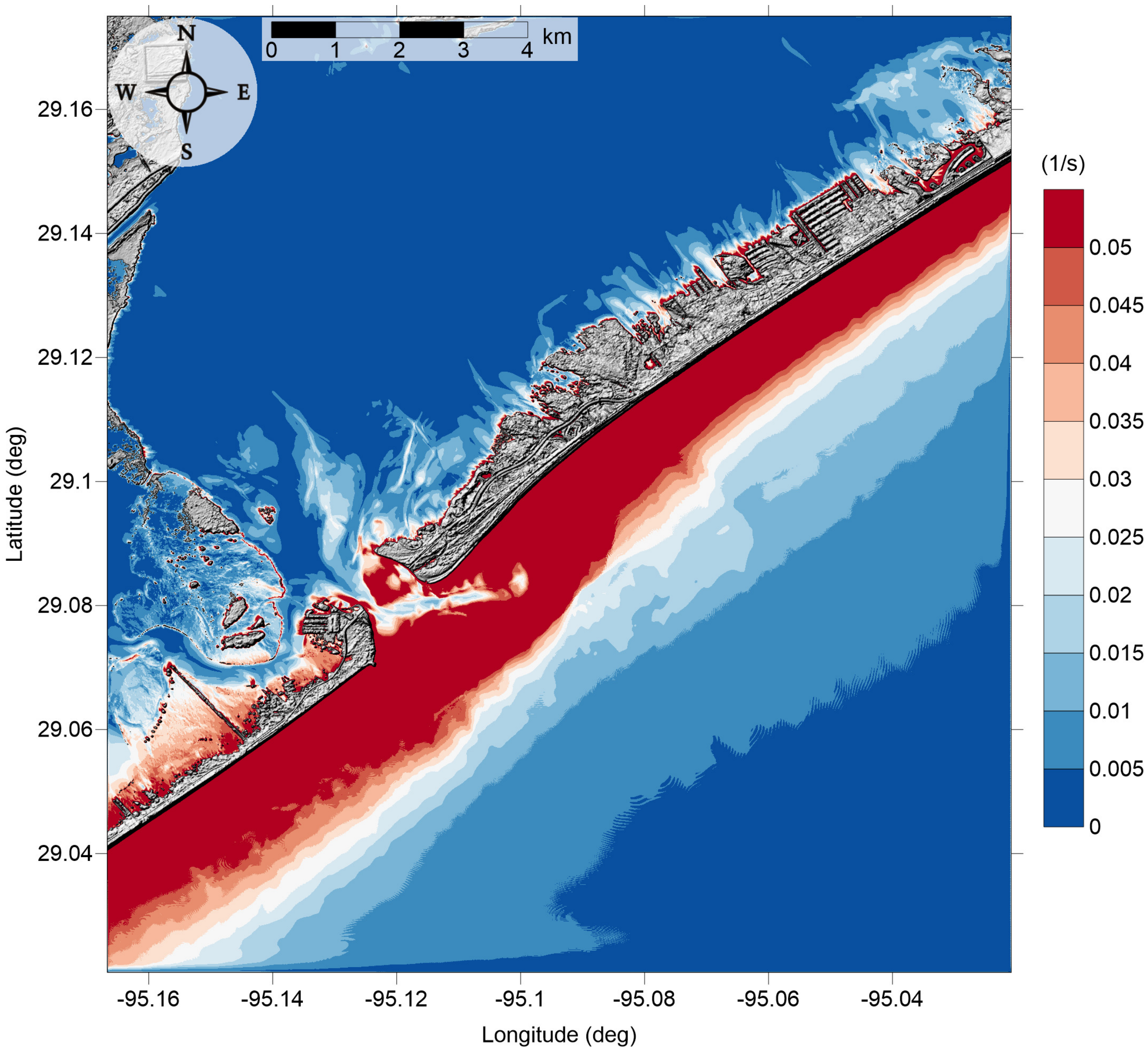

Figure 78: Maximum of maximum vorticity magnitude contour in San Luis Pass, TX Grid 5 (1/3 arcsecond) for all landslide scenarios.

7 Meteosunami

As the name implies, the source of a meteorological tsunami (a.k.a. meteotsunami) is a moving atmospheric pressure disturbance such as a squall line, storm system, derecho, frontal motion, or atmospheric gravity wave train. Unlike seismic sources, these sources are extended both spatially and in time. Many meteotsunami attributes are otherwise similar to those of their seismic cousins [Pattiaratchi and Wijeratne, 2015].

Ground level pressure disturbances from known meteotsunami sources are typically under 5 hPa, but can build rapidly over the course of several minutes. Because sea level changes attributed to the inverted barometer effect are small, resonance effects are required to produce a damaging meteotsunami. As the speed of these sources at ground level is typically in the range of 15 - 30 m/s, resonance can occur where the shallow water wave speed ($c = \sqrt{gd}$) matches that of the moving source. This restricts the generation zone to ocean depths under 100 m and with significant "fetch" where resonant effect like Proudman resonance [Proudman, 1929] can be expected to increase wave amplitude. Additional means of amplification include shoaling (Greens Law), shelf slope effects known as Greenspan resonance [Greenspan, 1956], and the matching of atmospheric gravity wave and harbor seiche periods. The extensive shelves of the Gulf of Mexico, shown in Fig. 79 provide both the area and "fetch" for generation.

In the following, first we present a numerical simulation of a 2010 Florida gulf coast meteotsunami event and compared results with field gauge recordings. Secondly we present several possible scenarios for characterization of physical parameters both globally and locally in specific regions susceptible to meteotsunami in the GOM.

7.1 Numerical Simulation of a February 2010 Florida Gulf Coast Meteotsunami Event

Olabarrieta et al. [2017] analyzed the meteotsunami events recorded by several northeastern GOM NOAA gauges and found seasonal variance in meteotsunami occurrence in different regions and the link to climate variability like the El Niño. One of the prominent events mentioned in Olabarrieta et al. [2017] is the Florida gulf coast meteotsunami of February 2010 that generated a 1.0 meter high wave at Clearwater Beach gauge. Here we present the model's physics, setup, and numerical results of this event. A web-based meteotsunami model has been developed to facilitate this study, which can be used for hindcasting or forecasting.

Atmospheric Source

The source used in this investigation is based on a simple surface pressure function of the general form:

$$P(x, y) = \begin{cases} A_c * x * exp(-(y)^2 - \left(\frac{x}{L_c}\right)^2) & , x < 0 \\ A_t * x * exp(-(y)^2 - \left(\frac{x}{L_t}\right)^2) & , x > 0 \end{cases} \tag{2}$$

where subscript c indicates crest and t indicates trough. Parameters A and L are amplitude and length respectively, chosen to produce a compact pressure footprint with a leading edge trough and trailing edge crest. Coordinates x, y are taken to be longitude and latitude excursions from the source center. The pressure distribution translates at 20 m/s in a SSE direction following the shelf break and is curved slightly along the travel direction (Fig. 79).

In this case, we used $A_c = 5$ mbar, $A_t = -1$ mbar, $L_c = 0.7$ deg, $L_t = 1.05$ deg. The pressure disturbance travels from (-85.6070, 30.7470) deg to (-82.0620, 23.4480) deg.

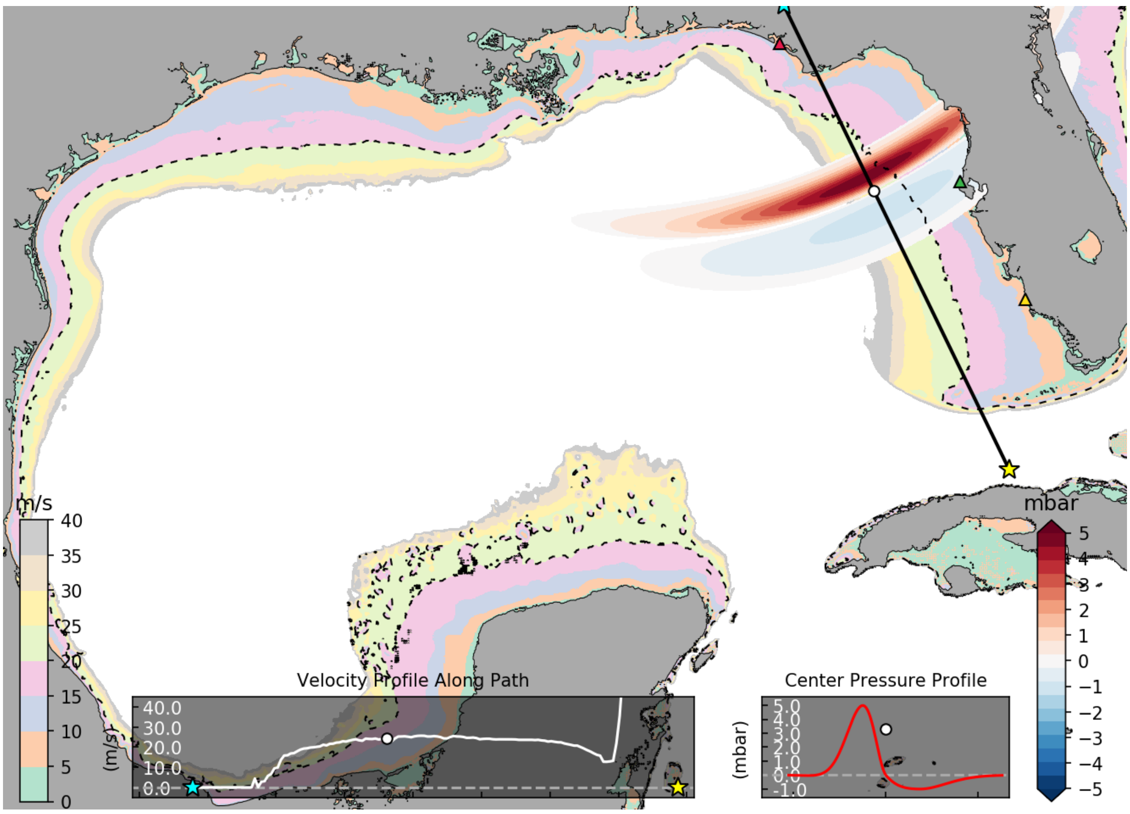

Figure 79: Meteotsunami atmospheric pressure contour plot and travel path. Black solid straight line shows the path on which pressure disturbance travels (from blue to yellow star). Pressure disturbance is plotted in red-blue contours in mbar. The bottom right inset plot depicts the pressure profile along the path, where the crest amplitude is 5 mbar and the leading trough amplitude is 1 mbar. The bathymetry is plotted in the form of shallow water wave celerity $c = \sqrt{gd}$, ranging from 0 - 40 m/s, where d is depth of ocean floor. Bottom left inset plots the velocity profile along the travel path. In this case, it more or less follows the 20 - 25 m/s celerity contour lines. The white dots appearing in all three plots mark the same center of pressure location. Three gauges in Panama City, Clearwater Beach, and Naples, FL, are marked by red, green, and yellow dot, respectively.

Model Setup

The numerical model used for meteotsunami study is a non-linear, shallow water wave model in spherical coordinate, modified to include time and space dependent atmospheric pressure. Bottom friction is based on the Manning model with Manning coefficient of 0.025 $sm^{1/3}$. Tides have not been included in the computation. The model domain covers the full Gulf of Mexico as shown in Fig. 79. Bathymetry data was downloaded from the Etopo1 dataset at https://maps.ngdc.noaa.gov/viewers/wcs-client/, and was interpolated to 15 arcsecond. A coastal wall is set up at water depth of 0.3 m to avoid runup. Marigrams are computed at several near-coastal tide gage locations and moved as needed to the nearest point close to 5 m depth. The Alaska Tsunami Forecast Model (AFTM) model [Knight, 2011] is also used for simulations and to verify the results.

Results

Model results show a combination of refraction, reflection, resonance, and shoaling which combine to produce wave heights varying with coastal coordinate from near zero up to 0.5 m. Fig. 80 shows the time evolution of water levels in the three numerical gauges at Panama City, Clearwater Beach, and Naples, FL. Clearwater Beach and Naples both recorded a prominent wave, with wave height of approximately 1.0 m and 0.5 m, respectively. Fig. 81 compares numerical result and NOAA gauge record at Clearwater Beach, FL. Good agreement can be found from the first major wave crest and trough, especially the peak and trough amplitude. However, the second wave is not reproduced well in our results. This indicates that additional investigation of the parameters in the simplified Eq. 2 is in order. For example, while obtaining the crest and trough amplitudes is relatively easy, it can be difficult to determine their lengths (e.g. from radar reflectivity data). According to Hibiya and Kajiura [1982], the more abrupt the pressure jump, the stronger is the amplification of meteotsunami wave generation, and thus the pressure wave length plays an important role. In addition, the inclusion of wind stress may also have an impact on these comparisons.

Fig. 82 plots the maximum wave amplitude after 20 hour of the 2010 Florida Meteotsunami event. It can be observed that energy focuses toward Clearwater Beach and the south coastline. Colored stars indicate the path of the maximum wave amplitude at 15 min intervals with the first section directing to Clearwater Beach, and the second section following the coastline (like an edge wave) toward Naples. The first section aligns well with the velocity contour line at 20 m/s because of Proudman resonance. The wave energy built up continues straight and refracts toward Clearwater Beach, producing the highest water elevation during this event. We noticed that the meteotsunami wave is almost traveling in phase with the atmospheric pressure. The bottom subplot shows the time evolution of this maximum wave amplitude, with the first peak detected at Clearwater Beach gauge. Less than four hours later, a 0.25 m wave reached Naples, FL. Moreover, Florida Keys also took a strong hit by catching the remnant wave energy collected by the southwestern Florida shelf.

7.2 Numerical Experiment for Meteotsunami Effect in West Florida

In order to gain a better understanding of meteotsunami effect on west Florida from different source regions in the GOM and under different physical conditions, we carried out the following numerical experiments. The US GOM coast is divided into several meteotsunami source regions based roughly on continental slope orientation (Fig. 83). Within each region, a series of parallel travel paths are selected, and for each path, pressure disturbance travel speed is varied from 10 m/s to 40 m/s. For this pilot study, the pressure disturbance's geometric parameters are kept the same as the 2010 Florida case (Section 7.1).

For instance, experiment indicated in Fig. 83(h) uses pressure disturbances traveling from NW to SE. Results of this experiment (Fig. 84) show the maximum wave amplitude recorded at each gauge (#01, #02 and #03 correspond to Panama City, Clearwater Beach, and Naples, FL gauges, respectively) for each travel path and velocity. In each gauge plot,

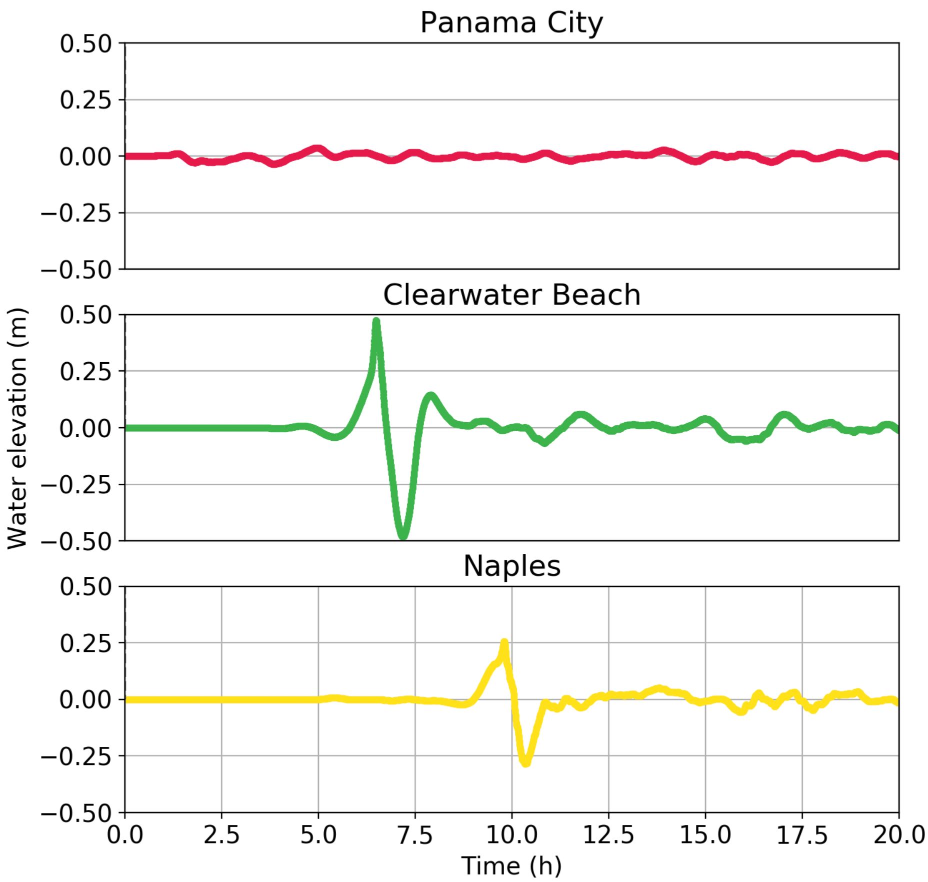

Figure 80: Numerical gauge water elevation time evolution, corresponding to Panama City, Clearwater Beach, and Naples, FL NOAA gauges, and are marked by red, green, and blue colors, respectively. Refer to Fig. 79 for location.

colored lines represent different travel paths (Fig. 83(h)). Results demonstrate that highest wave amplitudes are usually achieved at pressure disturbance traveling velocity between 20 m/s and 30 m/s because the majority of the GOM continental shelf depth lies in this Proudman resonance velocity range (see Fig. 79). Source regions in the western GOM have shown less meteotsunami influence on Florida. The maximum wave amplitude at Panama City (gauge #01) occurred at range of 20 m/s - 30 m/s for the red, green, blue and magenta (#1 #2 #3 and #4) paths due to the resonance at Florida panhandle shelf; Clearwater Beach (gauge #02) at 20 m/s for the cyan, gray and pink (#7, #8 and #9) due to resonance at nearby shelf; and Naples (gauge #03) at range of 20 m/s - 25 m/s for the magenta, black and olive (#4, #5 and #6). It can be observed from the results that meteotsunami waves affecting different locations can be generated from different regions along the same travel path.

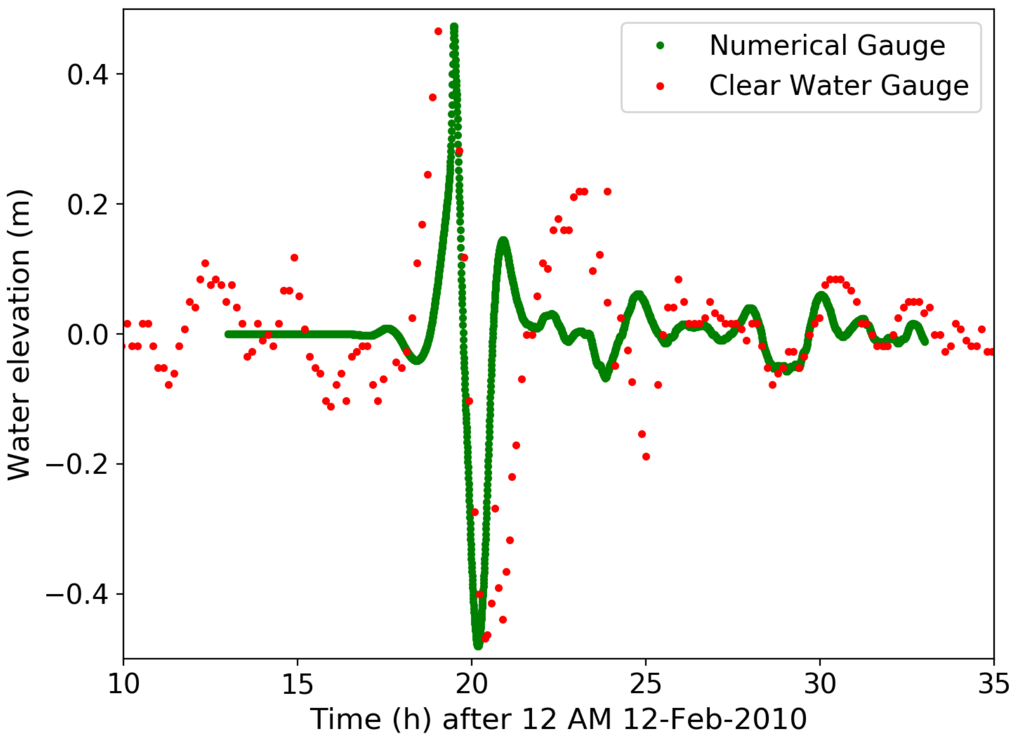

Figure 81: Numerical result and NOAA gauge record comparison at Clearwater Beach, FL.

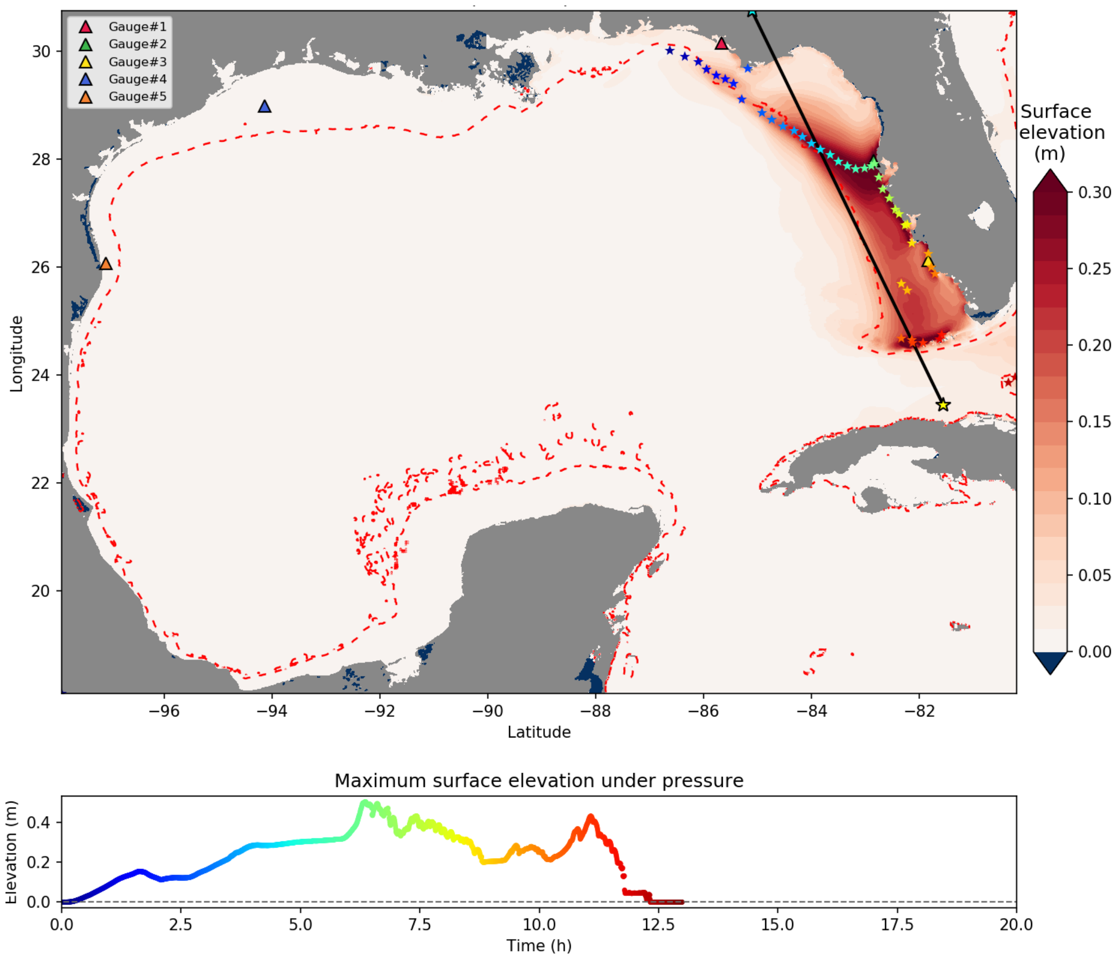

Figure 82: Contour plot (red) showing the maximum surface elevation at each grid point after 20 hour simulation of the 2010 Florida Meteotsunami event. Black solid straight line shows the path on which pressure profile moves from the blue star toward yellow. Red dashed line marks the contour line where Proudman resonance would occur (20 m/s). Colored stars track the location with the maximum elevation of all grid points at 15 min intervals. Bottom plot shows the time evolution of this maximum elevation with color matching the star locations.

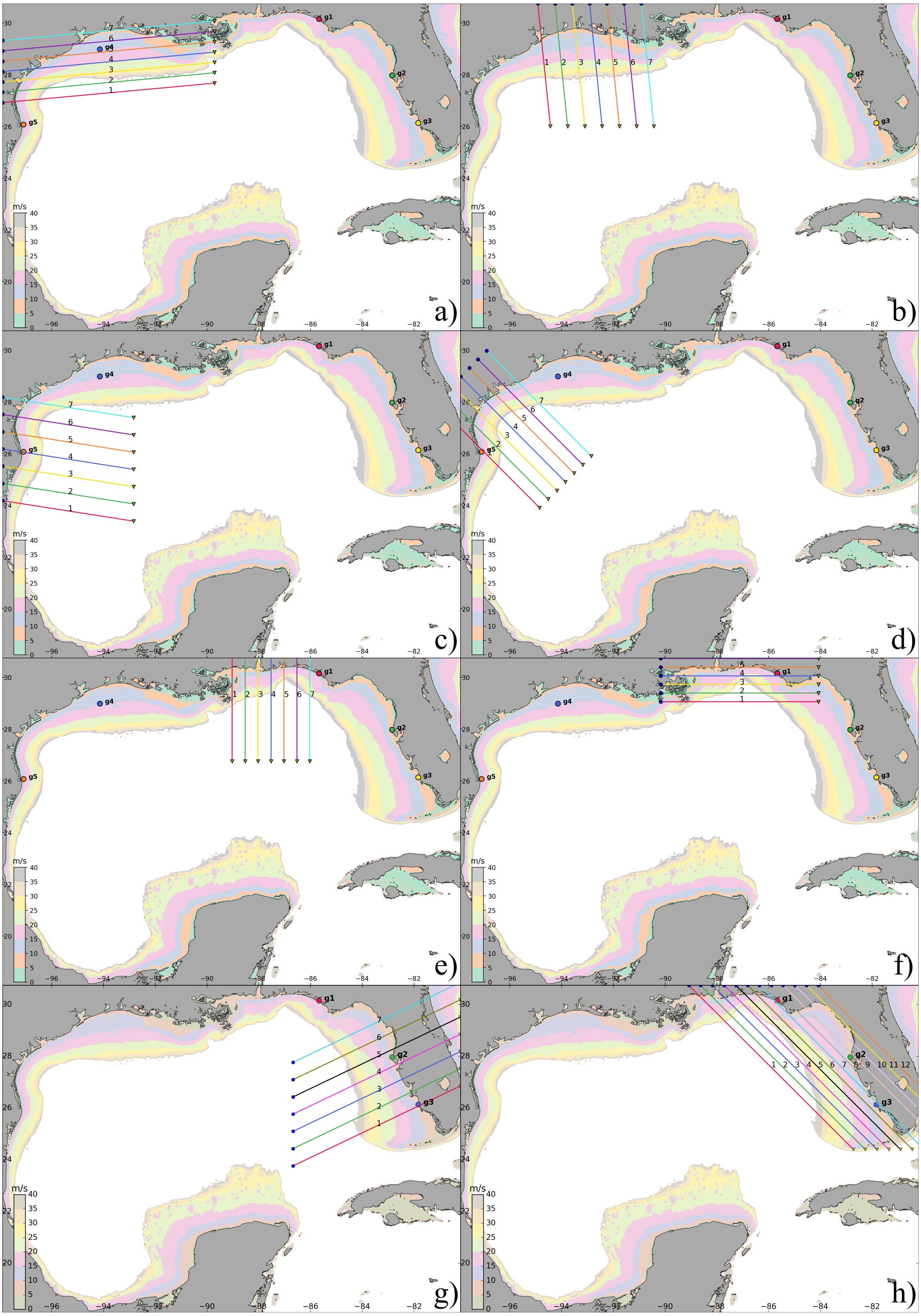

Figure 83: Numerical experiment transects covering U.S. coastlines.

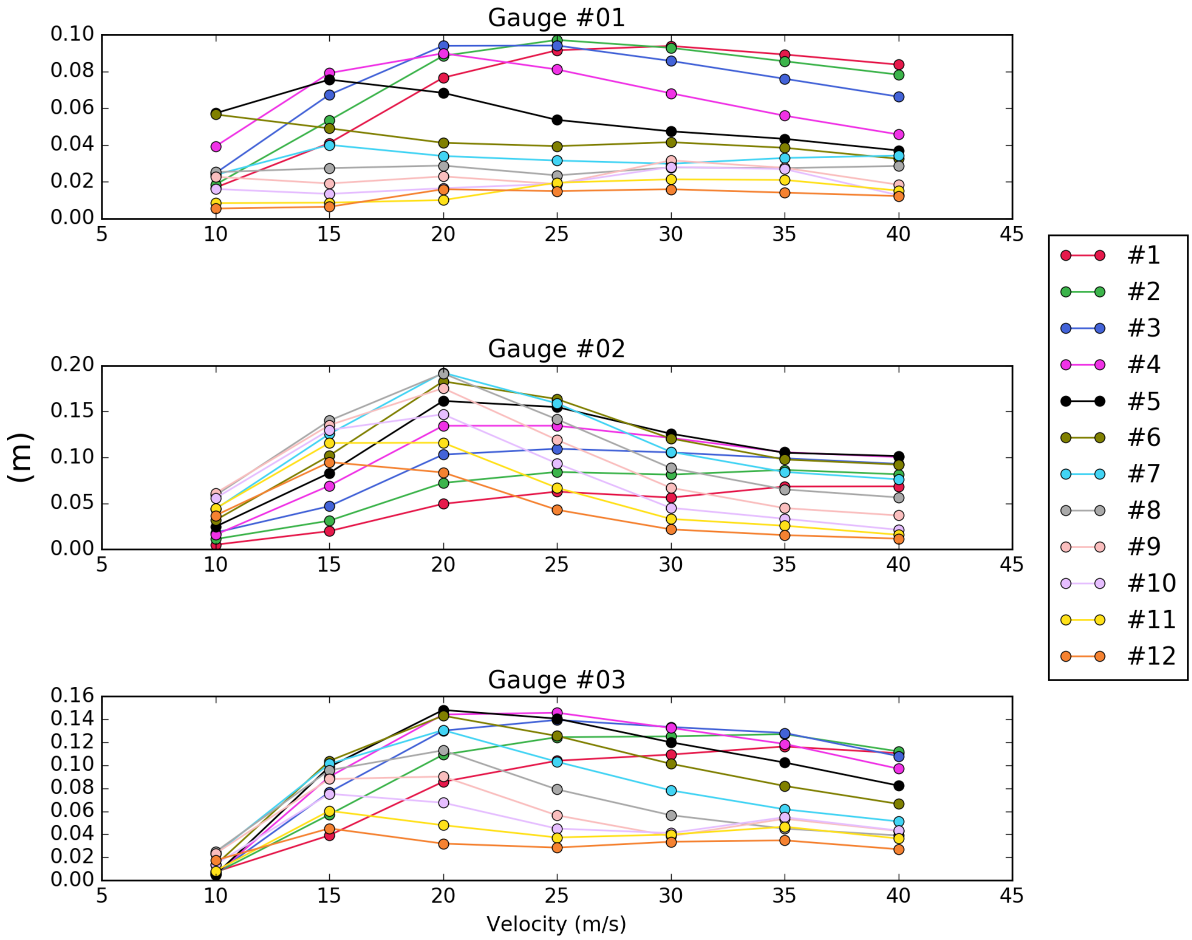

Figure 84: Maximum wave amplitude (meter) recorded at each gauge for each travel path and velocity (Scenario h) in Fig. 83). Gauge #01 #02 #03 corresponds to Panama City, Clearwater Beach, and Naples, FL numerical gauges, respectively. In each subplot, x-axis is velocity and colored lines represent different travel paths.

To further understand how different travel path locations influence the maximum wave amplitude at selected gauge locations, we carried a path location sensitivity experiment (Fig. 85) where three travel paths are selected, with the middle one (#2) being the same as

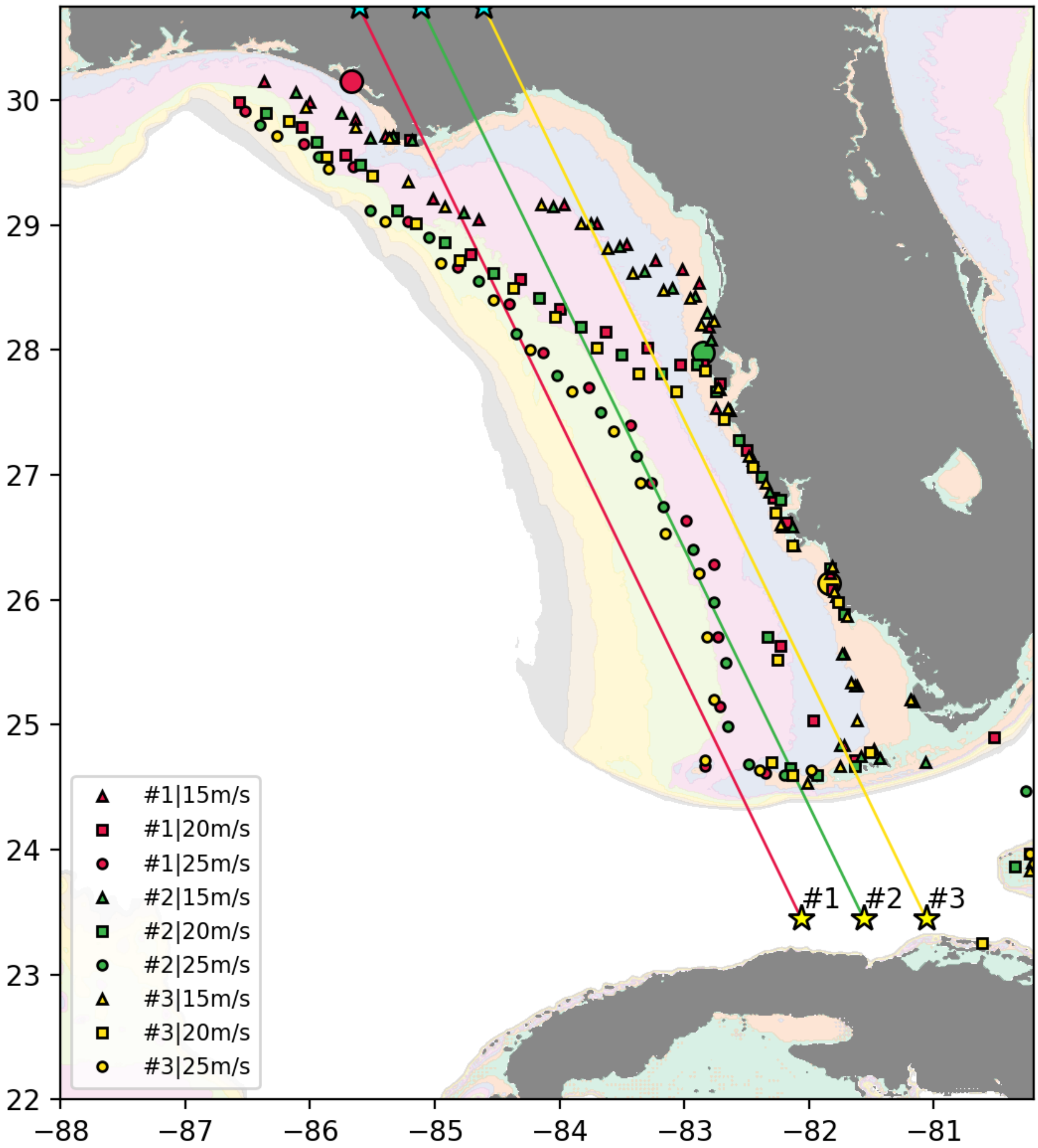

Figure 85: Maximum wave amplitude tracking at 15 min intervals for 3 travel paths and 3 velocities. Different shapes mark velocities and colors correspond to travel paths.

the 2010 Florida case, and three different travel velocities of the pressure disturbance. The atmospheric pressure disturbance parameters are kept the same as the Florida case.

Fig. 85 shows the track of maximum wave amplitude at 15 min intervals for three pressure travel paths and three velocities. Different shapes mark velocities, and colors correspond to travel paths. At Clearwater Beach (big green circle), for both 15 m/s and 20 m/s velocities, all travel paths resulted in that the maximum wave amplitude track hits Clearwater Beach. However, the 25 m/s velocity tracks hit Florida Keys directly. For this particular experiment, the insensitivity of meteotsunami maximum wave track with respect to pressure travel path demonstrates that shelf configuration (depth and shape, etc.) is the more dominant factor, under the assumption of a straight travel path with a constant velocity.

7.3 Summary

In this pilot meteotsunami study, we successfully recreated the 2010 Florida gulf coast meteotsunami, and carried out numerical experiments to investigate the influence of pressure disturbance travel path and velocity on selected Florida locations. For future work, we plan to expand to other locations, expand the current parameter range to gain a better understanding of the two most important parameters (path and velocity), and possibly include more parameters like variability in travel path direction, variability in velocity, and different pressure profiles. Additionally, wind stress can be incorporated into the model to investigate its effects.

Overall, the numerical study could aid in predicting meteotsunami trajectory, identifying vulnerable coastal communities, estimating water levels, and hopefully help prevent damage.

8 Conclusions

This project focused on the implementation of recent developments in the tsunami science recommended by the National Tsunami Hazard Mitigation Program - Modeling Mapping Subcommittee - Strategic Plan (NTHMP-MMS-SP) into our current Gulf of Mexico (GOM) tsunami mitigation products. Three main developments for tsunami mitigation have been created under this project for two new communities in the GOM (Grand Isle, LA and Freeport, TX) that will provide guidance to state emergency managers for tsunami hazard mitigation and warning purposes. The first task is the development of tsunami inundation maps for the two selected communities with nine landslide sources. The second is the comparison between existing SLOSH hurricane flooding data and our tsunami inundation result for the two new communities in order to facilitate temporal-low-order estimate for tsunami hazard areas (community) where inundation studies have not yet been assigned/executed or where little bathymetric and elevation data exists. The third is to produce maritime products (maximum of maximum (MOM) velocity and velocity magnitude maritime maps) for both communities to help identify impact specifically on ship channels, bay inlets, harbors, marinas, and other infrastructures. The fourth task is to identify meteotsunami physical parameters and to obtain an understanding of this phenomenon through the characterization of physical parameters both globally and locally in a specific region susceptible to meteotsunami in the GOM. We have chosen Panama City, Clearwater Beach, and Naples, FL as the prime locations for this pilot study to gain a better understanding of the meteotsunami phenomenon on the eastern Gulf of Mexico and west coast of Florida, and to determine which tools (methodology) are most appropriate for EMs and tsunami warning operators for mitigation and hindcasting/forecasting of these types of events.

Tsunami wave propagation and inundation in Grand Isle, LA and Freeport, TX was also modeled to obtain inundation, momentum flux, current velocity and vorticity maps considering the entire suite of nine landslide sources. Grand Isle is in a unique location, being just 60 km north of the Mississippi source. As a result, almost the whole barrier island is overtopped, with the seaward portion inundated by at least 5 m. At Freeport, the barrier island provides nice protection for the mainland against tsunami inundation. While inundation depth at the barrier island ranges from 1 to over 3 m, the mainland is mostly less than 2 m. The more populated Surfside Beach and San Luis Pass areas have similar inundation patterns. Although the reinforced dune at the beach provides somewhat protection, the communities behind it can experience tsunami inundation as high as 2 to 3 meters. For both communities, MOM tsunami inundation is produced solely by the Mississippi Canyon failure. This historical failure is the largest in both area and volume of material removed, and therefore produces the highest amplitude wave of all simulated sources.

Comparisons of MOM tsunami inundation results with the SLOSH MOM high tide storm surge inundation indicate that while the details of referencing tsunami inundation to hurricane storm surge is dependent on local topographic effects, general regional trends can be identified. Grand Isle's tsunami inundation exceeds Category 5 by as high as 4 m except for the islands northwest of Bay Joyeux where it is Category 4. The difference between hurricane flooding and tsunami inundation (from -1.5 m to -4 m, meaning hurricane < tsunami) indicates that tsunami produces significantly higher water depth even when comparing to the most severe hurricane. At Freeport, the matching hurricane category distribution closely reflects that of tsunami inundation. West of the Freeport jetty is dominated by Category 3 and 4, and Category 2 appears around the two small communities at Compass Ct. and Deep Sea Dr. On the east side of the jetty, beachfront inundation corresponds to Category 3 while other parts of the barrier island Category 2. Over at the mainland, the majority of the inundated area corresponds to Category 1, with few exceptions. The difference between hurricane flooding and tsunami inundation $\Delta\zeta$ is generally within $\pm$ 0.5 m.

The San Luis Pass area is clearly divided into three tiers following the inundation pattern. South of San Luis Pass Rd is dominated by Category 3, and it transitioned into Category 2 on the other side of the road and finally to Category 1 at the bayside barrier island coast. The difference between hurricane flooding and tsunami inundation is larger than 1 m (hurricane $>$ tsunami) around the Chocolate Bay, and less than 0.5 m (absolute value) at the barrier island.

Since even general, low-resolution inundation information is useful for hazard mitigation efforts, we believe that these results can be extended to provide a preliminary, first-order estimate of potential tsunami hazard zones for other Gulf Coast communities that is accessible and understandable to regional emergency managers and more appropriate for the low-lying Gulf Coast than methods such as the 10 m (33 ft) elevation contour line. We anticipate that communities which lack detailed tsunami inundation maps, but which have modeled hurricane storm surge information, would be able to use the results presented here to estimate their potential tsunami hazard level based on their regional topographical/bathymetric features. We stress, however, that such results should be used only in a broad, regional sense given the differences seen among and within communities based on local details of bathymetry, topography, and geographical location within the GOM basin. There is no guarantee that comparison results will be identical in areas with similar topography, and comparisons should only be made after understanding the limitations and simplifications of the methodology presented here. Improvements to the methodology would clearly improve the reliability of comparisons. For example, given the large difference in resolution of the SLOSH model data (1 km) and tsunami inundation data (1/3 arcsecond $\approx$ 10 m), the comparison between the two datasets would be greatly improved with increased resolution of the SLOSH model runs, or alternate data on category-specific hurricane storm surge. Additionally, a more detailed comparison could also be accomplished by comparison with probabilistic storm surge parameters, e.g. 100-year or 500-year hurricane surge events, which may provide more/better information in areas where there are large differences between the modeled tsunami inundation and that of the best-match hurricane category. Successful implementation of this approach would certainly require the availability of probabilistic data for the locations of interest in order to develop a generalized probabilistic tsunami - storm surge comparison.

Finally, we produced the MOM velocity and velocity magnitude maps for all the landslide scenarios, for Grand Isle, LA and Freeport, TX, based on a simplified current velocity damage scale where we associate 0 - 3 knots to unharmful currents, 3 - 6 knots to minor damage, 6 - 9 knots to moderate damage, and over 9 knots to major damage. The four damage levels are denoted with white, blue, yellow and red colors, respectively.

From the MOM velocity magnitude results in the entire Gulf of Mexico (Fig. 68), it can be observed that, potential damaging currents (> 3 knots, blue, yellow and red areas) tend to be present in most of the area shallower than the minimum offshore safe depth. However, damaging currents could reach areas deeper than 200 m close to most of the landslide generation regions. Major damaging currents (> 9 knots, red) can be expected in most of the landslide generation regions, in the continental shelf adjacent to Mississippi Canyon, offshore northwest Florida, and Yucatán shelf. Moderate (> 6 knots and < 9 knots, yellow) damaging current areas are scattered over the continental shelf, but mostly close to areas with major damage currents.

General trends can be observed from the different domain levels of the MOM velocity for Grand Isle, LA. In the vicinity of the barrier island and the open ocean, there are mostly major damaging currents (> 9 knots, red). Again the large area of major damaging currents is attributed to the nearby Mississippi landslide source. Current velocity decreases toward the mainland with contour lines following the orientation of the barrier islands. In Freeport, TX, the situation is much less severe than Grand Isle, LA. Major damaging current area appears as a thin strip seaward of the barrier island and diminishes toward the gulf to minor currents. In the interior bays and channels, the tsunami currents are less severe which can be used as shelter to minimize tsunami impact.

Tsunami hazard maritime products such as tsunami current magnitude, vorticity, safe/hazard zones would be central for future developments of maritime hazard maps, maritime emergency response and as well as infrastructure planning.

In this pilot meteotsunami study, we successfully recreated the 2010 Florida gulf coast meteotsunami. Good agreement can be found from the first major wave crest and trough, especially the peak and trough amplitude. However, the second wave is not reproduced well in our results. Model results show a combination of refraction, reflection, resonance, and shoaling which combine to produce wave heights varying with coastal coordinate from near zero up to 0.5 m. We noticed that the meteotsunami wave is almost traveling in phase with the atmospheric pressure in most of the cases. Secondly, we carried out numerical experiments to investigate the influence of pressure disturbance travel path and velocity on selected Florida locations. For this particular experiment, the insensitivity of meteotsunami maximum wave track with respect to pressure travel path demonstrates that shelf configuration (depth and shape, etc.) is the more dominant factor, under the assumption of a straight travel path with a constant velocity. For future work, we plan to expand to other locations, expand the current parameter range to gain a better understanding of the two most important parameters (path and velocity), and possibly include more parameters like variability in travel path direction, variability in velocity, and different pressure profiles. Additionally, wind stress can be incorporated into the model to investigate its effects. Overall, the numerical study could aid in predicting meteotsunami trajectory, identifying vulnerable coastal communities, estimating water levels, and hopefully help prevent damage.

Although the recurrence of destructive tsunami events have been verified to be quite low in the GOM, our work has confirmed that submarine landslide events with similar characteristics to those used here, have indeed the potential to cause severe damage to GOM coastal communities. Therefore, this work is intended to provide guidance to local emergency managers to help managing urban growth, evacuation planning, and public education with the final objective to mitigate potential tsunami hazards in the GOM.

Acknowledgments

This work was supported by the National Tsunami Hazard Mitigation Program (NTHMP) under awards NA18NWS4670078, "Development of two tsunami inundation maps in the GOM and inclusion of the Meteotsunami characterization for Panama City, FL". The authors wish to thank all NTHMP modeling and Mapping Subcommittee members and GOM's emergency manager representatives for their helpful insights. Special thanks go to Brad Baker for their helpful insight and support. Also thank Kelly Carignan and Kelly Stroker for providing the DEMs. High resolution inundation maps are available from `http://www.tamug.edu/tsunami/NTHMP/NTHMP.html` or by contacting corresponding author upon request.

References

D. Basco and C. Klentzman. On the classification of coastal storms using principles of momentum conservation. In *Proc. 31st Int. Conf. on Coastal Eng.* ASCE, 2006.

J. D. Chaytor, E. L. Geist, C. K. Paull, D. W. Caress, R. Gwiazda, J. U. Fucugauchi, and M. R. Vieyra. Source characterization and tsunami modeling of submarine landslides along the yucatán shelf/campeche escarpment, southern gulf of mexico. *Pure and Applied Geophysics*, 173(12):4101–4116, Dec 2016. ISSN 1420-9136. doi: 10.1007/s00024-016-1363-3. URL `https://doi.org/10.1007/s00024-016-1363-3`.

D. D. Churchill, S. H. Houston, and N. A. Bond. The daytona beach wave of 34 july 1992: A shallow-water gravity wave forced by a propagating squall line. *Bulletin of the American Meteorological Society*, 76(1):21–32, 1995. doi: 10.1175/1520-0477(1995)076⟨0021:TDBWOJ⟩2.0.CO;2. URL `https://doi.org/10.1175/1520-0477(1995)076<0021:TDBWOJ>2.0.CO;2`.

B. Dugan and J. Stigall. Origin of overpressure and slope failure in the Ursa region, northern Gulf of Mexico. In D. C. Mosher, R. C. Shipp, L. Moscardelli, J. D. Chaytor, C. D. P. Baxter, H. J. Lee, and R. Urgeles, editors, *Submarine Mass Movements and Their Consequences*, pages 167–178. Springer Netherlands, 2010.

P. K. Dunbar and C. S. Weaver. *U.S. States and Territories National Tsunami Hazard Assessment: Historical Record and Sources for Waves.* U.S. Department of Commerce, National Oceanic and Atmospheric Administration, National Geophysical Data Center Tech. Rep.No. 3, 2008.

E. L. Geist, J. D. Chaytor, T. Parsons, and U. ten Brink. Estimation of submarine mass failure probability from a sequence of deposits with age dates. *Geosphere*, 9(2):287–298, 2013.

H. P. Greenspan. The generation of edge waves by moving pressure distributions. *Journal of Fluid Mechanics*, 1(6):574–592, 1956.

S. T. Grilli, O.-D. S. Taylor, C. D. P. Baxter, and S. Maretzki. A probabilistic approach for determining submarine landslide tsunami hazard along the upper east coast of the United States. *Mar. Geol.*, 264:74–97, 2009.

C. B. Harbitz, F. Løvholt, and H. Bungum. Submarine landslide tsunamis: How extreme and how likely? *Nat. Hazards*, 72(3):1341–1374, 2014.

T. Hibiya and K. Kajiura. Origin of theabiki phenomenon (a kind of seiche) in nagasaki bay. *Journal of the Oceanographical Society of Japan*, 38(3):172–182, Jul 1982. ISSN 1573-868X. doi: 10.1007/BF02110288. URL `https://doi.org/10.1007/BF02110288`.

C. W. Hirt and B. D. Nichols. Volume of fluid method for the dynamics of free boundaries. *J. Comput. Phys.*, 39:201–225, 1981.

J. Horrillo. *Numerical Method for Tsunami calculations using Full Navier-Stokes equations and the Volume of Fluid method*. PhD thesis, University of Alaska Fairbanks, 2006.

J. Horrillo, A. Wood, C. Williams, A. Parambath, and G. Kim. Construction of tsunami inundation maps in the Gulf of Mexico. Technical report, Award Number: NA09NWS4670006 to the National Tsunami Hazard Mitigation Program (NTHMP), National Weather Service Program Office, NOAA, 2011. avail. from http://www.tamug.edu/tsunami/NTHMP.html.

J. Horrillo, A. Wood, G.-B. Kim, and A. Parambath. A simplified 3-D Navier-Stokes numerical model for landslide-tsunami: Application to the Gulf of Mexico. *J. Geophys. Res.-Oceans*, 118:6934–6950, 2013. doi:10.1002/2012JC008689.

J. Horrillo, A. Pampell-Manis, C. Sparagowski, L. Parambath, and Y. Shigihara. Construction of five tsunami inundation maps for the Gulf of Mexico. Technical report, Award Number: NA12NWS4670014 and NA13NWS4670018 to the National Tsunami Hazard Mitigation Program (NTHMP), National Weather Service Program Office, NOAA, 2015. avail. from http://www.tamug.edu/tsunami/NTHMP.html.

J. Horrillo, W. Cheng, A. Pampell-Manis, and J. Figlus. Implementing nthmp-mms strategic plan in tsunami hazard mitigation products for the Gulf of Mexico. Technical report, Award Number: NA14NWS4670049 to the National Tsunami Hazard Mitigation Program (NTHMP), National Weather Service Program Office, NOAA, 2016. avail. from http://www.tamug.edu/tsunami/NTHMP.html.

J. Horrillo, W. Cheng, and J. Figlus. Development of four additional tsunami inundation maps with revision of Port Aransas, TX and updating existing ones with maritime products. Technical report, Award Number: NA15NWS4670031 and NA16NWS4670039 to the National Tsunami Hazard Mitigation Program (NTHMP), National Weather Service Program Office, NOAA, 2017. avail. from http://www.tamug.edu/tsunami/NTHMP.html.

J. Horrillo, W. Cheng, and J. Figlus. Development of two tsunami inundation maps in the GOM and inclusion of the USGS' Yucatan landslide tsunami sources. Technical report, Award Number: NA17NWS4670015 to the National Tsunami Hazard Mitigation Program (NTHMP), National Weather Service Program Office, NOAA, 2018. avail. from http://www.tamug.edu/tsunami/NTHMP.html.

J. L. Irish and D. T. Resio. A hydrodynamics-based surge scale for hurricanes. *Ocean Eng.*, 37:69–81, 2010.

L. Kantha. Time to replace the Saffir-Simpson hurricane scale? *Eos, Transactions American Geophysical Union*, 87(1):3–6, 2006.

B. Knight. ATFM Alaska Tsunami Forecast Model, Proceedings and Results of the 2011 NTHMP Model Benchmark Workshop (NOAA Special Report). 2011.

W. Knight. Model predictions of Gulf and Southern Atlantic Coast tsunami impacts from a distribution of sources. *Sci. of Tsunami Hazards*, 24:304–312, 2006.

A. M. López-Venegas, J. Horrillo, A. Pampell-Manis, V. Huérfano, and A. Mercado. Advanced tsunami numerical simulations and energy considerations by use of 3D - 2D coupled models: The October 11, 1918, Mona Passage tsunami. *Pure Appl. Geophys.*, 172(6):1679–1698, 2015.

P. J. Lynett, J. C. Borrero, R. Weiss, S. Son, D. Greer, and W. Renteria. Observations and modeling of tsunami-induced currents in ports and harbors. *Earth and Planetary Science Letters*, 327:68–74, 2012.

P. J. Lynett, J. Borrero, S. Son, R. Wilson, and K. Miller. Assessment of the tsunami-induced current hazard. *Geophysical Research Letters*, 41(6):2048–2055, 2014.

S. Maretzki, S. Grilli, and C. D. P. Baxter. Probabilistic SMF tsunami hazard assessment for the upper east coast of the United States. In V. Lykousis, D. Sakellariou, and J. Locat, editors, *Submarine Mass Movements and Their Consequences*, pages 377–385. Springer Netherlands, 2007.

D. Masson, C. Habitz, R. Wynn, G. Pederson, and F. Lovholt. Submarine landslides: Processes, triggers and hazard protection. *Philos. Trans. R. Soc. A*, 364:2009–2039, 2006.

S. Monserrat, I. Vilibić, and A. B. Rabinovich. Meteotsunamis: atmospherically induced destructive ocean waves in the tsunami frequency band. *Natural Hazards and Earth System Science*, 6(6):1035–1051, Dec. 2006. URL `https://hal.archives-ouvertes.fr/hal-00299394`.

M. Olabarrieta, A. Valle-Levinson, C. J. Martinez, C. Pattiaratchi, and L. Shi. Meteotsunamis in the northeastern gulf of mexico and their possible link to el niño southern oscillation. *Natural Hazards*, 88(3):1325–1346, Sep 2017. ISSN 1573-0840. doi: 10.1007/s11069-017-2922-3. URL `https://doi.org/10.1007/s11069-017-2922-3`.

A. Pampell-Manis, J. Horrillo, Y. Shigihara, and L. Parambath. Probabilistic assessment of landslide tsunami hazard for the northern Gulf of Mexico. *J. Geophys. Res.-Oceans*, 2016. doi:10.1002/2015JC011261.

C. B. Pattiaratchi and E. Wijeratne. Are meteotsunamis an underrated hazard? *Philosophical Transactions of the Royal Society A: Mathematical, Physical and Engineering Sciences*, 373(2053):20140377, 2015.

C. K. Paull, D. W. Caress, R. Gwiazda, J. Urrutia-Fucugauchi, M. Rebolledo-Vieyra, E. Lundsten, K. Anderson, and E. J. Sumner. Cretaceous–paleogene boundary exposed: Campeche escarpment, gulf of mexico. *Marine Geology*, 357:392–400, 2014.

J. Proudman. The effects on the sea of changes in atmospheric pressure. *Geophysical Journal International*, 2:197–209, 1929.

U. S. ten Brink, H. J. Lee, E. L. Geist, and D. Twichell. Assessment of tsunami hazard to the U.S. East Coast using relationships between submarine landslides and earthquakes. *Mar. Geol.*, 264:65–73, 2009a.

U. S. ten Brink, D. Twichell, P. Lynett, E. Geist, J. Chaytor, H. Lee, B. Buczkowski, and C. Flores. Regional assessment of tsunami potential in the Gulf of Mexico. *U. S. Geol. Surv. Admin. Rep.*, 2009b.

R. Wilson, C. Davenport, and B. Jaffe. Sediment scour and deposition within harbors in california (usa), caused by the march 11, 2011 tohoku-oki tsunami. *Sedimentary Geology*, 282:228–240, 2012.

R. I. Wilson, A. R. Admire, J. C. Borrero, L. A. Dengler, M. R. Legg, P. Lynett, T. P. McCrink, K. M. Miller, A. Ritchie, K. Sterling, et al. Observations and impacts from the 2010 chilean and 2011 japanese tsunamis in california (usa). *Pure and Applied Geophysics*, 170(6-8):1127–1147, 2013.

Y. Yamazaki, Z. Kowalik, and K. F. Cheung. Depth-integrated, non-hydrostatic model for wave breaking and run-up. *Int. J. Numer. Meth. Fl.*, 61:473–497, 2008.